



**University of
Nottingham**
UK | CHINA | MALAYSIA



**British
Geological Survey**
Expert | Impartial | Innovative

The Variability of Gas Diffusion in Soils

by

Lewis Sam Rose *MSci* (Hons)

Thesis submitted to the University of Nottingham for the degree of

Doctor of Philosophy

January 2020

With thanks to synthetic organic chemistry, for destroying me so that I would become indestructible

-and to Michael Stipe, Peter Buck, Mike Mills, and Bill Berry; Michael Shanks, Amanda Tapping, and David Hewlett.

Thank you to my supervisors George Shaw, Neil Crout and Andy Tye for their advice and assistance whenever it was needed, and also for supporting my extra-curricular work whether it was going off travelling with NERC, with STARS, or just returning with another concussion from racing.

Thank you to Phil Haygarth, Davey Jones, Olivia Lawrenson, the rest of the STARS management and my fellow STARS students for an unforgettable PhD experience. Special mention to my fellow dream-team members Alex Williams and Dan Evans. I couldn't have got through this without the adventures we've been on. The book of quotes will have to be an appendix...

Thanks also goes to John Alcock, Matt Tovey and Will Spracklen from the University of Nottingham Farm for their help in field set-ups, the Forestry Commission, Allerton Project, BGS field team, and Leicestershire County Council for access to their field sites, David Boorman at COSMOS for their meteorological data, and Wright Engineering Co. (Nottingham) Ltd. for the soil gas sampler manufacture. Apologies to anyone I have forgotten, I'm so good at asking for help!

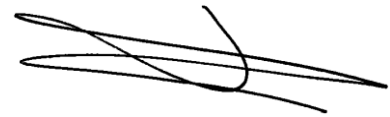
Thanks to Prof. Pete Licence for the opportunities he has supported me in getting hold of. They have done me a lot of good.

Cheers to the whole of BladeSoc, the University of Nottingham Inline Skating Society, for electing me president and making the excursions I organised massive successes.

At home I'd like to thank my mum Nina, sister Lucy, and cat Jake for putting up with me for years before this even started, as well as Bekah Smith, for the same during this most difficult part.

-and thank you to the Japanese Society for the Promotion of Science for what comes next!

Lewis S. Rose

A handwritten signature in black ink, consisting of several overlapping, fluid strokes that form a cursive representation of the name Lewis S. Rose.

December 2019

Contents

| | | |
|-------|--|------|
| 1 | Abstract..... | 1:1 |
| 2 | Introduction | 2:4 |
| 2.1 | Composition and movement of soil gas | 2:4 |
| 2.2 | Modelling of diffusion processes in soil | 2:6 |
| 2.2.1 | Mathematical representations of diffusion | 2:6 |
| 2.3 | Tracer gases for soil gas measurements..... | 2:10 |
| 2.3.1 | Radon gas in soils..... | 2:10 |
| 2.4 | Sampling of soil gas for laboratory analysis | 2:17 |
| 2.4.1 | Passive and active methods of sampling | 2:18 |
| 2.5 | Research aims and objectives | 2:20 |
| 2.5.1 | General objective | 2:20 |
| 2.5.2 | Aims of research: field section | 2:21 |
| 2.5.3 | Aims of research: modelling section..... | 2:22 |
| 2.6 | The theoretical soil gas concentration curve..... | 2:24 |
| 3 | Methods | 3:25 |
| 3.1 | Field sites..... | 3:25 |
| 3.2 | Gas sampling and measurement in soils..... | 3:26 |
| 3.2.1 | Soil gas sampling method..... | 3:26 |
| 3.2.2 | Soil gas analysis | 3:35 |
| 3.2.3 | Sample analysis for ²²² Rn | 3:35 |
| 3.2.4 | Sample analysis by gas chromatography | 3:37 |
| 3.3 | Solid characterisation of soils..... | 3:38 |
| 3.3.1 | Soil solid sampling | 3:38 |

| | | |
|--------|--|-------|
| 3.4 | Liquid characterisation of soils | 3:51 |
| 3.5 | Monitoring of meteorological conditions..... | 3:51 |
| 3.6 | Computational modelling of soil gas transport..... | 3:52 |
| 3.6.1 | Crank-Nicolson implementation | 3:53 |
| 3.6.2 | System size and boundary conditions..... | 3:55 |
| 3.6.3 | Testing..... | 3:57 |
| 3.7 | Initial conditions | 3:60 |
| 3.8 | Differences in the number of measured values..... | 3:64 |
| 3.9 | Comparison with a closed-form expression | 3:64 |
| 3.10 | Parameter estimation..... | 3:67 |
| 3.10.1 | Relating space and time | 3:67 |
| 3.10.2 | Source term..... | 3:68 |
| 3.11 | System length..... | 3:68 |
| 3.12 | <i>DS</i> value selection: grid search | 3:70 |
| 3.13 | Temporal variability of <i>DS</i> (ex-ASGARD site) | 3:71 |
| 3.13.1 | Assessing fit of model to the data | 3:72 |
| 3.13.2 | Radon source term | 3:74 |
| 3.13.3 | Model implementation | 3:77 |
| 4 | Results: soil time-series (ex-ASGARD site)..... | 4:79 |
| 4.1 | Site description: ex-ASGARD | 4:79 |
| 4.2 | Subsurface soil gas recharge rate..... | 4:87 |
| 4.3 | Annual variation in soil gas concentrations | 4:90 |
| 4.3.1 | Annual variation findings | 4:90 |
| 4.3.2 | Annual variation discussion | 4:98 |
| 4.4 | Diurnal variation in soil gas concentrations..... | 4:101 |
| 4.4.1 | Diurnal variation findings..... | 4:102 |

| | | |
|-------|---|-------|
| 4.5 | Discussion: ex-ASGARD site soil gas..... | 4:111 |
| 5 | Results: radon measurements in sites with varying soil textures and treatments..... | 5:115 |
| 5.1 | Overview..... | 5:115 |
| 5.2 | Kingston field site (sandy farmed soils)..... | 5:115 |
| 5.2.1 | Site description: Kingston..... | 5:115 |
| 5.2.2 | Findings | 5:118 |
| 5.3 | Hollin Hill field site..... | 5:120 |
| 5.3.1 | Site description: Hollin Hill (slipping clay soils) 5:120 | |
| 5.3.2 | Findings | 5:123 |
| 5.4 | Bagworth Heath field site (reclaimed colliery soils) 5:127 | |
| 5.4.1 | Site description: Bagworth Heath | 5:127 |
| 5.4.2 | Findings | 5:129 |
| 5.5 | Allerton Project field site (farmed clay soils) | 5:133 |
| 5.5.1 | Site description: Allerton Project..... | 5:133 |
| 5.5.2 | Findings | 5:135 |
| 5.6 | Boundary Plantation field site (Sherwood Forest soils) 5:137 | |
| 5.6.1 | Site description: Boundary Plantation..... | 5:137 |
| 5.6.2 | Findings | 5:139 |
| 5.7 | Discussion: field section | 5:143 |
| 6 | Results: computational soil gas modelling | 6:145 |
| 6.1 | Temporal variability of gas diffusion in soil (ex-ASGARD site) 6:146 | |

| | | |
|--------|--|--------|
| 6.2 | Spatial variability of gas diffusion in soil (Boundary Plantation, Sherwood Forest). | 6:154 |
| 6.3 | Discussion: modelling soil gas dynamics | 6:156 |
| 7 | General Discussion..... | 7:158 |
| 7.1 | Literature estimations of soil gas diffusivity | 7:159 |
| 7.2 | Literature approaches | 7:164 |
| 7.2.1 | Fitting method | 7:165 |
| 7.2.2 | Goodness of fit and statistical significance .. | 7:166 |
| 7.2.3 | General model assumptions | 7:167 |
| 7.2.4 | Model parameter selection | 7:174 |
| 7.2.5 | Model confirmation and further prediction... | 7:180 |
| 7.3 | Summary of soil gas sampling | 7:185 |
| 7.3.1 | Soil gas samplers | 7:185 |
| 7.3.2 | Soil gas sampling process..... | 7:186 |
| 8 | Conclusions..... | 8:189 |
| 9 | References..... | 9:194 |
| 10 | Appendix: Scripts | 10:214 |
| 10.1 | Authorship | 10:214 |
| 10.2 | Conversion of particle size analyser results | 10:214 |
| 10.3 | Soil gas diffusion model..... | 10:216 |
| 10.3.1 | Primary algorithm: <i>Main()</i> | 10:216 |
| 10.3.2 | Secondary algorithm: <i>Diff_1D()</i> | 10:223 |
| 10.3.3 | Tertiary algorithm: <i>RSS()</i> | 10:228 |

1 Abstract

Soil acts as a major transport pathway for various solids, liquids, and gases. Many processes observed across different scales, from gas exchange in the soil surrounding a single plant to landslides consuming hectares of forest, all begin with small changes in the subsurface and are affected by various external processes. Knowledge of gas movement in soils is critical for effective management and remediation.

Gases in soil are often studied with the aim of elucidating other properties of the system. One property of interest is the effective soil gas diffusion coefficient, a value indicative of the rate at which a specific gas moves through a soil. The soil gas diffusion coefficient is often presented in relation to the rate of movement in free air. Determination of a specific diffusion coefficient is possible with a high degree of precision in laboratory studies, but the heterogeneity of natural soils (as well as the environmental conditions often present at field sites) make more "realistic" values difficult to obtain. The variability in undisturbed soils can be high both spatially and temporally.

Soil gas is a complex mixture. The components of soil gas include the greenhouse gases carbon dioxide, methane, and nitrous oxide. Movements of such gases are of great interest when studying soil responses to climate and land use change. The major problem with attempting to model the movement of these gases is that they are all being created and destroyed at varying rates through the soil profile through biological and chemical interactions. This complexity easily conceals the underlying physical transport processes and makes determining physical characteristics very difficult.

There are two main ways in which information can be obtained about soil gas movement: gas can be collected, and its properties measured, or information (often proxies) about soil gas composition can be measured in-situ. A useful tracer for soil gas movement is the ubiquitous radioisotope radon-222 (^{222}Rn). The inert nature of radon-222 makes it an ideal soil gas tracer, and its negative health effects have been the driver of research into its detection and quantification in the environment. The radioactive decay of the nuclide radium-226 to radon-222 occurs at a constant rate with time and is a source of gas moving into the soil system at all points in space. Radioactive decay is a physical process unaffected by temperature, pressure, moisture content, biological or chemical conditions.

Many literature methods have been devised to collect soil gas and to quantify radon activity concentrations in a gas sample. Laboratory and field studies often involve a large amount of invasive field work such as drilling soil cores or digging large soil pits. Field work takes energy and time, and risks fundamental change to the soil's physical behaviour. Due to the heterogeneous nature of soils, data for one area does not necessarily apply to another. It does not make much sense to engage in a large field exercise only to produce data that is no longer applicable; a minimally invasive method of soil gas extraction is therefore attractive. As well as having a better chance that resulting data will represent the field site, minimally invasive methods can be employed on sensitive sites, including existing experimental plots, without causing undue damage or distress.

Recent studies of radon gas, specifically, have displayed a move toward more intricate and expensive equipment for a more detailed analysis of the soil system. Whilst the science might

not be disputable, the approach is not always appropriate: many areas of the world where radon is a major human health hazard, or where its use as a tracer may lead to a greater understanding of the local soil systems, require methods which are less expensive, easier to use, and more suited to remote or extreme environments than currently exist. The research reported in this thesis attempts to address this gap.

In the studied soils, gas diffusion coefficients as resolved by the employed model varied by a factor of 2 over 12 months, and by a factor of 1.5 over 50 m. Over 18 months, soil gas radon concentrations themselves varied by a factor of 6 at a depth of 10 cm, and by a factor of 1.5 at a depth of 100 cm.

The probe sampling method developed performed well in homogeneous, sandy soils; soil gas was easily extracted, and the depth concentration profile was closely approximated by diffusive theory in the form of Fick's Second Law. The developed method of fitting soil gas diffusion coefficients to data was found to be sensitive to the gas production parameter. Clayey soils and soils with properties such as compaction or horizonation due to land slippage, were both more susceptible to error in gas sampling and produced depth concentration profiles that were not valid for fitting a single diffusion coefficient value.

2 Introduction

2.1 Composition and movement of soil gas

The composition and movement of the gas within soil pore networks are vitally important for the functioning of soils, particularly soil biological processes. Atmospheric air averages 0.04 % CO₂ (though increasing each year) and 21.0 % O₂. Soil gas in UK arable soils averages 0.25 % CO₂ and 20.6 % O₂ but these concentrations vary by up to 50 % with soil treatments such as manure spreading (Russel and Appleyard, 1915). The remaining gas in soil pores includes, in variable proportions, nitrogen, methane and radon. Carbon dioxide and methane are produced and consumed at different rates throughout the soil profile (Davidson and Trumbore, 1995). Soils used for laboratory studies are often treated to exclude many parameters, such as soil biological activity, that may serve to increase or decrease localised gas concentrations (De Jong, 1973). Larger soil aggregates can support different biological communities than the bulk soil (Certini et al., 2004), so the behaviour of biologically significant gases may be difficult to represent when soil is homogenised or otherwise altered for laboratory experiments.

Compared with the free atmosphere, the soil atmosphere is quiescent, so the movement of soil gases is dominated by diffusion. Molecular diffusion is a transport phenomenon occurring because of the random motion of particles with temperatures above absolute zero. When concentrations in a system are unequal, diffusion results in the movement of particles from areas of high concentration to areas of low concentration until these concentrations are equalised.

The diffusion coefficient, or diffusivity, D of a gas is a parameter which indicates the rate at which it moves through a specific medium, in response to a concentration gradient, as the result of molecular diffusion. The SI unit for diffusivity is m^2s^{-1} . Different gases (including different isotopic forms of gases) possess different diffusion coefficients (Huxol et al., 2013). Gas diffusivity in a soil, D_s , is governed mainly by the air-filled volume and tortuosity of the pore space, both of which vary with soil volumetric water content (Moldrup et al., 2004, Hassan et al., 2009). When soil volumetric water content increases, the movement of gas within the soil relative to free air (D_0) becomes more hindered, i.e. the tortuosity of the soil pore network increases. The diffusion coefficient of a gas is 10^4 times higher in air than in water, so even the most water-soluble gases have diffusion coefficients determined primarily by the air-filled porosity of the medium.

In the environment, gas transport also occurs due to non-diffusive pathways such as mass flow due to temperature difference (convection), or pressure-induced flow due to heterogeneous porosity. Any measured gas transport constant can be represented by an effective gas diffusion coefficient D_{eff} (Maier et al., 2010).

Gas transport in soils can be affected by factors such as macroscopic soil cracks, which increase gas exchange and movement substantially (Penman, 1940), or gas build-up beneath impermeable layers such as clay caps (Ota et al., 2007) or snow cover (Fujiyoshi et al., 2010). Changes in barometric pressure have been measured to have an effect on gas transport in some soils (McNerney and Buseck, 1973), but not in others (Reimer, 1980); influence of barometric pressure on

soil gas movement is probably restricted to the short-term and to the surface of the soil (Clements and Wilkening, 1974).

2.2 Modelling of diffusion processes in soil

Diffusion in the environment is subject to variable boundary conditions, non-constant diffusivities, and changes in soil properties such as texture in dynamic systems. Simplifying assumptions have been challenged as not adequately representing realistic conditions (Hafez and Awad, 2016); gas diffusion in soils is widely modelled numerically using computers, often in one dimension assuming that diffusivity is independent of depth (Lehmann et al., 1999; Dörr and Munnich, 1990). At single soil depths, temporal changes in both diffusivity and soil moisture content require greater study (Lehmann et al., 2000; Call, 1957; Papendick and Runkles, 1965).

2.2.1 Mathematical representations of diffusion

Numerical models are based upon the diffusion equation (2.1, from Fick's Second Law). The diffusion equation is a partial differential equation (PDE) relating the concentration of a substance in space and in time.

$$\frac{dC}{dt} = -D \frac{d^2C}{dx^2} \quad (2.1)$$

Fick's second law in one dimension where C is concentration, t is time, x is space, and D is the diffusion coefficient in $m s^{-2}$.

Closed-form expressions of Fick's second law are available, and their solutions are readily computed ((3.1)). These exact solutions are only for specific geometrical arrangements, boundary conditions and source terms, however. Closed-form expressions are usually too restricted for practical application in the environment.

$$C(x, t) = \sqrt{\frac{t_0}{t}} e^{\left(\frac{-x^2}{4Dt}\right)} \quad (2.2)$$

–given the initial condition:

$$C(x, t_0) = e^{\left(\frac{-x^2}{4Dt_0}\right)} \quad (2.3)$$

–where $t > 0$, with spatial boundary conditions:

$$C(\pm x_0, t) = \sqrt{\frac{t_0}{t}} e^{\left(\frac{-x_0^2}{4Dt}\right)} \quad (2.4)$$

Closed-form expression and boundary conditions for Fick's Second Law where C is concentration, t is time, and x is space. Valid only when the given conditions are met. Derivation provided in Section 3.9 and presented graphically (Figure 22).

In whichever way Fick's diffusion equation is solved, the key parameter in any model of gas diffusion is the diffusivity, D , of

an individual gas. As described above, the effective diffusivity of a gas in soil varies according to a range of varying soil properties. Empirically derived representations of gas diffusivity in soils attempt to express the 'effective' diffusivity of gases as the ratio of the diffusivity in the soil pore space in relation to the diffusivity in the free atmosphere. These expressions vary in terms of their scope and complexity; over several decades ever more parameters derived mathematically or measured from the environment have been incorporated (Table 1). Often, diffusivity is presented as $\frac{D_s}{D_o}$, simply the ratio of the species' diffusivity in the soil and in air.

Table 1 Notable literature representations of soil gas diffusion where ϕ is soil porosity (m^3m^{-3}), θ is soil volumetric water content, m is a constant ($m = 3$ for undisturbed soils and $m = 6$ for sieved, repacked soils).

| <i>Source</i> | <i>Diffusivity representation</i> |
|------------------------------|--|
| <i>Buckingham (1904)</i> | $\frac{D_s}{D_o} = \phi^2$ |
| <i>Penman (1940)</i> | $\frac{D_s}{D_o} = 0.66(\phi - \theta)$ |
| <i>Marshall (1959)</i> | $\frac{D_s}{D_o} = (\phi - \theta)^{1.5}$ |
| <i>Jin and Jury (1996)</i> | $\frac{D_s}{D_o} = \frac{\phi^2}{\theta^{\frac{2}{3}}}$ |
| <i>Moldrup et al. (1997)</i> | $\frac{D_s}{D_o} = 0.66(\phi - \theta) \left(\frac{\phi - \theta}{\phi} \right)^{\frac{12-m}{3}}$ |
| <i>Moldrup et al. (2000)</i> | $\frac{D_s}{D_o} = \frac{(\phi - \theta)^{2.5}}{\phi}$ |

The number of parameters included in these representations of effective diffusivity means that deciding which to utilise in a soil study is often difficult. Many representations are derived from (and therefore applicable mainly to) artificial soils and are of little use to those who require a model applicable to the real world. Uses of more complex representations are more restricted because there are more parameter values to quantify, which is possible for repacked soil cores in the laboratory but more difficult for natural soils *in situ*. In cases where both simpler and more complex representations can be applied, the largest difference between estimated diffusion coefficients was 14 % (Allaire et al., 2008). Generally, the different representations of soil gas movement yield similar estimations of the diffusion coefficient in soils; greater complexity in a 'model' representing effective diffusivity does not necessarily mean greater accuracy in the predicted diffusion coefficient.

Soils are inherently variable, and models from all publication years are still employed. Broad assumptions within simpler models are not always met (Pingingtha et al., 2010). The Moldrup et al. (1997) model (Table 1) makes an important distinction between soils in the field and in the laboratory, and implies a much larger soil-type dependency in undisturbed soils compared to those used in laboratory columns.

2.3 Tracer gases for soil gas measurements

In order to inform and/or confirm model predictions of soil gas movement, data from soil measurements are required. The individual gases quantified are referred to as tracers (Etiope and Martinelli, 2002) and can either be gases present naturally in soils, such as carbon dioxide (De Jong and Schappert, 1972), methane (Born et al., 1990) or radon (Holý et al., 2007), or gases introduced to the soil specifically as tracers, such as sulphur hexafluoride (SF_6 , Boon et al., 2013). Of the commonly used tracer gases only radon and SF_6 have no biological or chemical interaction with the soil, a property that is highly desirable in a tracer as it removes complexity from the observed behaviour of the gas (Laemmel et al., 2017). In field experiments radon has a major advantage over SF_6 : it is naturally produced and ubiquitous. No invasive gas injection is required when using radon as a tracer in soil gas diffusion studies.

2.3.1 Radon gas in soils

Measured diffusion coefficients of radon gas in different materials vary by more than 7 orders of magnitude, in dry soils by 1 order of magnitude (Table 2).

Table 2: Reported diffusion coefficients of different gases in different media. ¹Allaire et al. (2008), ²Boon et al. (2013), ³Hirst and Harrison (1938), ⁴Nguyen et al. (2018), ⁵Durrani and Ilic (1997), ⁶Schery et al. (1980), ⁷Hansen and Damkjaer (1987), ⁸Folkerts et al. (1984), ⁹Quindós-Poncela et al. (2005), ¹⁰Lehmann et al. (2000), ¹¹Chauhan et al. (2008).

| Gas | Material | Diffusion coefficient (<i>D</i>) / m ² s ⁻¹ |
|-------------------------|--|--|
| Argon | Free air ¹ | 2×10 ⁻⁵ |
| Neon | Free air ¹ | 6.5×10 ⁻⁵ |
| Radon | Free air ³ | 1.2×10 ⁻⁵ |
| | Water ⁵ | 1×10 ⁻⁹ |
| | Concrete ⁸ | 6.8×10 ⁻¹⁰ |
| | "radon-proof" barriers ⁹ | 1×10 ⁻¹² |
| | Wet clay soil ⁷ | 8×10 ⁻¹¹ –6.2×10 ⁻¹⁰ |
| | Soil ¹⁰ | 2.6×10 ⁻⁷ |
| | Soil ^{6,7} | 7×10 ⁻⁷ –8.5×10 ⁻⁶ |
| | Soil ⁴ | 2×10 ⁻⁷ –1.4×10 ⁻⁶ |
| | Sand ¹¹ | (3.3–3.6)×10 ⁻⁶ |
| Sulphur hexafluoride | Repacked soil ² | (1.5–9.4)×10 ⁻⁷ |

Most soils contain detectable uranium, made up of 99 % uranium-238 (²³⁸U) and ~1 % uranium-235 (²³⁵U). The world average soil uranium concentration is 1 mg kg⁻¹ (UNSCEAR, 1993). During the radioactive decay of ²³⁸U to the stable isotope lead-206 (²⁰⁶Pb) in the uranium series decay chain (Figure 1) the radioactive isotope radon-222 (²²²Rn) is formed. Radon-222 (hereafter referred to as radon) is the longest-lived isotope of

the radioactive noble gas, with a half-life of 3.8 days. Other, shorter-lived radon isotopes are produced within the thorium-232 (^{232}Th) decay series (decaying to ^{206}Pb via "thoron", ^{220}Rn , $T_{1/2}=55.6$ seconds) and the uranium-235 (^{235}U) decay series (decaying to ^{207}Pb via "actinon", ^{219}Rn , $T_{1/2}=3.96$ seconds). As thoron and actinon are considerably shorter-lived than ^{222}Rn they make up <1 % of total 'radon' in natural systems (Chamberlain 1991). In terms of macroscale environmental processes such as soil gas transport, only ^{222}Rn is of relevance.

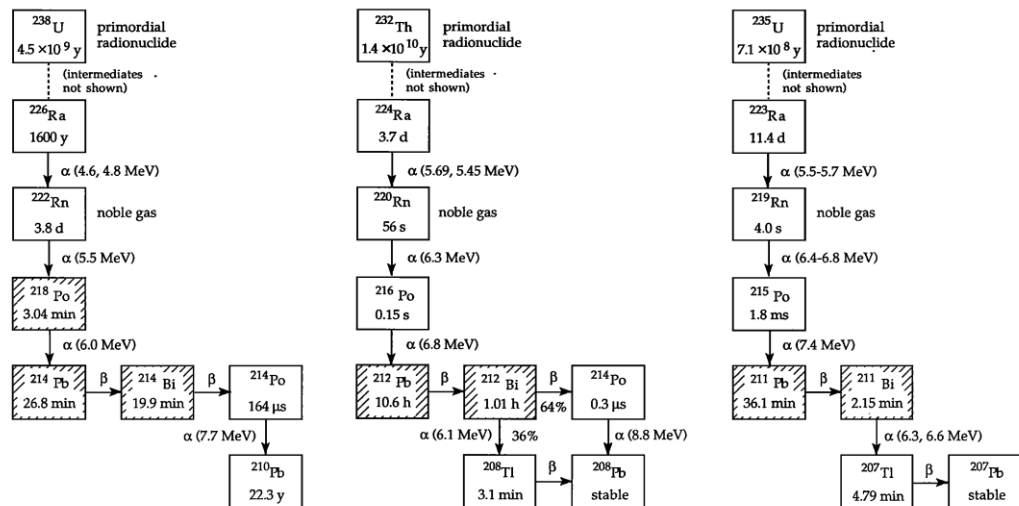


Figure 1: The ^{238}U , ^{232}Th and ^{235}U decay chains. Shaded isotopes are the most hazardous to health. From Nazaroff (1992).

2.3.1.1 Quantification of radon gas activity concentrations

Radon gas is a human health hazard (Clarke and Southwood, 1989) although it can also be used in several applications such as environmental pollution assessment (Hunkeler et al., 1997) and prediction of geological (specifically volcanic) activity (Fu et al., 2009). The features of radon gas mean that studies of radon in the environment are numerous in the literature and measurement methods are well-established.

A radon nucleus decays by alpha emission: the loss of two protons and two neutrons (i.e. a helium nucleus) from the nucleus as an energetic particle. The decay of radon by alpha particle emission makes its detection relatively straightforward, and an array of measurement techniques are available. Measurement techniques for radon activity concentration include spectrometry of alpha particles (detection as they induce current), scintillation (detection of visible light emitted by certain molecules following interaction with charged particles), and solid-state track detectors in which impacts of alpha particles alter a solid material such that impact events can then be counted. Results from radon measurement methods are comparable for most techniques (Castelluccio et al., 2010) and so choice of method can be made on the basis of “ease of use in the field, degree of convenience, sensitivity and accuracy” (Papastefanou 2007, Table 3), rather than on precision alone.

Table 3: An overview of common radon measurement methods.
Table from Papastefanou (2007).

| Method | Type | Field area | Volume | Sensitivity | Time period |
|-------------------------------|---------------|------------|--------------|---|--------------------------------|
| Alpha scintillation detectors | Instantaneous | Gas/water | 0.1 l-3.0 l | 0.8-16 cph/Bq m ⁻³ | 1-5 min |
| Alpha track-etch detectors | Integrated | Gas | 456 ml | 0.03-0.09 tracks cm ⁻² /kBq m ⁻³ h | 1-2 weeks |
| Electret ion chambers | Integrated | Gas | 50 ml-960 ml | 3 Bq m ⁻³ h-1.05 kBq m ⁻³ h | 2-40 days |
| Barasol detectors | Continuous | Gas | 590 ml | 0.02 pulses h ⁻¹ /Bq m ⁻³ | 15-240 min |
| Clipperton detectors | Continuous | Water | 590 ml | 1 cph/362 Bq m ⁻³ | 1 min-48 h |
| Radon/thoron monitors | Continuous | Gas/water | 0.27 l | 0.01 cpm/Bq m ⁻³ | 1 min-24 h (standard 6 min) |

2.3.1.2 The process of radon emanation from soil solids

When a ²²⁶Ra atom (the progenitor of ²²²Rn in the ²³⁸U decay chain) within a soil grain decays, kinetic energy is imparted to the daughter ²²²Rn atom (Sasaki et al., 2004). A fraction of the ²²²Rn atoms created will escape into the soil pore space. Of the ²²²Rn atoms reaching the soil pore space, some will cross the full width of the pore and become embedded into adjacent grains (Bossus, 1984; Tanner, 1980; Nazaroff, 1992; Sakoda et al., 2011, Figure 2). The fraction of ²²²Rn atoms propelled into, and remaining within, the soil pore space compared with the number originally produced by decay of the parent ²²⁶Ra within soil grains is termed the ²²²Rn emanation factor, *EF*.

Several external factors affect the radon emanation factor, particularly soil moisture content: as the diffusivity of atoms in water is much smaller than that in air, thin films of water on the surface of soil grains increase the radon emanation factor. The effect of moisture content on the radon emanation factor concerns only soils with volumetric water contents <5–10 %

(Sakoda et al., 2011). At >10 % volumetric water content, most soil grains are surrounded by a thin film of water. The water surrounding soil grains acts as a mediator for the kinetic energy of the daughter atoms, and the radon emanation rate approaches a constant value determined by other physical characteristics of the soil.

Soil drying and other pre-analysis treatments in the laboratory may facilitate certain chemical reactions and destroy biofilms (Girault and Perrier, 2012b). Knowing the effects of moisture content alone on soil radon emanation, treatment of soils for laboratory studies is likely to alter radon production and therefore transport characteristics in comparison with undisturbed soils.

In addition to moisture content, soil radon emanation is controlled by complex interactions with many other factors including radium distribution within soil grains, soil organic matter content, temperature (Iskandar et al., 2004, though <5 % environmental conditions), weather modification of soil grains, mineral type, and soil grain size (Kikaj et al., 2016). The current picture of radon emanation at the soil grain scale is probably incomplete (Krishnaswami and Seidemann, 1988; Rama and Moore, 1990; Nazaroff, 1992). Current understanding of radon emanation is summarised in Figure 3 (Sakoda et al., 2011).

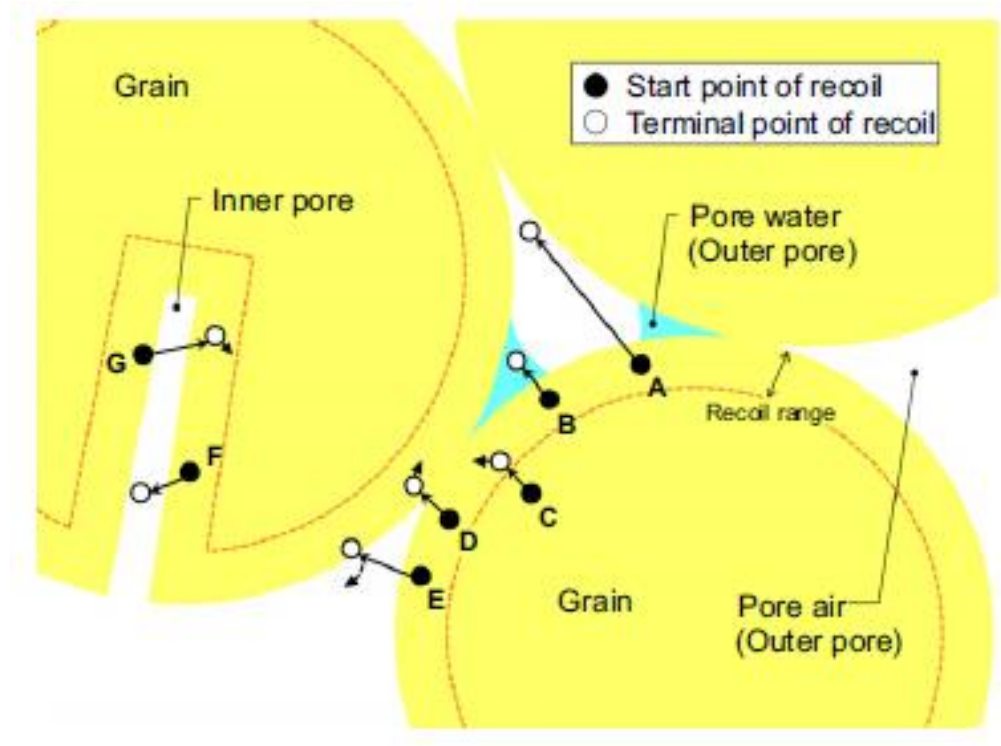


Figure 2: Scheme of radon emanation phenomenon. A, B, E and F result in emanation of radon from the soil grain (not to scale). From Sakoda et al. (2011).

2.3.1.3 Radon exhalation from soil to atmosphere

As with radon emanation, soil moisture also affects radon exhalation, defined as the movement of radon from the soil pore space to the free atmosphere above the soil surface. Soil conditions approaching saturation increase radon exhalation in the short-term due to “degassing” of soil by infiltrating water, even though less pore space is available for gas diffusion and the soil gas diffusivity drops in response to higher water pore water content (Lehmann et al., 2000).

Considering that soil and atmospheric properties such as lithology, water content, temperature and air pressure influence gas transport in soils, the spatial variability of radon emanation

can be high (Kikaj et al., 2016). It is well known that seasonal variations in radon activity concentration exist and these temporal fluctuations are often due to changes in soil moisture levels. Daily oscillations can be increased in the summer months due to cracking in soils resulting in accelerated convection (Baykut et al., 2010).

Variations in radon exhalation have been observed on diurnal timescales (Clements and Wilkening, 1974) as well as annual timescales (Szabó et al., 2013): soil gas radon activity concentrations are generally higher at night and in winter.

2.4 Sampling of soil gas for laboratory analysis

There are two main ways in which information can be obtained about soil gas: gas can be collected physically, and its properties measured *ex situ* (usually in the laboratory), or information (often proxies) about soil gas composition can be measured *in situ* instrumentally. Collection of soil gas would ideally be non-disruptive and possess an adequate temporal and spatial resolution (Laemmel et al., 2017); however, accuracy and precision in space and time is not always possible. Installation of any equipment potentially disturbs the soil's physical structure. Cracking of dried soils upon sampler insertion will increase local porosity dramatically, compromising gas samples. Pilot hole methods would also encourage soil venting. Animal burrows, utility conduits and other barriers to migration can yield false results, while topographic variations can also distort data (Ullom, 2018).

Active methods of soil gas collection involve either continuous automated withdrawal of gas by an electronically controlled pump, or discrete manual sampling of points, often over time. Passive methods of soil gas collection rely on diffusion of material into containers, or the chemical or physical change in a material due to the presence of certain species. Passive methods of soil gas measurement can suffer from low temporal resolution compared to active methods (Abjoassim, 2017; Fuhrmann et al., 2019), although for some applications such as large-scale mapping, a lower spatial resolution sampling method can be desirable (Bem et al., 2020).

2.4.1 Passive and active methods of sampling

Passive measurements of radon concentrations can be cheaper and require less maintenance than active methods. Active methods are sometimes employed alongside passive methods for quality control (Beresford et al., 2012).

Methods of passive radon measurement include nuclear track detectors, traditionally used within existing subsurface structures such as caves and animal burrows (Beresford et al., 2012). On the surface of the soil, chambers are often employed involving either temporary (Uchida et al., 1997) or permanent (Schroth et al., 2012) installation of a collar to create an enclosed space for gas build-up and collection. Chamber measurements are limited to quantifying surface fluxes and provide no information on radon distribution with respect to depth. Chambers shield the soil system from possible external effects such as wind and sudden changes in barometric pressure (Ota and Yamazawa, 2010), moderating the influence of non-

diffusive factors but, like laboratory experiments, moving the soil system from its natural state. In order to keep soils beneath chambers as close to natural conditions as possible, the chambers are often electronically opened for equilibration at regular time intervals (Butterbach-Bahl et al., 2002; Rubio and Detto, 2017). Installation of passive samplers brings the same risks of soil system disturbance as active methods, though over long-term installation it is likely that smaller disturbances will have a smaller effect on collected data.

Active soil gas collection results in some degree of induced gas transport within the soil being sampled. Gas pumps can be battery-operated and left in the field for long time periods (Lehmann et al., 2000), though continuous pumping can create large gradients in soil gas concentrations. Pressure gradients bring unnatural convective flows within the soil structure and make accurate measurement of natural soil gas behaviour difficult, especially at high temporal resolution (Hirano et al., 2003). Where relatively large amounts of gas are moved in a soil gas system (Beresford et al., 2012) possible dilution effects due to atmospheric draw-down cannot be ignored.

Active methods for soil gas sampling include the use of rigid tubes to penetrate the soil and withdraw gas from specific depths. Soil gas probes are an approach favoured in many experiments, with many different types of installation possible depending on the desired measurement pattern (Kabrt et al., 2017; Huxtable et al., 2017). Theoretical sampling radii for soil gas probes have been calculated based on an assumption of homogeneous and isotropic pore structure in soils (Huxtable et al., 2017); minimum spacing between samplers and minimum sampling depth are heavily dependent on soil properties and the

volume of gas extracted. For the presented research, a similar probe was devised (Figure 5, Figure 8).

2.5 Research aims and objectives

2.5.1 General objective

The overall aim of the presented research was to use measurements of radon (^{222}Rn) in soils, in combination with numerical model fitting, a) to estimate *in situ* diffusion coefficients for radon in soils and b) to use these estimates to quantify the diffusive characteristics of soils applicable to other important soil gases. The overall aim was achieved by developing and extending a previously published method of sampling and measuring ^{222}Rn in soil gas from various soil types under field conditions (Huxtable et al., 2017). The method was used to collect data in the long- and short-term. A bespoke computer model of soil gas transport by diffusion was fitted to the data to provide estimates of the soil gas transport characteristics of different soils under different conditions, based on effective *in situ* soil gas radon diffusion coefficients.

2.5.2 Aims of research: field section

2.5.2.1 Temporality

Observe annual variation in soil gas radon activity concentration as observed in literature (Reimer, 1980; Dmitriev; 2018), in an inexpensive and easily implemented way.

Observe a similar pattern to that observed over seasonal timescales but on a diurnal timescale. Diurnal variation will not be observable in winter if night/day temperature variation is insufficient to induce thermal inversion at the soil surface (Rubio and Detto, 2017).

2.5.2.2 Weather Events

Observe higher variations in carbon dioxide and methane concentrations during dry periods, as soils respond more dynamically to wetting (Ma et al., 2012); however, extreme changes in environmental conditions may affect radon activity concentrations, masking other effects.

2.5.2.3 Soil textural effects

Ascertain the applicability of the method to different soil types. Clay soils will possess reduced porosity, so extraction of soil gas may be more difficult than from sandier soils.

Ascertain the applicability of the method to different soil treatments within agriculture. Topsoil regularly disturbed will be

much easier to penetrate with the sampler than undisturbed soils.

2.5.2.4 Tracer production requirements

Ascertain whether employed detection methods can detect radon from all soil types (soils with extremely low radon production rate may not produce enough radon to detect).

2.5.2.5 Site-specific characteristics

Ascertain whether soil gas radon activity concentration profiles can be used to identify soil treatment changes, such as that between ploughed and zero-tillage soils.

Determine whether a soil gas probe sampler is unduly hindered by the presence of trees and other established flora.

2.5.3 Aims of research: modelling section

Enable the tracking of the variability in gas movement across study sites and/or study periods by calculating the theoretical soil gas radon activity concentrations for the soils in question and then fitting a variable D_S value to the measured data.

It is hypothesised that any surface organic matter will have little effect on the soil gas radon activity concentration profile due to its proximity to the atmosphere, and that more complex soil gas radon activity concentration profiles will result from the mixing

of different soil textures leading to profiles not conforming to theory.

2.6 The theoretical soil gas concentration curve

According to Fick's Second Law (2.1), assuming net constant production of gas with depth, and a single diffusion coefficient with depth, an open upper boundary and a closed lower boundary, a characteristic radon activity concentration curve develops with respect to soil depth (Figure 3).

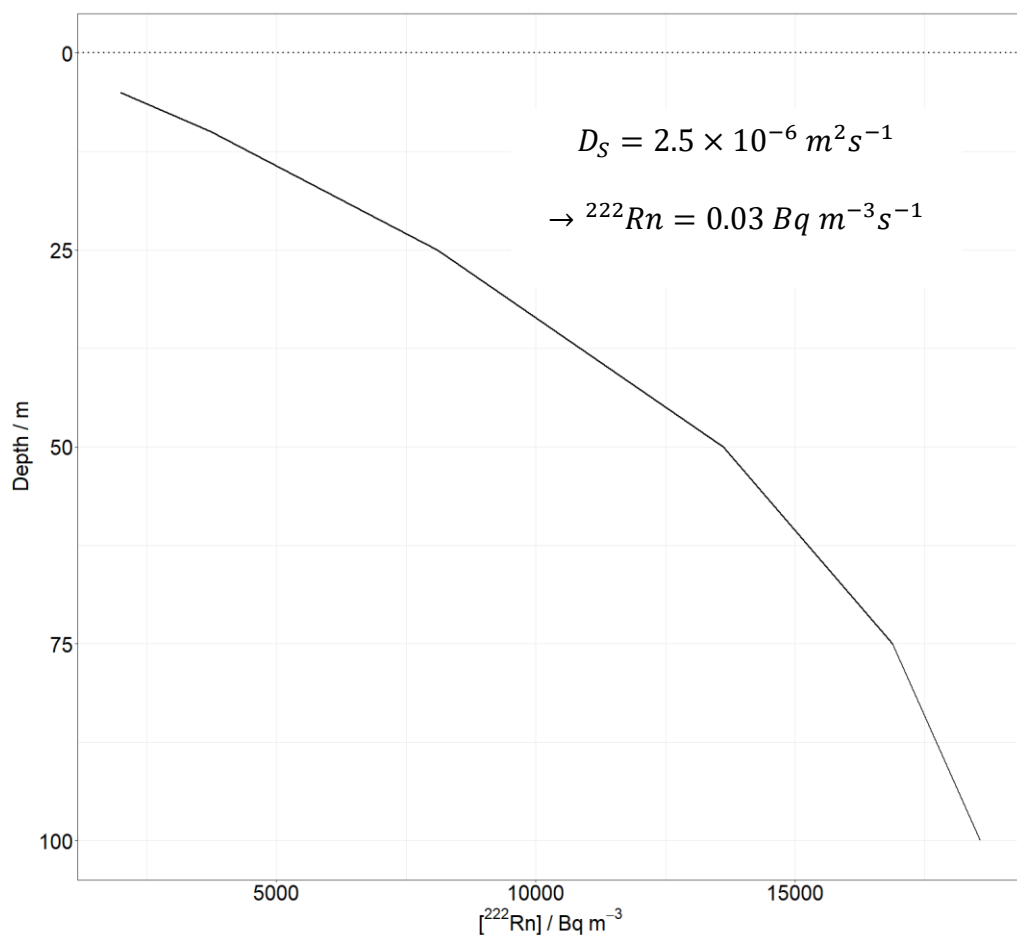


Figure 3: An example of the depth-activity concentration curve ("concentration profile") of radon in soil assuming net constant production and diffusion coefficient with depth, atmospheric concentrations of zero and constant concentration at depth.

3 Methods

3.1 Field sites

Field sites visited were all in the central United Kingdom (Figure 4). Sites are described in detail in their respective sections.

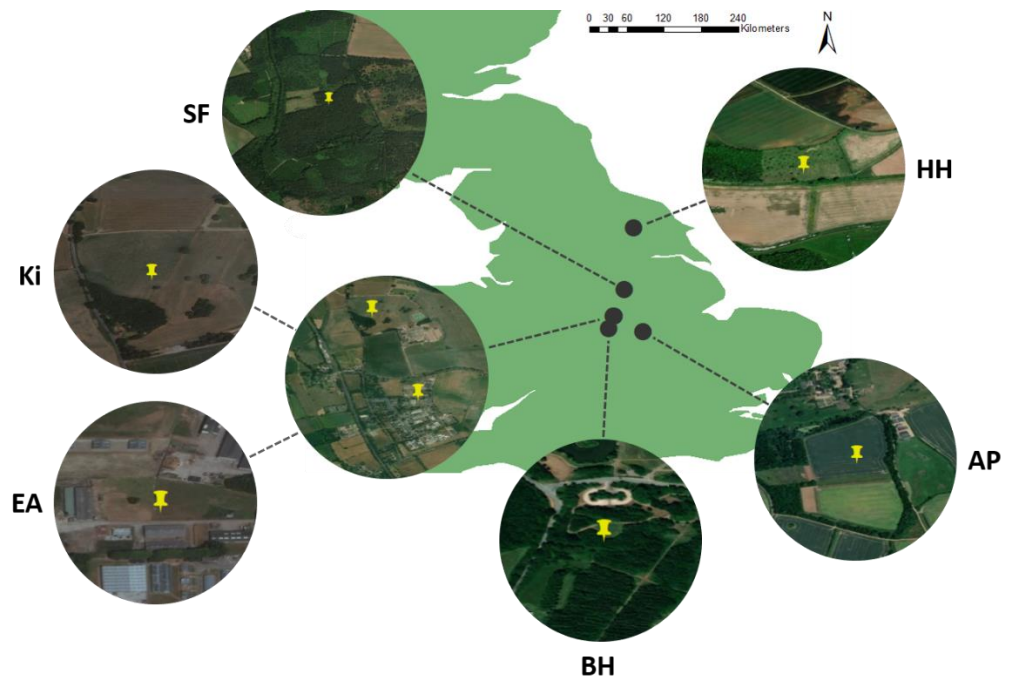


Figure 4: Location of field sites within the UK. Clockwise from top-right: Hollin Hill (HH), Allerton Project (AP), Bagworth Heath Demonstration Woodland (BH), Sutton Bonington [top: Kingston (Ki), bottom: ex-ASGARD (EA)], Sherwood Forest Boundary Plantation (SF).

3.2 Gas sampling and measurement in soils

3.2.1 Soil gas sampling method

3.2.1.1 Sampling apparatus

To facilitate active sampling of small volumes of soil gas, a probe was designed consisting of stainless steel tubing (316 grade, length <2 m, 8 mm external diameter, 5 mm internal diameter) with a thread at one end to which a pointed tip can be attached (Figure 5). The sampler tip is perforated by twelve 1 mm \varnothing holes leading to the interior of the sampler. Immediately behind the sampling tip was fixed a narrow (0.8 mm) internal diameter flexible silicone rubber tube. The silicone rubber tube was passed through the sampler body and fixed to a plastic tap with a Luer fitting *via* a brass elbow joint at the upper end of the tube, allowing a disposable syringe to be attached. The syringe was used to draw soil gas through the sampling probe from the required soil depth.

The design of the soil gas sampler minimises 'dead space' of gas within the internal volume. The approximate volumes in the sampler head and in the silicone tube are 0.5 cm³ m⁻¹ and result in total internal volume <1.5 mL for the longest (2 m) sampler.

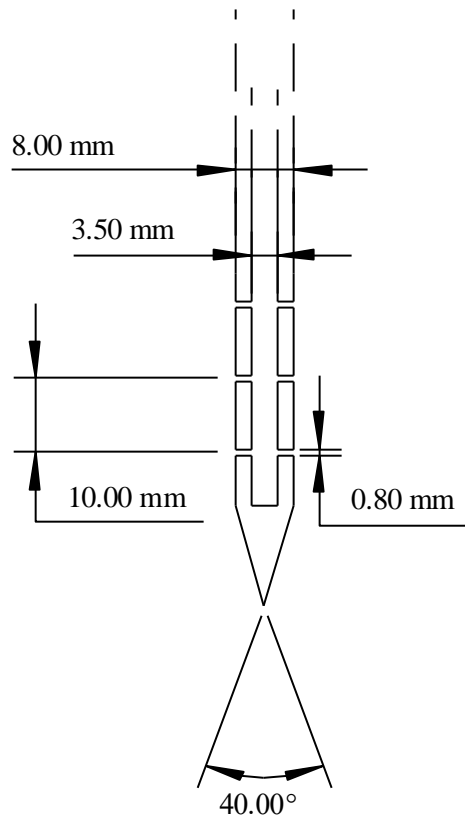


Figure 5: Schematic of soil gas sampler tip.

If samples are taken too closely together there is a danger that the volumes of soil from which the gas samples are drawn will overlap, thus compromising the data obtained from each sample. The potential for overlap depends on the radius of the 'sphere of influence' around the sampler tip which, in turn, depends on the sample volume and the effective porosity of the soil.

The theoretical sphere of influence during soil gas sampling has previously been calculated (Huxtable et al., 2017; Figure 6). The optimum volume of soil gas for counting of ^{222}Rn by liquid scintillation has been determined as 45 cm^3 (Huxtable et al., 2017). The soil volume affected by extraction of a 45 cm^3 sample will vary with the air-filled porosity of the soil: at 10 % air-filled porosity, the "sampling sphere" has radius $\sim 5 \text{ cm}$, and

the sampling sphere radius decreases with increasing porosity to a value of ~ 3 cm at 40 % air-filled porosity.

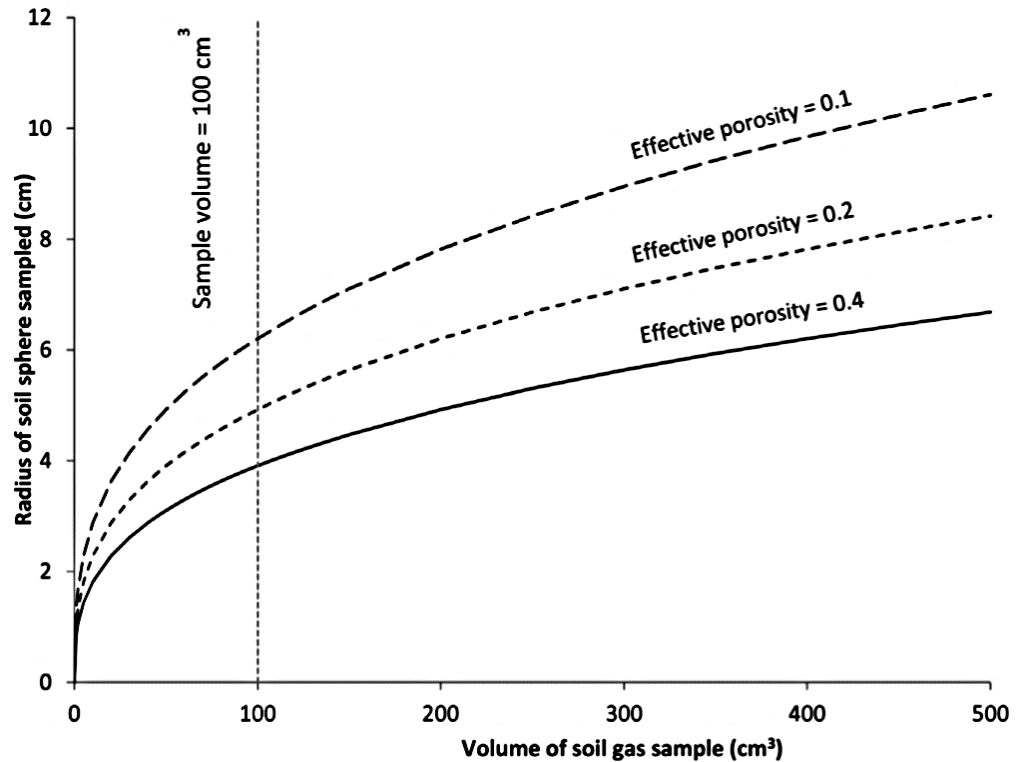


Figure 6 Theoretical soil gas sampling spheres of influence (Huxtable et al., 2017).

There is no known method for determining air-filled porosity in the field. Instead, soil samples must be taken and bulk density as well as volumetric water content measured. From bulk density and volumetric water content, soil air-filled porosity can be calculated by (3.1):

$$\text{Total Porosity} = \left(1 - \frac{bd}{pd}\right) * 100 \quad (3.1)$$

Where *bd* is bulk density [g cm^{-3}] and *pd* is particle density, taken as 2.65 g cm^{-3} in mineral soils. Air-filled porosity is calculated by subtracting volumetric water content from the total porosity of the soil [**both dimensionless**].

It is too laborious to calculate the possible inter-sample spacing for every set of samples taken. Instead, an assumed porosity of >0.1 was used. In highly variable areas, however, bulk density could be estimated in order to increase spatial resolution as much as possible.

Agricultural soils in the UK have mean porosity 0.38 (min. 0.28, max. 0.66) at 10 cm depth (Ball et al., 2000). It was decided that a minimum sampling radius of 5 cm for sample volumes $<50 \text{ mL}$ could be assumed to be free of interference from adjacent samples.

3.2.1.2 Sampler installation

For sampling a single spatial point or depth profile at one point in time, a sampler was inserted vertically into the soil to a depth of 10 cm and a 45 cm^3 soil gas sample withdrawn as described above. After a sample was taken, the probe was driven downwards into the soil in 10 cm increments and soil gas samples taken at each depth until the deepest desired / possible soil depth had been sampled.

The strategy described for sampling soil gas from different depths is preferable to sampling from depth in the soil before moving toward the surface, as the radon concentration and any soil disturbance caused at the surface can be assumed to increase with depth.

For sampling soil gas in a single vertical profile at more than one point in time, long-term sampler installation is necessary. In order to minimise the effect of any rainfall events on the soil-sampler interface, samplers were installed at 45 ° to the soil surface so that sampler tips were positioned in the same vertical axis as with the single point sampling procedure described previously (Figure 7). Sampler tips were installed at depths of 5, 10, 25, 50, 75 and 100 cm, greater than the minimum radius (<0.1 m) estimated by Huxtable et al. (2017, Figure 6). To meet the criterion of <0.1 m between sampler tips (a sampling radius of ~0.05 m), the sampler for 0.05 m depth was offset by ~9 cm.

A buffer zone measuring 1.5 m × 2 m (Figure 7) was maintained surrounding the sampling area at the surface to reduce disturbance to the ground during the sampling process and to exclude grazing animals.

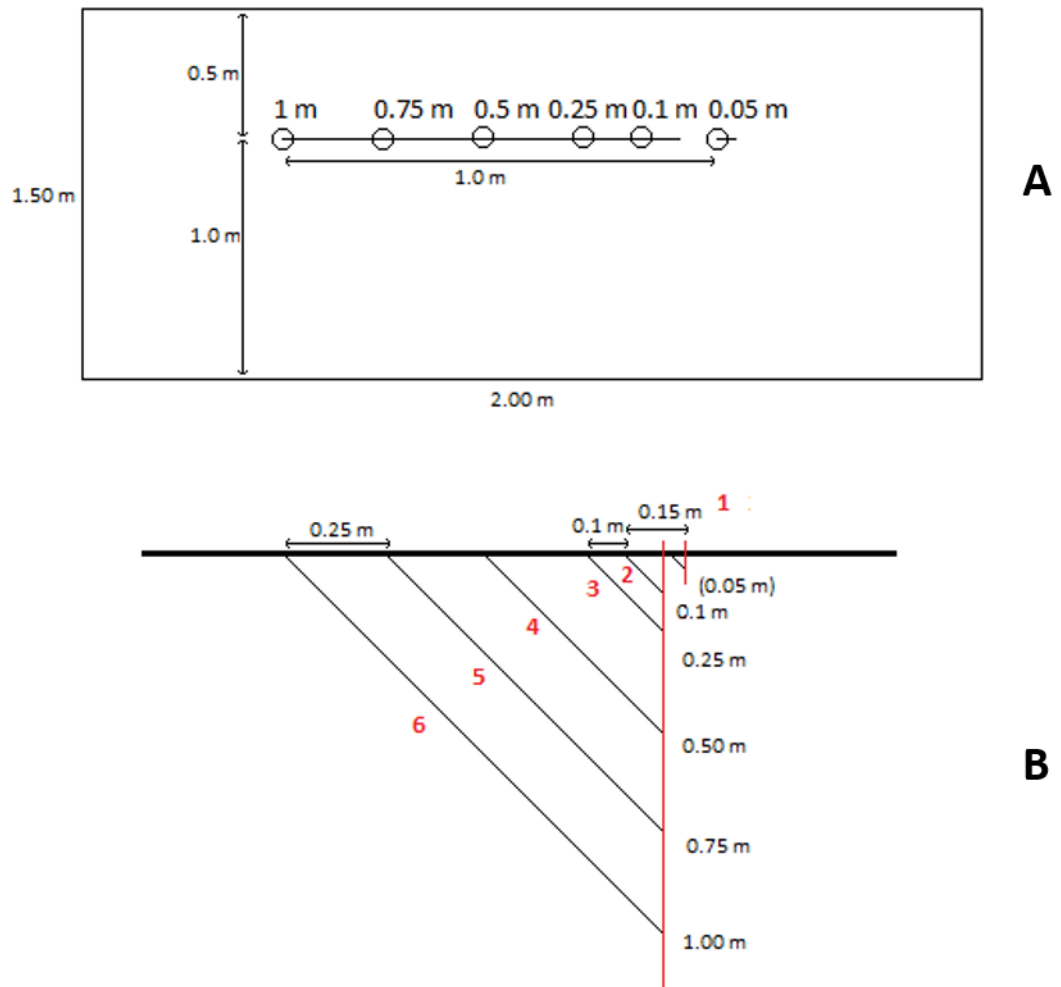


Figure 7: Installation of samplers at 45 ° to the soil surface in plan view (A) and profile view (B).

3.2.1.3 Soil gas sampler development

After soil sampling on the first field site (Section 5.2) using the apparatus as described in Huxtable et al. (2017), a redesign was carried out (Figure 8). New soil gas samplers were manufactured by Wright Engineering Co. (Nottingham) Ltd., using 316 stainless steel with wall thickness 1.5 mm (OD 8 mm, ID 5 mm). The advantage of 316 stainless steel over aluminium is a tensile yield strength of 206 MPa. Stainless steel samplers

are nearly 4 times as strong as those made from aluminium (EZ-LOK, Tool Components Inc., www.ezlok.com, AZoM, AZoNetwork UK Ltd., www.azom.com). A later manufacture included a handle attachment for removal of samplers (Figure 8).

3.2.2 Soil gas analysis

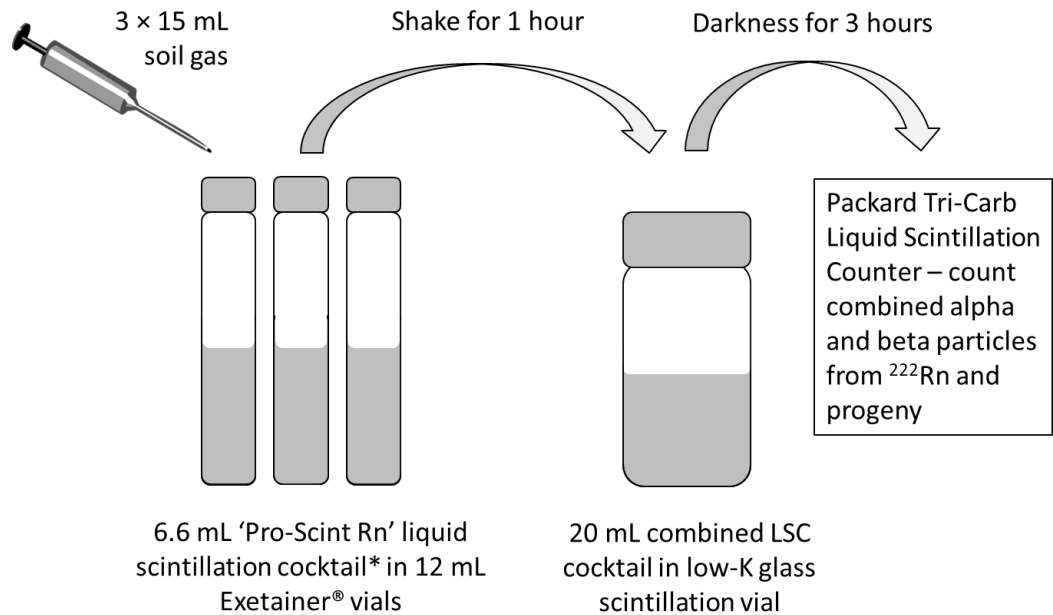
3.2.3 Sample analysis for ^{222}Rn

Samples of soil gas were actively extracted in the field for subsequent analysis in the laboratory. In order to eliminate any 'dead volume' effect due to the samplers' internal volume, an initial volume of 5 mL was extracted at the sample point and discarded.

For analysis of radon (as ^{222}Rn) within soil gas, 3 × 15 mL soil gas samples were extracted sequentially using a 20 mL syringe; each sample was injected into a separate 12 mL Exetainer® vial (Labco Ltd.). Vials for radon gas analysis were prepared in advance by adding 6.6 mL ProScint Rn liquid scintillation cocktail (Meridian Biotechnologies, UK) then partially evacuating the headspace gas from the vial using a syringe. Care was taken to prevent loss of sample during transfer from syringe to cocktail-containing vial. After injecting the gas samples into the Exetainers, they were manually shaken at 15-minute intervals over the next 2 h, then combined in a single low potassium borosilicate vial for liquid scintillation counting. Samples were then placed in darkness for >1 h before further analysis in order to allow for any chemiluminescent reactions to subside. The overall sample processing time, including the dark adjustment period, ensured that any residual ^{220}Rn ($T_{1/2} = 55$ seconds) had completely decayed prior to measurement.

Radon activity concentrations were determined in the dark-adjusted samples which were counted for 1 hour across an energy range of 0–2000 keV using a Packard Tri-Carb 2100-TR

Liquid Scintillation Counter. The overall procedure is summarised in Figure 10.



(*mineral oil based with 'pseudocumene' scintillator)

Figure 10: Schematic summary of soil gas preparation and counting for ²²²Rn activity concentration.

Net sample activities were calculated from the number of counts detected during the count period, minus the activity recorded in a reagent blank background sample. A counting error (2σ i.e. 95 %) is reported for the raw counts in the instrument. After decay correction of reported count rates to the sampling time and calculation of original sample radon activity concentrations, values are reported as Bq m^{-3} of soil gas.

3.2.4 Sample analysis by gas chromatography

An additional 5 mL soil gas was extracted at the time of sampling in the field; the 5 mL sample was injected into a 3 mL Exetainer® vial (Labco Ltd.) for the analysis of greenhouse gases (GHGs – specifically CO₂, CH₄ and N₂O) in the laboratory. Vials for greenhouse gas analysis were prepared in advance by removing a nominal 8 mL gas from the vial at atmospheric pressure.

The 5 mL soil gas samples were analysed using a GC-2014 gas chromatograph (Shimadzu Corp., Japan) fitted with a custom auto sampler (HTA S.R.L., Italy). A 3 mL total volume dual-loop system enabled analysis of each sample for its concentrations of CO₂, CH₄ and N₂O, using a combination of Thermal Conductivity Detector (TCD), Flame Ionization Detector (FID) and Electron Capture Detector (ECD), respectively. Two gas calibration standards (BOC, UK) were used: standard 1 was certified at 500 ppm CO₂, 50 ppm CH₄ and 500 ppb N₂O; standard 2 was certified at 10 ppm CO₂, 2 ppm CH₄, 100 ppb N₂O.

Data analysis was performed using GCSolution software (Shimadzu Corp., Japan).

3.3 Solid characterisation of soils

Unless stated otherwise, soil properties were characterised by extracting three soil cores and splitting them into sections for analysis in the laboratory. From the core sections, soil porosity was determined according to Rowell (1994), assuming the density of water as 1 g cm^{-3} and soil particle density as 2.66 g cm^{-3} . Other soil physical characteristics such as, dry bulk density (Section 3.3.1.1), soil particle size distribution (Section 3.3.1.2), and soil penetration resistance (Section 3.3.1.3) were also measured.

3.3.1 Soil solid sampling

Unless stated otherwise, a triplicate 90 cm (length) cores were collected using a graduated soil corer (3 × 30 cm sections, diameter 5 cm, 3.5 cm, 2 cm, respectively). Randomised sampling was carried out after soil gas sampling had been completed, or approximately 2 m from the site of soil gas sampling in the case of long-term installation, to minimise soil disturbance. Variations in soil properties with depth were noted, as well as differences between the three cores. Each core was separated into 5 cm sections before transport to the laboratory.

Where dry soils were required (for gamma-ray spectrometry and particle size analysis), each sample was oven-dried for >8 h at 105 °C. Following oven drying, samples were milled and sieved to <2 mm.

3.3.1.1 Soil bulk density analysis

For determination of soil bulk density, soil samples of known volume were extracted from the face of a soil pit (Figure 28) at 10 cm intervals. Each of these was processed as previously described and their mass measured.

From the known volume of each section and the measured masses, the bulk density can be calculated (Figure 29).

3.3.1.2 Soil particle size analysis

For soil particle size analysis, triplicate cores were collected in the manner previously described and each divided into sections 10 cm in length. Individual sections were dried and homogenised.

Samples of 0.5 g from each section were reacted overnight with 10 mL hydrogen peroxide (H_2O_2), before being heated to 80 °C and introduced to more H_2O_2 until organic matter had been completely removed. In order to remove carbonates and prevent flocculation, 10 mL sodium hexametaphosphate ($\text{Na}(\text{PO}_3)_6$) was added.

Prepared samples were passed through a Beckman-Coulter LS 13 320 Multi-Wavelength Laser Diffraction Particle Size Analyser. Output was in the form of a histogram containing percentages for arbitrary size classes to a simple spreadsheet.

A script was written to convert the files into a useable format and then collate the results (Appendix: Scripts) Calculation of the fraction of clay, silt and sand in each soil sample was then carried out (clay, silt, and sand were taken as particle size

diameter <8 µm, 8–60 µm and >60 µm, respectively, according to Konert and Vandenberghe (1997)).

3.3.1.3 Soil penetration resistance

It has been noted (Langton 1999), that soil penetration resistance can be used as a proxy for soil bulk density at depth. Use of a proxy would allow an estimation of the bulk density of soils in sites analysed, without the need to extricate large cores.

A PANDA penetrometer was used to provide measurements of soil strength to depths of >1 metre (Insitu Test Pty. Ltd., insitutest.com.au). The PANDA is a lightweight dynamic cone penetrometer with variable input energy. As the device is driven into the ground using a hammer, both the energy input and cone penetration are recorded electronically (*via* an accelerometer and retractable tape, respectively). The dynamic cone resistance and depth are then displayed in real-time.

Dynamic cone resistance is calculated using the “Dutch formula” (3.2):

$$q_d = \frac{1}{A} \cdot \frac{\frac{1}{2}MV^2}{1 + \frac{P}{M}} \quad (3.2)$$

Formula for calculating penetration resistance q_d where A is the cone area [cm^2], M is the striking mass [kg], P is the struck mass [kg] and V is the impact speed [cm s^{-1}].

3.3.1.4 Gamma-ray spectrometry

Calculation of the soil gas radon activity concentration profile requires an estimate of the production rate of ^{222}Rn within the soil. For ^{222}Rn estimation, an analysis of radium-226 (^{226}Ra , the parent nuclide of ^{222}Rn) was carried out using gamma-ray spectrometry. Calibration of the gamma-ray spectrometer was carried out (Figure 12) using samples of standard geometries (within 3.5 cm and 5.4 cm diameter Petri dishes of approximate volume 9.5 cm^3 and 28.5 cm^3 , respectively) created using materials of different densities.

Triplicate cores were extracted from the soil to a depth of 90 cm and separated into 10 cm depth-wise sections before being prepared as previously described. Samples were placed into 5.4 cm diameter Petri dishes which were then sealed and left >3 weeks to allow ingrowth of ^{222}Rn and its short-lived progeny polonium-218 and -214 ($^{218}\text{Po}/^{214}\text{Po}$), lead-214 (^{214}Pb), and bismuth-214 (^{214}Bi). Once secular equilibrium had been reached, counting was carried out for 24 h using two high-purity germanium (HPGe) crystals shielded by lead and copper, connected through a multi-channel analyser (MCA) to a computer running the GENIE-2000 gamma spectrometry software (Canberra Inc. now Mirion Technologies, USA). Spectra were smoothed with an interval of 0.3 keV before being stripped of background activity.

Activity concentration of ^{226}Ra was quantified *via* the granddaughter nuclides' gamma energies at 295.2 and 351.9 keV (^{214}Pb) and 609.3 keV (^{214}Bi) and by application of a factor (0.57) to distinguish the contributions of ^{226}Ra and ^{235}U to the composite gamma peak at 186.2 keV (Tucker et al., 2012; Giles, 1998). The two methods yielded comparable results

(Figure 11) although there appears to be a consistent difference between the two sets of resulting values of approximately 10 %. The discrimination factor calculation may be used in future in order to minimise laboratory time required (equilibration period is not needed when simply applying a factor to a measured peak).

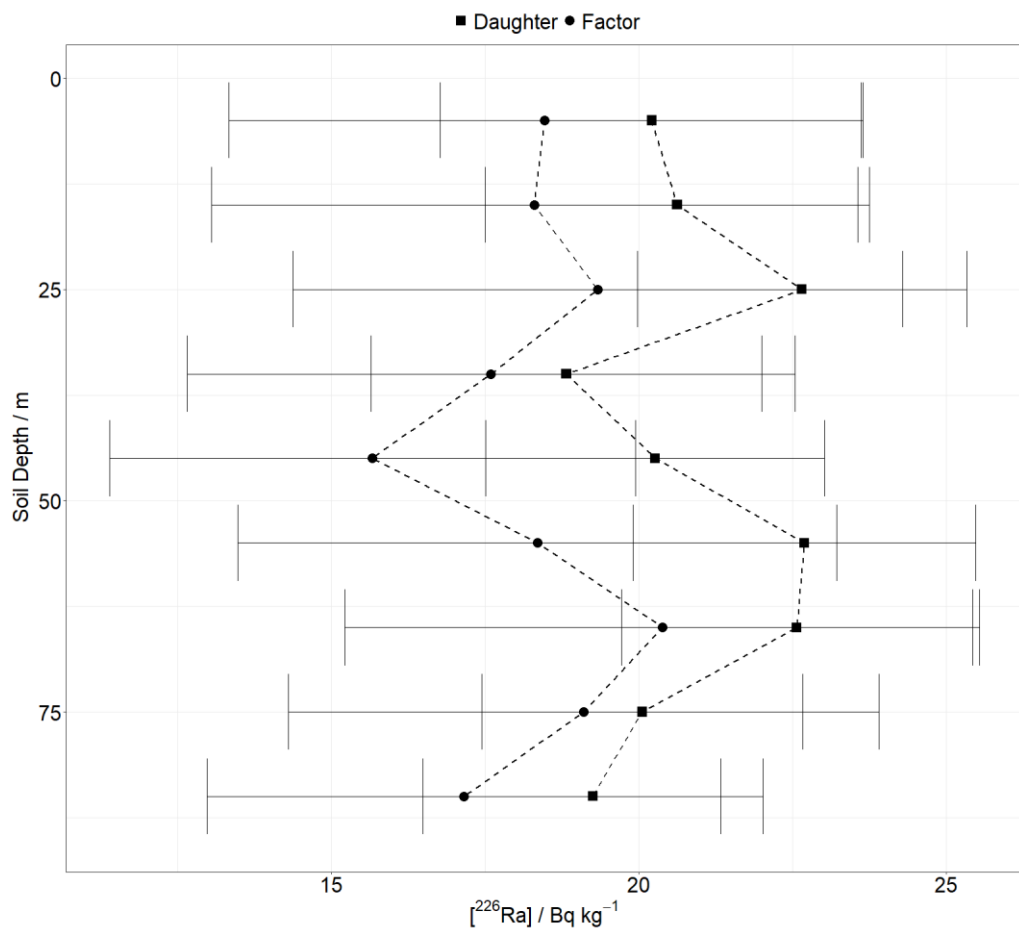


Figure 11: ^{226}Ra activity concentrations with depth determined via daughter radionuclides or by discrimination factor to resolve the 186.2 keV gamma ray peak. Both methods are within error of each other.

3.3.1.4.1 Preparation of gamma standard matrix

The materials utilised were sand, compost, leaf litter, and a mixture of sand and compost (an attempt to create a homogeneous material of intermediate density). Material was oven dried and sieved to <1 mm before doping with a standard solution of mixed radionuclides (NPL R08-01-2016040167-1).

Calculation precision was 4 decimal places. Unfortunately, in the 5.4 cm diameter petri dish the "Compost and Sand" petri dish had density very close to that of "Compost" (Figure 15). A summary of the employed standard is provided in Table 4:

Table 4 Mixed standard used for efficiency calibration.

| Nuclide | Activity / Bq g ⁻¹ |
|-------------------|-------------------------------|
| ⁵⁷ Co | 0.110 |
| ¹³⁹ Ce | 0.137 |
| ¹¹³ Sn | 0.348 |
| ⁸⁵ Sr | 0.429 |
| ²⁴¹ Am | 0.526 |
| ⁸⁸ Y | 0.519 |
| ⁵⁴ Mn | 0.541 |
| ¹³⁷ Cs | 0.587 |
| ⁶⁰ Co | 0.627 |
| ⁶⁵ Zn | 1.125 |
| ⁵¹ Cr | 2.216 |
| ¹⁰⁹ Cd | 2.920 |

3.3.1.4.2 Efficiency calculations

Efficiency of the gamma detector regarding an emission of specific energy is calculated by 3.3:

$$\varepsilon = \frac{cps}{Bq \cdot \gamma} \quad (3.3)$$

*Efficiency at specific energy (%) where **cps** is Counts per Second, **Bq** is radioactivity of specific nuclide, and γ is the gamma ray emission rate.*

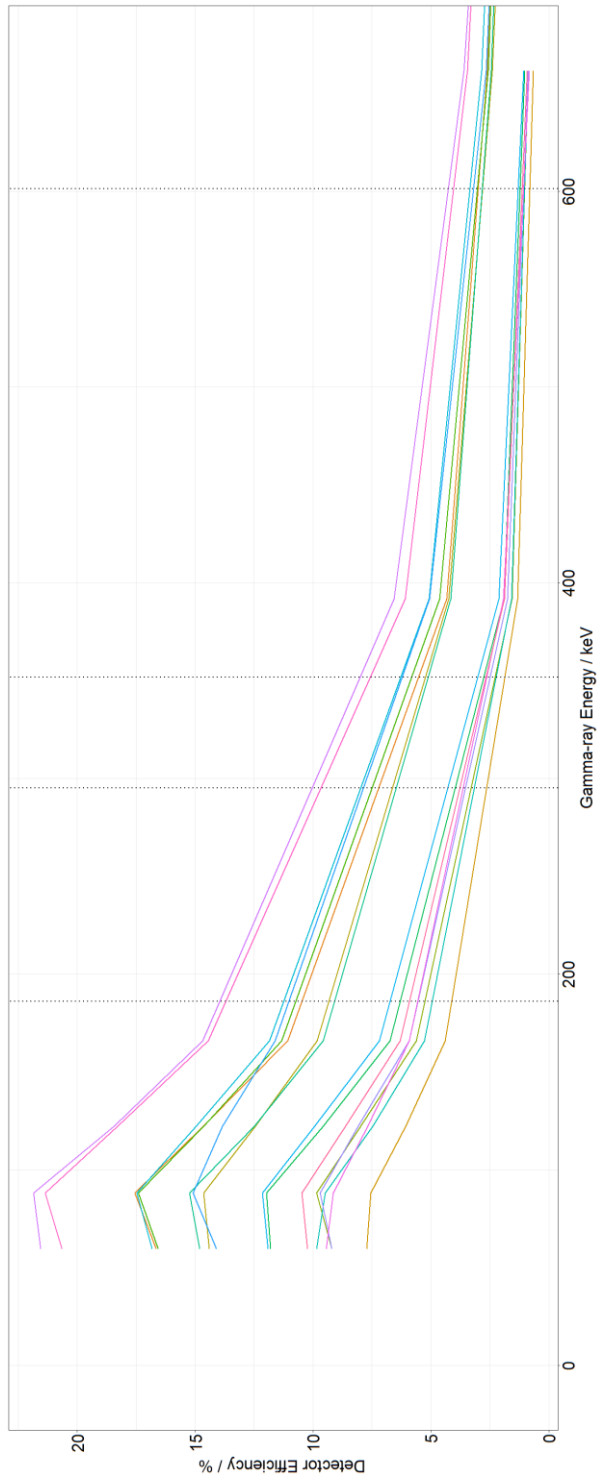


Figure 12 Fitted efficiencies for all standards. Vertical lines indicate the energies of ^{226}Ra (186.2 keV), ^{214}Pb (295.2 keV and 351.9 keV) and ^{214}Bi (609.3 keV) respectively.

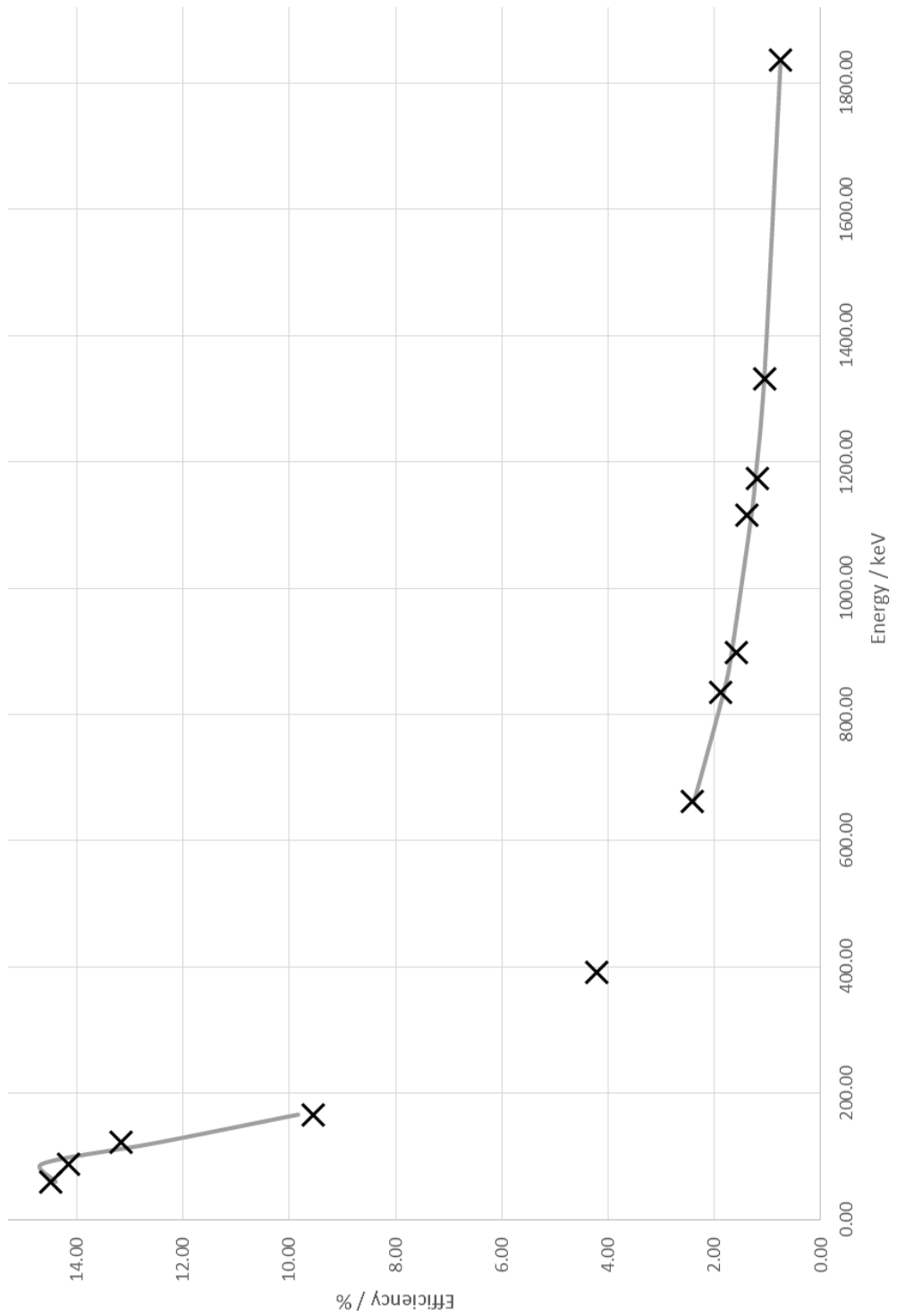


Figure 13 Comparison between the measured efficiency for each nuclide in the standard and the calculated efficiency curve for the energy range (5.4 cm, compost, MCA1).

Calibration was performed in the same manner as, and compared to, one previously carried out in the same manner (Itthipoonthanakorn 2017). Percentage changes in efficiency since the previous calibration were in the order of 1 %.

It is accepted that gamma counting efficiency is negatively correlated with sample density (Itthipoonthankorn 2017). Whilst previous calibrations of the instrument had indicated otherwise (Figure 14), the latest calibration displayed the generally accepted trend for isotopes such as ^{241}Am (59.54 keV) but not for ^{137}Cs (661.66 keV) (Figure 15). It is likely that density effects are not observed as easily in the case of high-energy gamma rays because of their ability to penetrate matter more easily, and so other factors affecting the result have a much larger impact.

In the case of the Sherwood Forest site (Section 5.6.1), a "Compost and Sand" calibration matrix was used for gamma spectra of the surface 5 cm as organic matter is >50 % (Figure 57). Organic matter content reduces with depth and so from 6 to 9 cm both "Compost and Sand" was employed. All other samples were analysed using the "Sand" calibration. For the Ex-ASGARD site (Section 4.1), all samples were analysed using the "Sand" calibration.

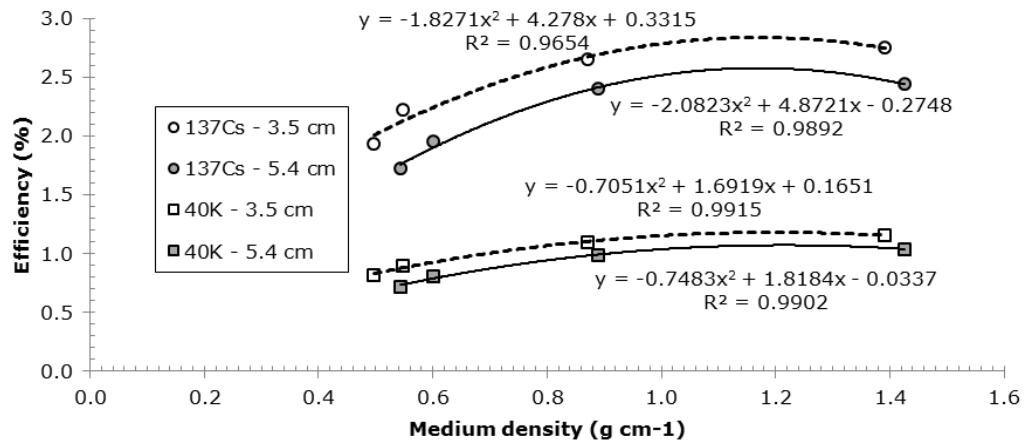


Figure 14 Relationship between density of medium and gamma counting efficiency found previously (Itthipoonthanakorn 2017).

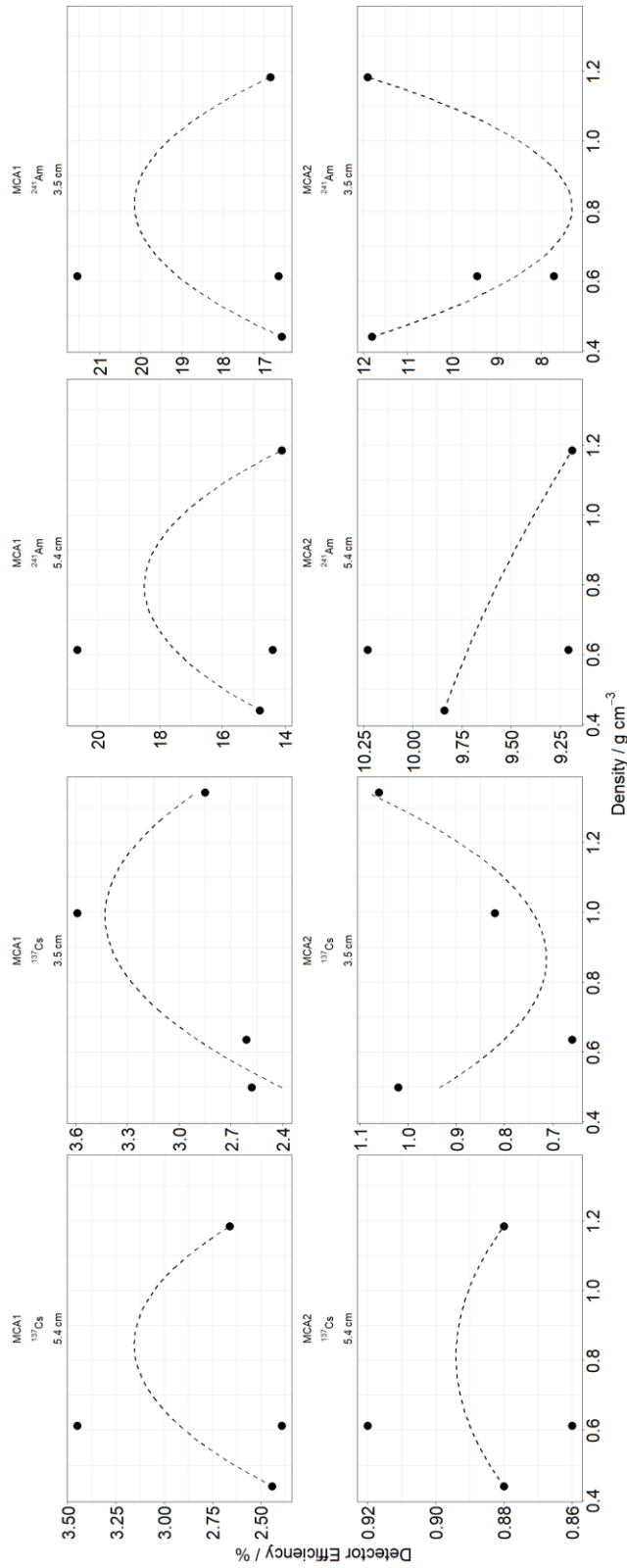


Figure 15 Density-efficiency relationships for ^{137}Cs and ^{241}Am in geometries 3.5 cm and 5.4 cm, found during the March 2017 calibration. Similar densities and few data points mean trends are not reliable.

3.3.1.5 ICP Mass Spectrometry

In order to provide a secondary estimate of ^{226}Ra activity in the soil samples, analysis of ^{238}U was undertaken by inductively coupled plasma mass spectrometry (ICP-MS) following acid digestion. The standard procedure for a hydrofluoric acid (HF) digestion was followed: 0.2 g of each soil sample were placed into a block digester tube. To each tube was added 2.0 mL HNO_3 and 1 mL HClO_4 . Blocks with tubes were heated to 80 °C for 8 hours, then 100 °C for two hours before cooling. 2.5 mL HF were added to each tube, before heating to 120 °C for 1 h, 140 °C for 3 h, and then 160 °C for 4 h. Tubes and samples were allowed to cool to 50 °C before adding 2.5 mL HNO_3 and 2.5 mL "MilliQ" ultrapure water (Merck). Tubes and samples were then maintained at 50 °C for one hour before being allowed to cool to room temperature. Each sample was then diluted to 50 mL with ultrapure water in a volumetric flask and further diluted 1:10 for analysis by ICP-MS.

3.4 Liquid characterisation of soils

One of the most important influencers of gas diffusion in soils, volumetric water content (VWC), was measured *in situ* using a PR2® probe coupled to an HH2® soil moisture meter (Delta-T Ltd., UK, delta-t.co.uk). The soil VWC probe was used in two locations, 60 cm from the sampling array on either end. At the measurement points, electrical resistivity was used to estimate soil VWC with an accuracy of $\pm 0.04 \text{ m}^3 \text{ m}^{-3}$. Volumetric water content was thus measured at six depths in the first metre of the soil profile: 10, 20, 30, 40, 60 and 100 cm. The soil VWC measurements are unidirectional, and so for each time point measurements were taken in three directions and the average taken. Intermediate distances were calculated by applying distance factors to the closest measured points.

3.5 Monitoring of meteorological conditions

Meteorological data were collected, where possible, from nearby stations. Where available, on-site COSMOS stations were utilised. COSMOS is a long-term network of soil moisture monitoring stations (cosmos.ceh.ac.uk). In the case of the University of Nottingham sites, some data were available from the University's meteorological station, with any omissions filled-in using data from the COSMOS station at Bunny Farm, 7 km away.

Data for a time point was taken as that recorded at the exact minute by the meteorological station in question.

3.6 Computational modelling of soil gas transport

Computational modelling of soil gas transport was carried out to estimate effective soil gas radon diffusion coefficients by fitting a gas diffusion model, based on a numerical solution to Fick's Second Law with variable values for D_g , to measured values of soil gas radon activity concentrations (Section 2.2). Once a solution has been approximated for a given set of parameters, it must then be compared to measured data in order to assess how appropriate those parameters are (Section 3.6.3).

Two main types of numerical methods are employed to approximate the solutions of PDEs: explicit and implicit. In "explicit" methods, each time step is solved entirely before progressing to the next. An explicit approximation divides the derivatives in (2.1) into discrete spatial and temporal units δx and δt to calculate an unknown value based on a known value close to it in space and time. Explicit methods are straightforward to implement but are not very useful for more complex environmental applications requiring high precision as they have high computational requirements. Implicit methods such as the Crank-Nicolson method (Crank and Nicolson 1947, Section 3.6.1) are more computationally efficient and enable the formulation of equations solvable for each other at numerous points in space and time simultaneously.

3.6.1 Crank-Nicolson implementation

Theoretical soil gas radon activity concentration profiles were calculated computationally using the Crank-Nicolson method. To approximate the diffusion equation, time and space were broken down into discrete units that can be visualised on a grid (Figure 16).

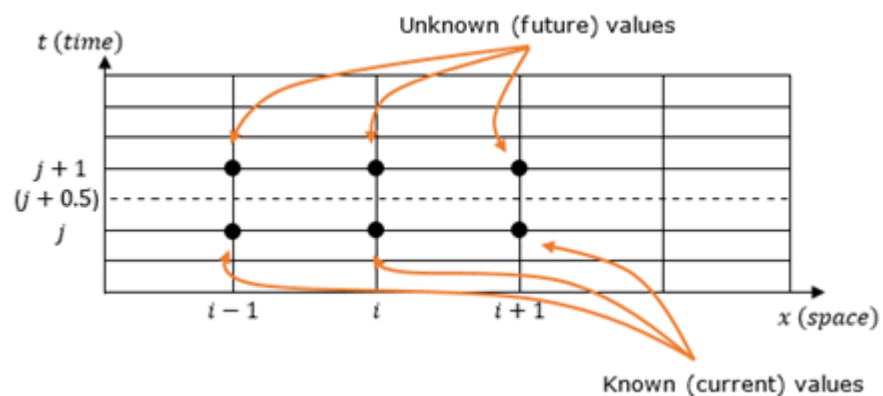


Figure 16: Representation of the Crank-Nicolson method for solving PDEs.

The Crank-Nicolson implicit method assumes that (2.1) is satisfied at the same point in space and exactly half-way between two points in time $\{i\Delta x, (j + \frac{1}{2})\Delta t\}$ (Figure 16). With the time point for satisfaction assumed, the function relating to space $\frac{d^2c}{dx^2}$ can be replaced by the mean of its finite-difference approximations at times j and $j + 1$; the diffusion equation is effectively reduced to a set of simultaneous equations for n unknown values in terms of known initial values and boundary conditions (3.7).

$$\left(\frac{\partial C}{\partial t}\right)_{i,j+\frac{1}{2}} = \left(\frac{\partial^2 C}{\partial x^2}\right)_{i,j+\frac{1}{2}} \quad (3.4)$$

From the discretised version of (2.1) the Crank-Nicolson scheme for Fick's Second Law (3.5) can be generated.

$$\frac{dC}{dt} = \frac{C_{i+1} - C_i}{\Delta x^2} = D \left(\frac{C_{j+1} - 2C_j + C_{j-1}}{\Delta x^2} \right) \quad (3.5)$$

Expanding and taking $r = D \frac{\Delta t}{\Delta x^2}$ yields (3.6):

$$\begin{aligned} -rC_{i+1,j+1} + (2 + 2r)C_{i,j+1} - rC_{i-1,j+1} \\ = rC_{i-1,j} + (2 - 2r)C_{i,j} + rC_{i+1,j} \end{aligned} \quad (3.6)$$

-where i is position in time and j is position along a 1-dimensional axis where. Introducing terms at the current timestep j for material production (i.e. radon emanation) P and material destruction λ (i.e. radioactive decay) yields the employed model (3.7):

$$\begin{aligned} -rC_{i+1,j+1} + (2 + 2r)C_{i,j+1} - rC_{i-1,j+1} \\ = rC_{i-1,j} + (2 - 2r)C_{i,j} + rC_{i+1,j} + P - \lambda \end{aligned} \quad (3.7)$$

Simultaneous equations resulting from the Crank-Nicolson method can be solved by matrix elimination (in this case Gauss-Jordan elimination) to give accurate solutions to the partial differential equation.

Time and space steps in a calculation need to be small in order to produce accurate results; explicit methods must follow $0 < \frac{\delta t}{\delta x^2} \leq 0.5$ but regarding this value the implicit methods are unconditionally stable. The numerical stability of implicit methods compared to explicit methods allows for larger time-steps to be used in calculations; saved computation time can be directed towards performing more calculations with different parameter values.

3.6.2 System size and boundary conditions

Since any model of a system must be restricted, an important topic is what happens at the spatial limits ("boundaries"). Model behaviour local to boundaries varies with the system studied (Smith, 1985). In terms of a soil gas system, boundary conditions were assumed as taking two common forms: open "Dirichlet conditions" in which the concentration of radon gas in the atmosphere is negligible in comparison to the soil, and closed "Neumann conditions" in which the concentrations of radon gas deeper in the soil mean that there is zero movement of gas downwards. Incorporation of an open boundary into (3.7) was achieved by forcing all points beyond the specified grid (Figure 16) to possess a concentration of zero at every time interval; incorporation of a closed boundary was achieved by requiring a concentration equal to that at a theoretical neighbouring point beyond the boundary at every time interval, i.e. $\frac{dC}{dt} = 0$ for all j at the edge of the spatial grid.

In order to combat a transient build-up of material adjacent to the closed boundary, the modelled system was extended in order to distance the effect from the points of interest. A distance of $40dx$ was selected as it was observed to provide enough computational space to accommodate the transient behaviour.

A set of calculated soil gas radon activity concentrations at different depths in the soil result from each trial value of D_S . A comparison of the calculated and measured soil gas radon activity concentrations at different depths in the soil yields a goodness of fit measure, which then is used in determining the next value of D_S to be attempted.

3.6.3 Testing

3.6.3.1 Diffusion model

A plot was created showing the performances of a closed-form expression (**Error! Reference source not found.**), the explicit solution, and the implicit, Crank-Nicolson solution, on diffusion in a simplified system (Table 5).

Table 5 Model system setup for algorithm testing.

| <i>Characteristic</i> | Value |
|----------------------------|---|
| <i>Boundary conditions</i> | Open |
| <i>Number of nodes</i> | 9 |
| <i>Initial conditions</i> | 0.2, 0.4, 0.6, 0.8, 1.0, 0.8, 0.6, 0.4, 0.2 (symmetrical) |

The calculated concentration at point $x = 0.3$ (initial condition 0.6), between times $t = 1$ and $t = 2$, is shown in Figure 17.

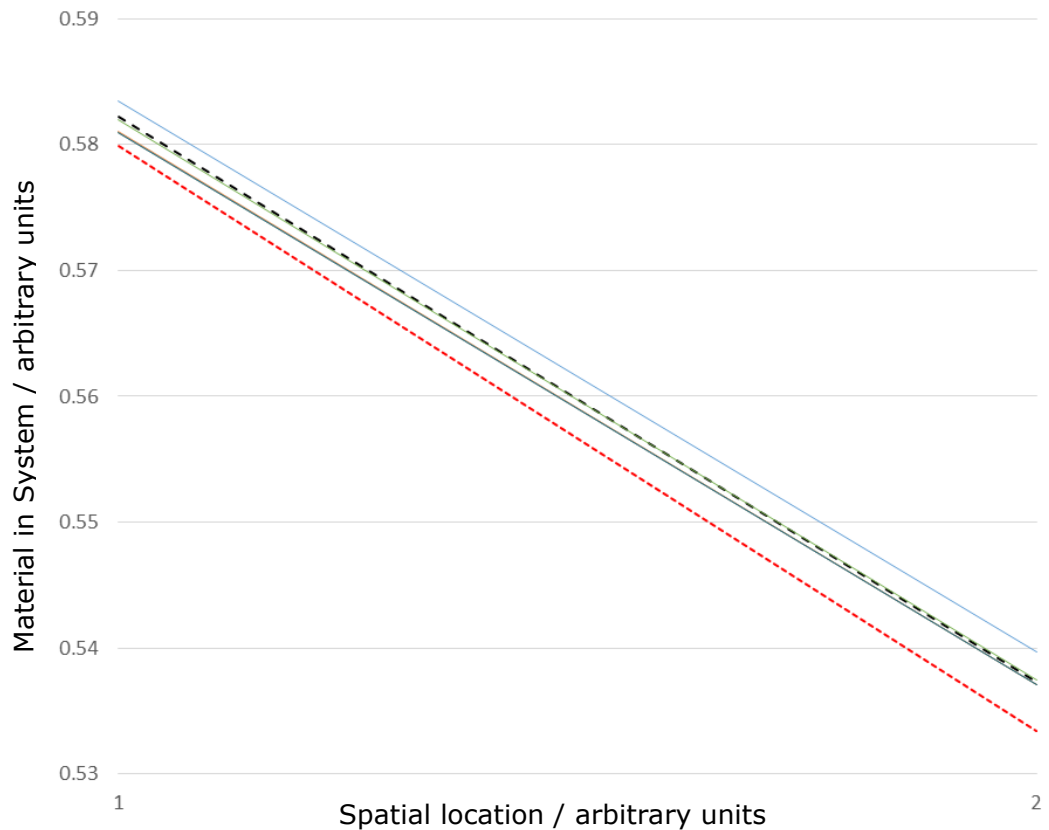


Figure 17 Solutions to simplified diffusion system (dimensionless), at $t = 1-2$. The red dotted line represents the closed-form expression, black dotted line represents explicit solution, blue, green, purple lines represent Crank-Nicolson solution with $r = 1.0, 0.5,$ and $0.1,$ respectively.

As seen in Figure 17, with $r = 1.0$ the Crank-Nicolson approximation is outperformed by the explicit solution, however, as the value of r is reduced the Crank-Nicolson calculated concentration approaches the analytical value. It is noted that calculation time increases with decreasing r -value, and suitable trade-offs are often necessitated.

3.6.3.2 Visualising calculation progress

A system proceeds to equilibrium from a user-specified initial state in a steady fashion, visualised in Figure 18.

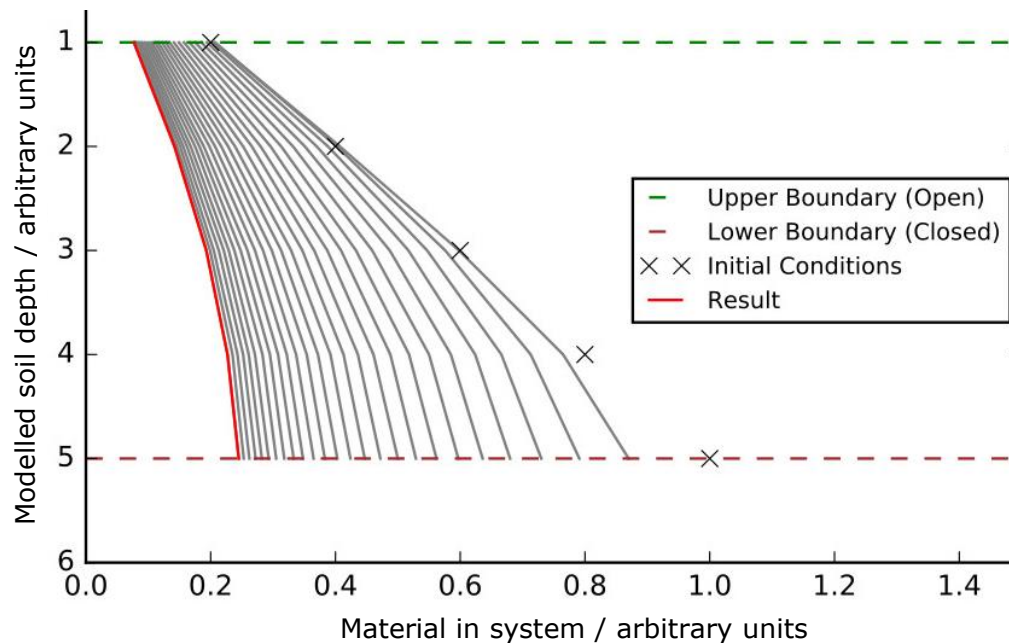


Figure 18 Graphical representation (Spyder) of calculation progression. Grey lines represent individual time-steps.

Depending on prescribed variables, solutions may possess equilibrium concentrations:

- i) Very low or zero. All material in the system has escaped through the open boundary
- ii) Within reasonable literature range for the desired system
- iii) Too high and so equilibrium higher than reasonable range, or beyond reasonable simulation time (Figure 19).

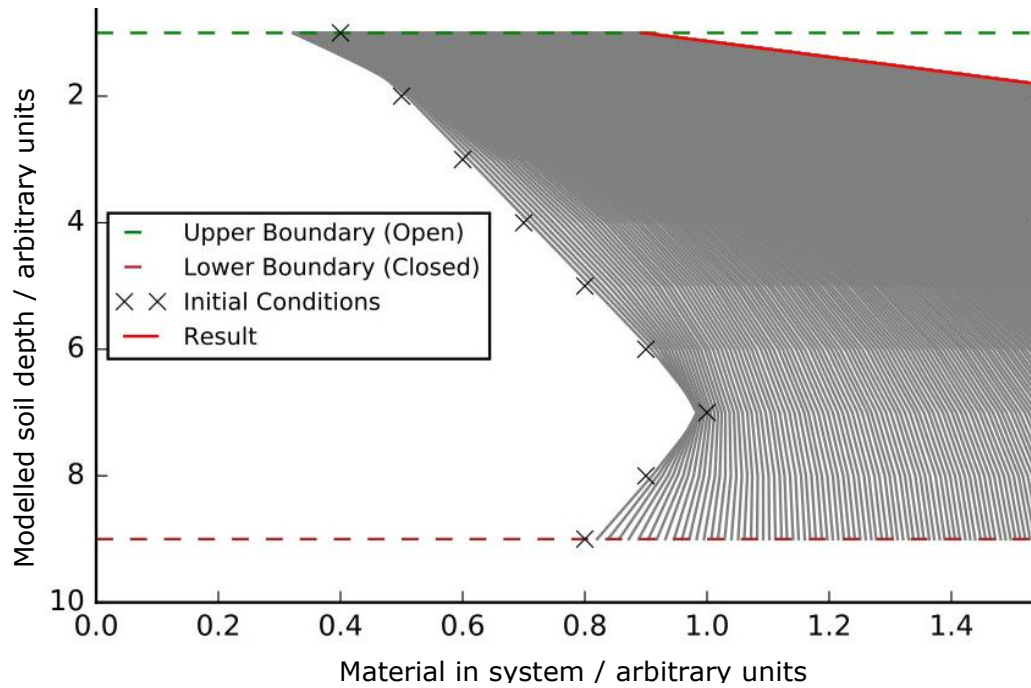


Figure 19 Example of simulation of system where equilibrium point is beyond a set range.

3.7 Initial conditions

To 'burn-in' each simulation starting from a radon activity concentration of zero each time is computationally intensive and wastes real-world time. Beginning from a larger concentration value however results in unwanted transient behaviour at the lower boundary. The overall effect of both methods is a similar increase in computation time. During a run, the initial conditions can be carried over from the result of the previous run and drastically reduce computation time.

Several variations of the initial conditions for the system were trialled on sample data and parameters, and it was found that while in certain cases, it may be beneficial to begin simulation runs from zero, the measured values or the result of the

previous calculation, had differing effects depending on the employed system; it is difficult to predict which set of initial conditions should be employed for a given setup. When differences are not inconsequential, and especially on long runs, it is likely that use of the previous calculation results is optimal as D_S values are attempted in order and so calculated results will not be far from each other in model space.

Static initial conditions are always the same distance from the measured values, but often far away from the desired points. Using the measured values brings the system closer to the desired answer but can still be far away from some values of D_S . Using the previous simulation values can be as far as or even further than zero at the start but gets progressively closer towards the end of a simulation. The use of large initial conditions has the advantage of moving towards the solution at a higher rate due to the open boundary condition employed having a greater rate of transfer than material is generated in the system, over most of model space.

Once a mesh was selected at 1 cm (0.01) intervals, initial conditions of 10^6 Bq were selected, followed by the result of the previous D_S value. Utilising the result of the previous run serves to only incur the time "penalty" of the initial "burn-in" once; D_S values being trialled in order of magnitude mean that the calculated equilibrium concentration will be close to the previous.

An initial transient steady state was observed in the system close to the lower closed boundary (Figure 20) when a static initial condition was employed. Such a steady state served to trigger the subroutine checking for equilibrium conditions, ending the calculations early; the system became trapped in a local minimum. Increasing the profile length by $40dx$ removed

the effect of the local minimum by lengthening the system, effectively moving it beyond the range which is assessed for the equilibrium condition.

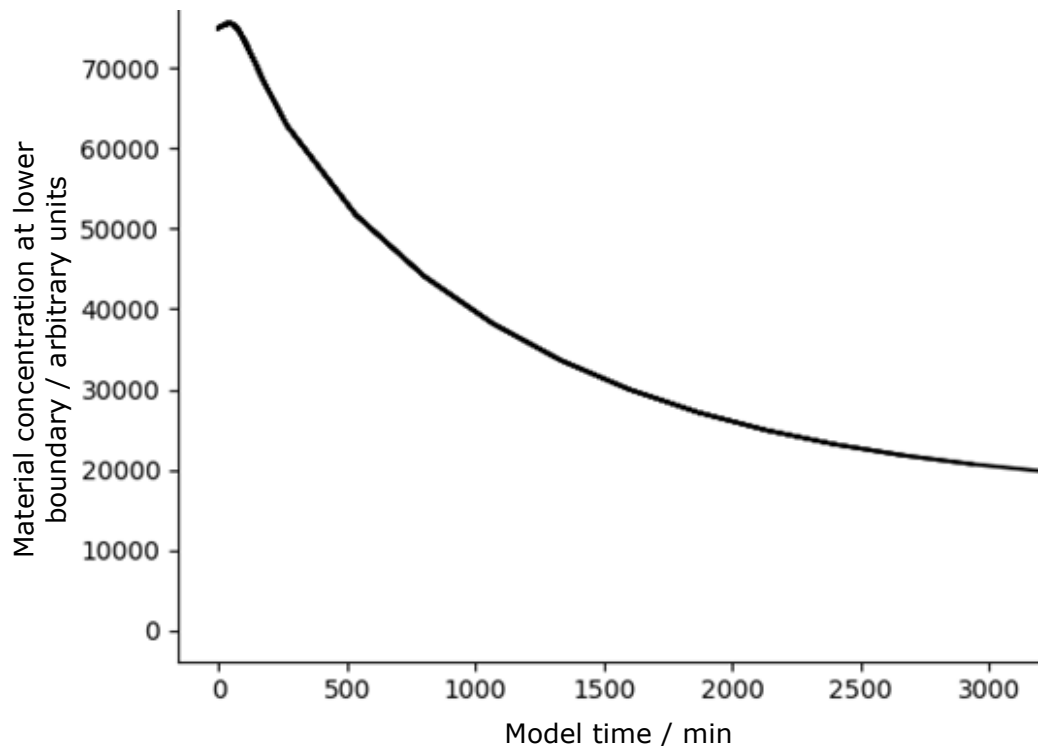


Figure 20 Initial, transient steady state of a system length 1 m, observable at low t .

3.7.1.1 Nodes and meshing

Variation of the length of the calculated mesh allows for different depths of soil to be modelled.

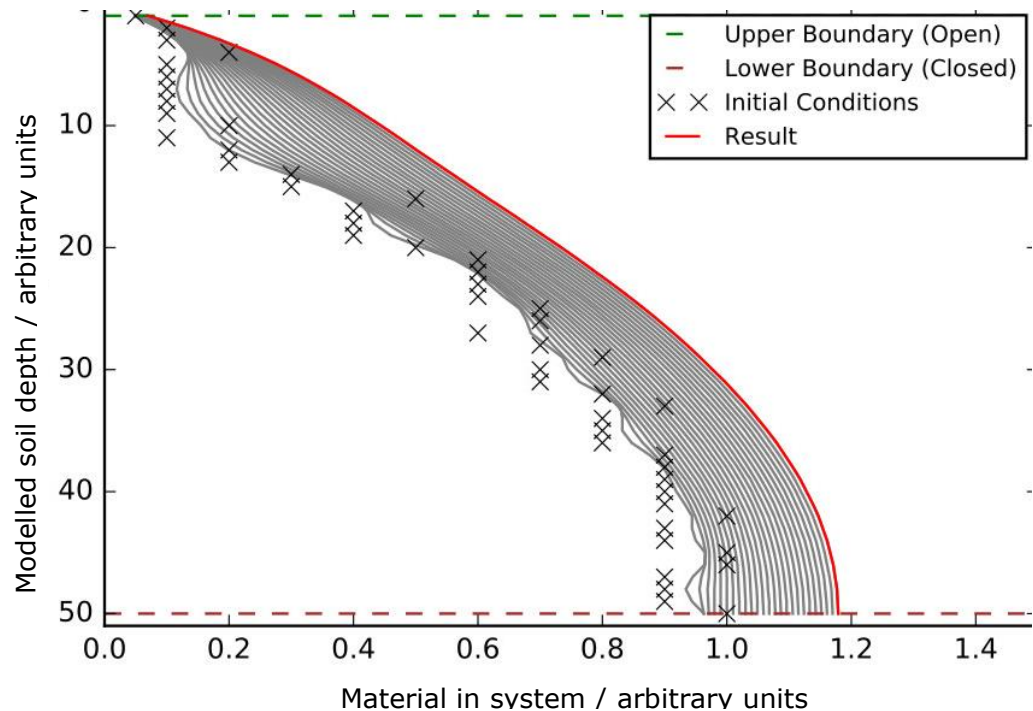


Figure 21 Simulation of a soil much deeper than previously attempted. There is no effect of initial conditions on the calculated result.

When using a finite grid based-model, diffusivity of material can be higher than intended, a phenomenon known as numerical dispersion (Crank, 1967). The employed Crank-Nicolson scheme is known to not suffer greatly from numerical dispersion (Fitzpatrick, 2006a). Nonetheless, comparisons were conducted between the employed system, and an explicit and analytical implementation of Fick's Second Law (Section 3.9).

3.8 Differences in the number of measured values

In some datasets (such as the long-term monitoring of radon activity concentrations on the ex-ASGARD site), a smaller number of measurements are taken for the depth of the profile than might be desirable, however, the representation of the modelled system that is compared with the measured values is acceptable.

3.9 Comparison with a closed-form expression

The progression of the closed-form analytical expression is indistinguishable from the explicit and Crank-Nicolson implicit solutions (Figure 22).

Expressing Fick's second law as dimensionless groups (derivation from Fitzpatrick (2006) based upon Crank (1967)):

$$\frac{C}{\left(\frac{M}{\sqrt{4\pi Dt}}\right)} = f\left(\frac{x}{\sqrt{4Dt}}\right) \quad (3.8)$$

Where C [$Bq\ m^{-3}$] is a function of M [$Bq\ m^{-3}$], x [m], and t [s].

Defining $\eta = \frac{x}{\sqrt{4Dt}}$ with constants found computationally (Fitzpatrick 2006), and evaluating (3.8) yields (3.9):

$$\frac{d}{d\eta}\left(\frac{df}{d\eta} + 2f\eta\right) = 0 \quad (3.9)$$

One solution to this is $\frac{df}{d\eta} + 2f\eta = 0$ with a solution in-turn

$f = A_0 e^{-\eta^2}$. As $M = \int_{-\infty}^{\infty} (C) dx$ so that $A_0 = M$, the solution is:

$$C(x, t) = \frac{M}{\sqrt{4\pi Dt}} e^{\left(\frac{-x^2}{4Dt}\right)} \quad (3.10)$$

Taking the specific case $M = C(t_0) = 1$ with constant D yields a specific analytical solution:

$$C(x, t) = \sqrt{\frac{t_0}{t}} e^{\left(\frac{-x^2}{4Dt}\right)} \quad (3.11)$$

–given the initial condition:

$$C(x, t_0) = e^{\left(\frac{-x^2}{4Dt_0}\right)}$$

–where $t > 0$, with spatial boundary conditions:

$$C(\pm x_0, t) = \sqrt{\frac{t_0}{t}} e^{\left(\frac{-x_0^2}{4Dt}\right)}$$

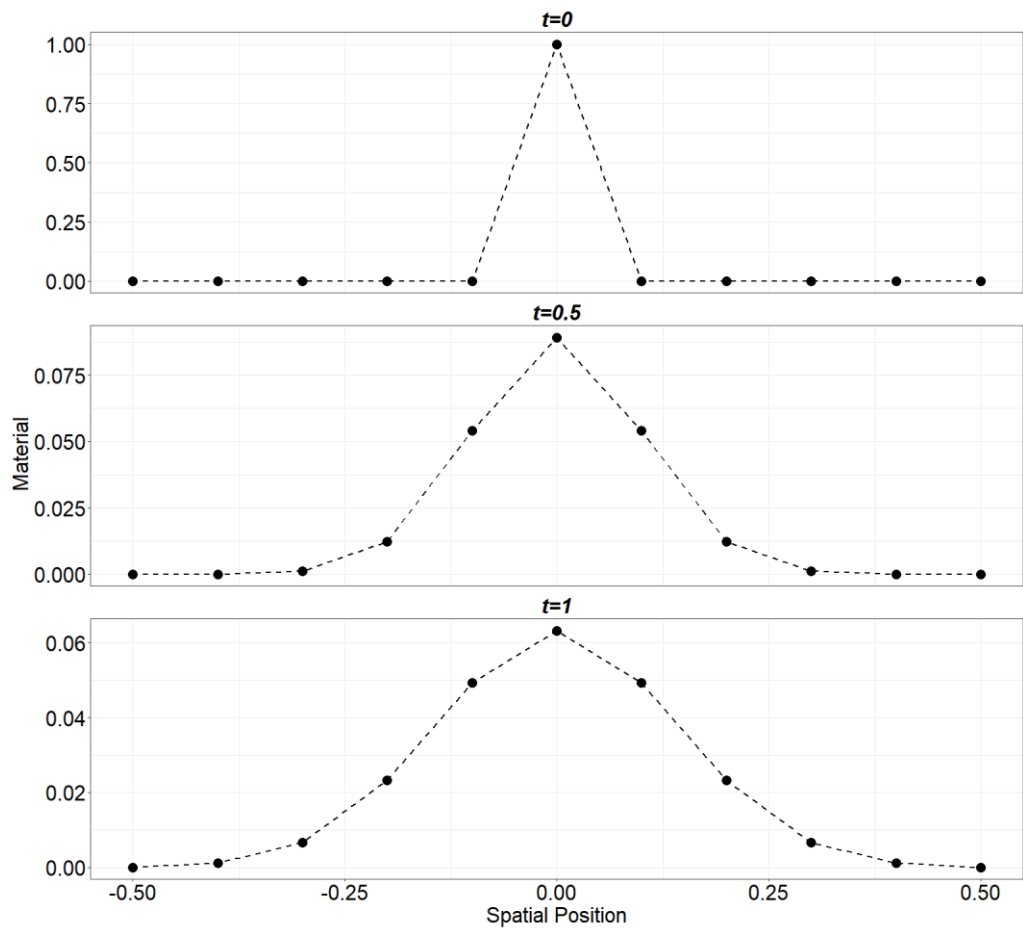


Figure 22 Graphical representation of the analytical solution (3.11) at $t = 0$, $t = 0.5$, $t = 1$. To a precision of 3 decimal places, the analytical, explicit, and Crank-Nicolson solutions are in agreement.

3.10 Parameter estimation

3.10.1 Relating space and time

The relationship between the diffusion coefficient, the space step and the time step is included within calculations as rd where $rd = \frac{D \cdot dt}{dx^2}$. The Crank-Nicolson scheme is unconditionally stable for all values of rd (Smith 1990). However, should the value of rd exceed 40, periodic oscillations occur in the system. Oscillations caused by a large rd value decay slowly with increasing t (Figure 23).

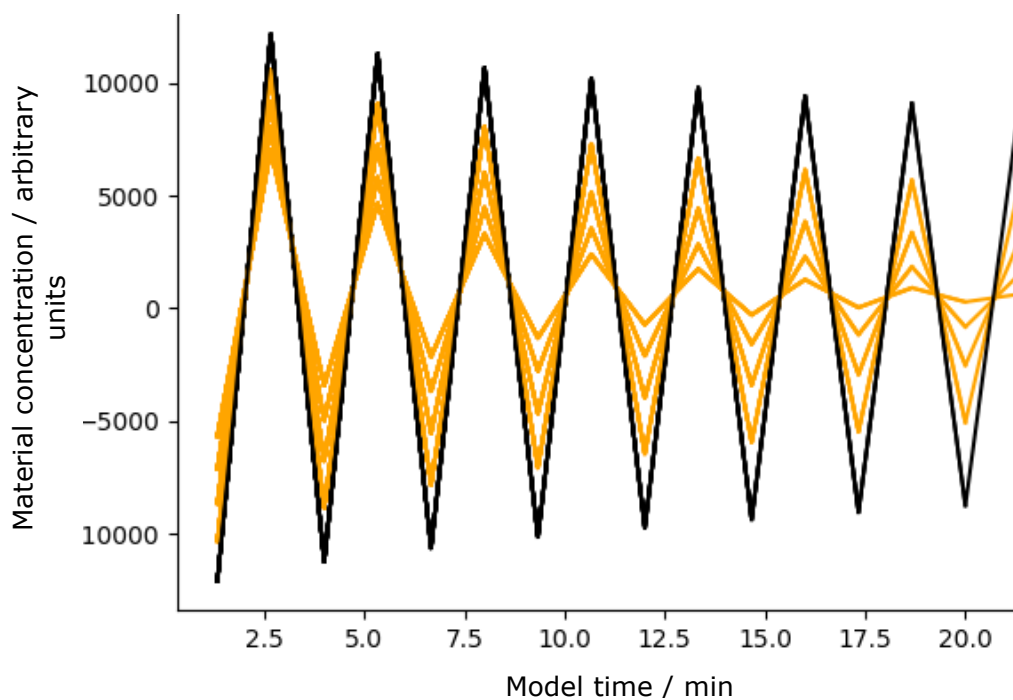


Figure 23 Examples of oscillations in the numerical solution should value of rd exceed 40. Lines represent each 10th node point (arbitrary units).

3.10.2 Source term

In order to inform the subtle shape of the soil gas concentration profile, the production of material at each spatial point is required. In order to inform the model, where possible, the radon source term calculated from soil moisture content, grain size and parent material concentration (Section 3.13.2).

3.11 System length

In order to remove the boundary effect, the modelled system was lengthened. Different relative lengths were trialled (Figure 24).

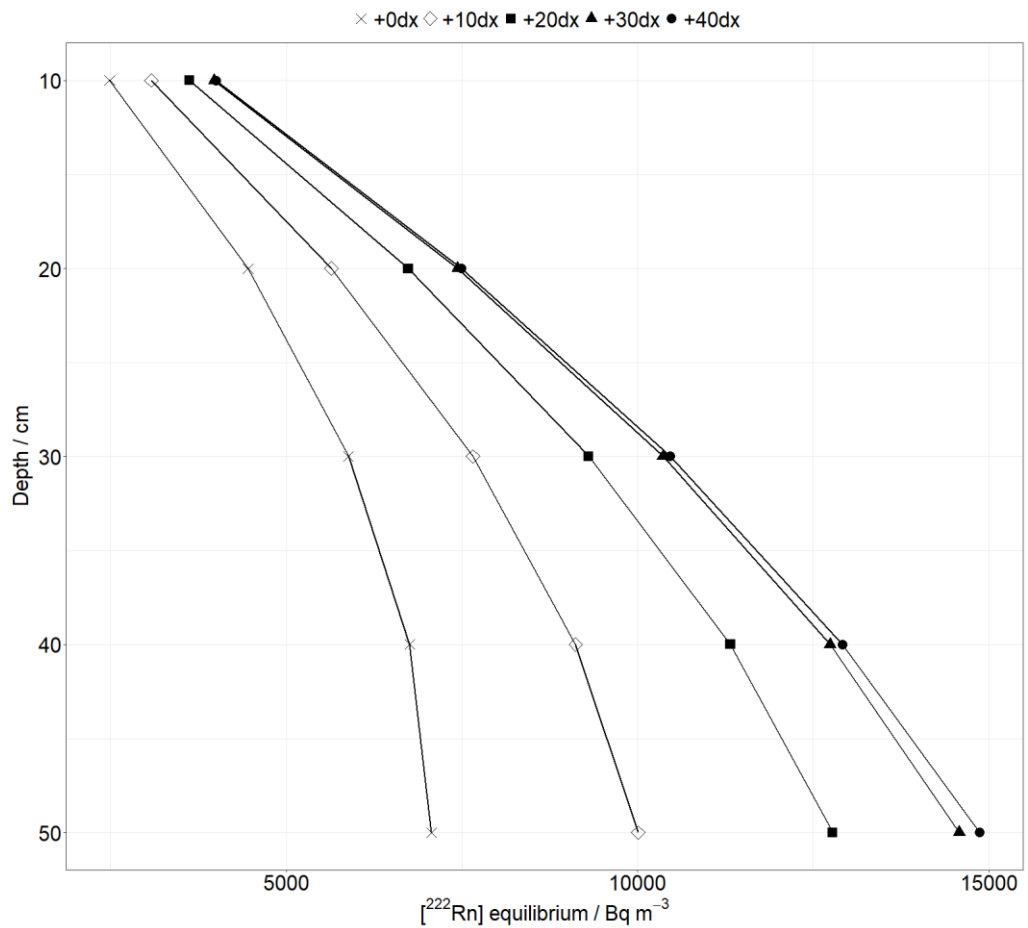


Figure 24 Lengthening the modelled system by 40dx was selected as a trade-off between proximity to equilibrium (asymptotic) and increased computational time.

It was found that a lengthening by 40dx is suitable for allowing the system to reach an accurate equilibrium concentration. The additional calculated values are removed prior to comparison with measured values.

3.12 D_S value selection: grid search

A linear range of values for the diffusion coefficient results in an uneven search of model space regarding the equilibrium concentration values, as these are mathematically related to the value $r = \frac{dt}{dx^2}$. A search was employed utilising a geometric progression of D_S values as it produces a more evenly-spaced grid in model space over which to search (Figure 25). In order to avoid preferentially selecting higher values of D_S (the profiles with lower concentrations), a new grid is regularly generated between the values with lowest residual values to the measured data.

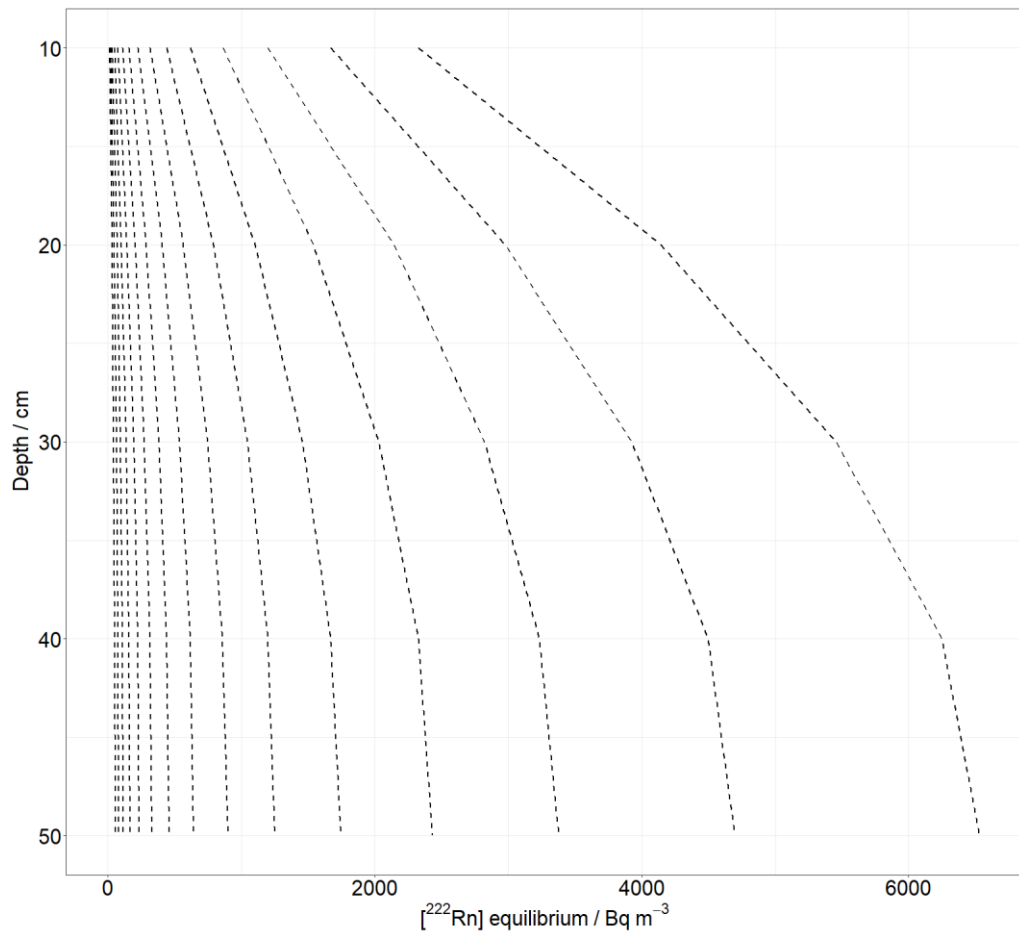


Figure 25 Illustration of the D_S grid search. When residuals begin to increase, a new grid is generated between the previous best values.

3.13 Temporal variability of D_S (ex-ASGARD site)

The permanent sampling array generates six data points which are not evenly distributed in space, and so a customised subroutine in the fitting algorithm $RSS()$ is employed. Samplers at the ex-ASGARD site are in closer proximity towards the surface of the soil and serve to better resolve the upper sections of the profile where changes in soil gas radon activity concentration vary at a much greater rate with depth.

3.13.1 Assessing fit of model to the data

The goodness of fit of a modelled activity concentration profile to the data was calculated as the r^2 using the residual sums of squares of the model to the data as per (3.14). In cases of data with known error component, errors can be weighted accordingly (3.15).

$$SS_{residual} = \sum_1^n (obs_i - mod_i)^2 \quad (3.12)$$

$$SS_{total} = \sum_1^n (obs_i - \overline{obs_i})^2 \quad (3.13)$$

$$r^2 = 1 - \frac{SS_{residual}}{SS_{total}} \quad (3.14)$$

*Formulae for sums of squares and coefficient of determination (r^2) values where **obs** is observed (field) value and **mod** is calculated value.*

$$RSS_W = \sum_1^n \left(\frac{obs_i - mod_i}{SE_i} \right)^2 \quad (3.15)$$

Weighted residual sums of squares. Values with smaller error have a greater 'weight' in the fitting process.

The use of r^2 over the residual sums of squares alone is desired as the division by total sums of squares (3.15) serves to normalise the calculated values. Despite normalisation, comparison between goodness of fit statistics is still only reliable

between profiles of the same number of measured values, and only alongside careful analysis of the plotted results.

Soil gas radon activity concentration profiles display large heteroscedasticity, i.e. there is a larger number of data points from shallower depths than from deeper in the soil, and the shallower samples with a lower activity will have a larger error due to the proportional relationship between counting errors and the number of counts. The over-population of shallower depth data yields several “shallow” profiles; weighting the sums of squared residuals would result in preferentially fitting points towards the top of the profile (soil surface) where the measurement errors are smallest. Since profiles tend to zero at the surface there is a risk of over-fitting to measured values from the uppermost layers in the soil. Smaller numbers of measured values will result in a less certain fit to the data, as statistical power is reduced, and so profiles of different sizes are assessed differently.

A grid search was employed in the developed model (Section 3.13.3) to vary the value of D_S to minimise residual sums of squares given the measured parameters. Several possible values for D_S need to be attempted in order to compare separate measurement points, be the difference spatial or temporal in nature. Simulations can be limited to a set number of subdivisions of n possible D_S values where $n \geq 6$. For fitting profiles in the current research, six possible D_S values were employed in each subdivision ($n = 6$), and calculation was continued until D_S was static to a precision of 3 significant figures.

3.13.2 Radon source term

For fitting to a measured profile, parameters must be estimated including the source term for radon generation (Section 2.3.1.2). Radon generation per time step can be determined by (3.16).

$$A_{Rn} = A_{Ra} * E * \lambda * \rho \quad (3.16)$$

Radon activity generated per unit time is a function of the ^{226}Ra content of the soil within the layer A_{Ra} [Bq kg^{-1}], radon gas emanation factor E , decay constant for radon λ [s^{-1}], layer soil bulk density ρ [g cm^{-3}].

Current understanding of ^{222}Rn emanation is poor. The ^{222}Rn emanation factor E can be affected by many factors not limited to soil grain radium activity concentration and distribution, soil moisture content (with which radon emanation factor can vary by factors of two to six according to Asher-Bolinder et al., 1990) and soil particle size (Chitra et al., 2018; Shiroma et al., 2015; Sakoda et al., 2010). Radon emanation factor has been predicted both to increase (Sakoda et al., 2010) and decrease (Markkanen and Arvela, 1992) with increasing soil particle size, and so E was taken as 0.1 for the dry soil at all temperatures (Chitra et al., 2018). It is necessary to include soil moisture content in the modelled system as it plays such a large role in radon emanation from soil grains (Section 2.3.1.2). Variation of radon emanation based upon soil volumetric water content was calculated using (3.17) (Zhuo et al., 2006). The relationship

between volumetric water content and soil radon emanation coefficient is displayed in Figure 26.

$$E = E_0[1 + k_1(1 - e^{-k_2 m})] \quad (3.17)$$

Radon emanation coefficient from moist soils E where E_0 is radon emanation coefficient for dry soil and m is soil volumetric water content. Value k_1 is 1.85, 1.73, 1.53 and k_2 is 18.8, 20.5, 21.8 for clays, silts, sands respectively.

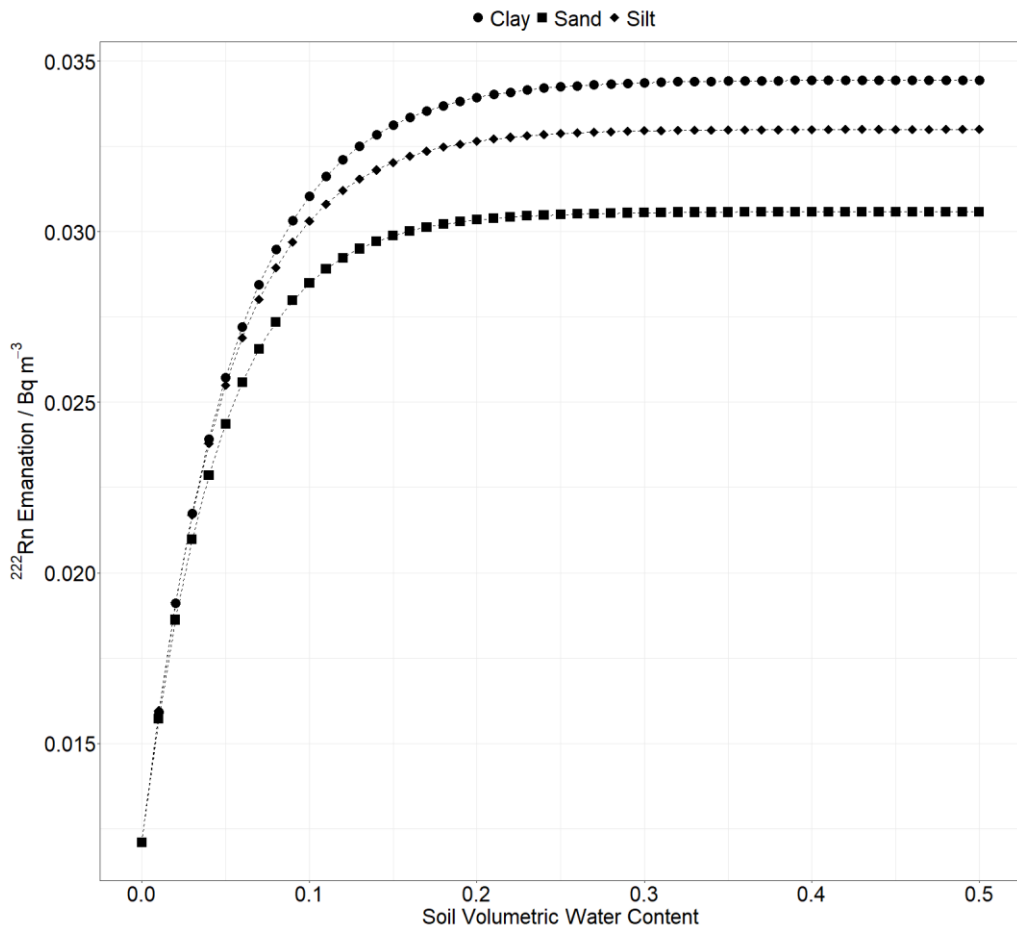


Figure 26: The relationship between soil volumetric water content and radon emanation coefficient as given by **Error!** Reference source not found..

3.13.2.1 Radon emanation calculations

Based upon radon emanation theory (Section 2.3.1.2), (3.16), and (3.17), radon emanation from University of Nottingham soil was estimated taking $E_0 = 0.1$, a value within literature ranges (Nguyen et al., 2018; Chitra et al., 2018):

Dry bulk density (Section 3.3) varies from 1.05 to 1.64 kg m⁻³, averaging 1.34 g cm⁻³;

²²⁶Ra activity concentration (Section 3.3.1) varies from 18.8 to 22.7 Bq kg⁻¹, averaging 20.8 Bq kg⁻¹;

The decay constant for ²²²Rn is 2.1 × 10⁻⁶ s⁻¹;

Soil volumetric water content is 8.8 % and soil textural makeup is 78 % sand, 9 % silt and 3 % clay, therefore ²²²Rn emanation factor will be according to Figure 27:

$$E = 0.78E_{sand} + 0.09E_{silt} + 0.03E_{clay}$$

where

$$E_{clay} = 0.1[1 + 1.85(1 - e^{-18.8(0.088)})]$$

$$E_{silt} = 0.1[1 + 1.73(1 - e^{-20.5(0.088)})]$$

$$E_{sand} = 0.1[1 + 1.53(1 - e^{-21.8(0.088)})]$$

Figure 27: Calculation of radon emanation factor for a specific soil under specific conditions.

Factoring the radium activity concentration (Bq kg^{-1}), dry bulk density (kg m^{-3}) and decay constant (s^{-1}) yields a “raw” radon production value for the soil ($\text{Bq m}^{-3} \text{ s}^{-1}$). Factoring of the emanation factor provides a specific radon production rate for the pore space of the specific soil under specific conditions.

If one or more parameters could not be, or were not, measured, they were estimated from similar field sites and literature-reported values. Without measured values, there is a risk that greater radon emanation in the model than in the sampled soil would lead to the fitting of a larger diffusion coefficient, and vice-versa.

Once a radon source term was estimated (Section 3.13.2.1), it was applied to the model assuming the 10 cm preceding the VWC measurement possesses the same emanation rate.

3.13.3 Model implementation

3.13.3.1 Model structure

The modelling algorithm itself draws on three custom algorithms written in Python 3.7 for this research. The algorithms comprising the model are provided in the Appendix:

Main() handles the core task of importing user-defined parameters from the *inputfile* (the time step *dt*; the space step *dx*; the lower and upper bounds for the diffusion coefficient *dstart* and *dend*; the number of values for the diffusion coefficient to model at each level *runcycle*; the number of levels; the depth of the measured profile; how many measurements have been made in the field; the sensitivity of

the algorithm to the equilibrium condition; the radon emanation rate of the soil). *Main()* generates the diffusion coefficient ranges to model and passes those forward, receiving back values relating to how well the model fits the data with those parameters, and then either returns a result or proceeds to generate more values for the diffusion coefficient, again as a user has defined.

Diff_mod() contains the core diffusion model. Taking a single diffusion coefficient as an argument, it proceeds to calculate an estimation of the equilibrium condition for the parameters specified.

RSS() is a residuals function. It takes the output from the diffusion model and compares the values with measured values imported from a comma separated values file (.csv). The subroutine returns to *main()* a value for the residual sum of squares between the measured and modelled values.

3.13.3.2 Equilibrium of modelled system

It was decided that the system can be assumed to be at equilibrium when the change at each modelled point in space is less than $2.5 \times 10^{-9} \text{ Bq s}^{-1}$, the maximum display precision of the employed software, as calculation time per set of measured values is driven overwhelmingly by the number of profiles calculated rather than the precision to which they are calculated. The time and space intervals for models can be varied to suit application and are presented where necessary.

4 Results: soil time-series (ex-ASGARD site)

In order to assess the applicability of the method for long-term installation, samplers were installed in the array described previously (Figure 7) and a time-series of data was collected from the site over approximately 18 months.

Unless otherwise stated, temporal trends are illustrated by non-parametric local regression (dashed line) with a 95 % confidence interval (shaded, for non-zero values). Concentration profiles in isolation are shown with 2σ (95%) counting errors as per Section 3.2.2.

Due to large differences in measured values, plot scales are not normalised.

4.1 Site description: ex-ASGARD

The “ex-ASGARD” site is located on the University of Nottingham Farm: 52.833369 °N, 1.250123 °W (“EA”, Figure 4). The area of interest is a grassland grazed occasionally since at least 2006, when a previous experiment (“ASGARD”) concluded (Gwosdz et al., 2016). The site slopes gently (approximately -2 %) to the NNE. Auger investigation around the perimeter of the study area revealed no obvious anthropogenic activity, corroborating previous findings (Ford, 2006).

Soil analysis corroborated previously reported results (West et al., 2009). Lithological variability increases with depth; horizonation is present in the form of an organic sandy loam “A” horizon of approximately 30 cm depth, a sandy “B” horizon from

30–80 cm depth, and a clayey sand “C” horizon beyond 80 cm depth (description based on post-sampling excavation, Figure 28).

Particle size analysis showed an average soil composition of 8.39 % clay, 14.0 % silt and 76.7 % sand (sandy loam), with gravelly river terrace deposits present at around 30–40 cm. The river terrace deposits contain significantly higher silt and clay fractions than the surrounding soil; however, the textural classification remains ‘sandy loam’. From 40–90 cm depth through the B horizon, sand content increases: the soil is a loamy sand. Into the C horizon, soil clay content increases again (Ford, 2006), typical of the underlying mudstones of the Mercia Mudstone Group.

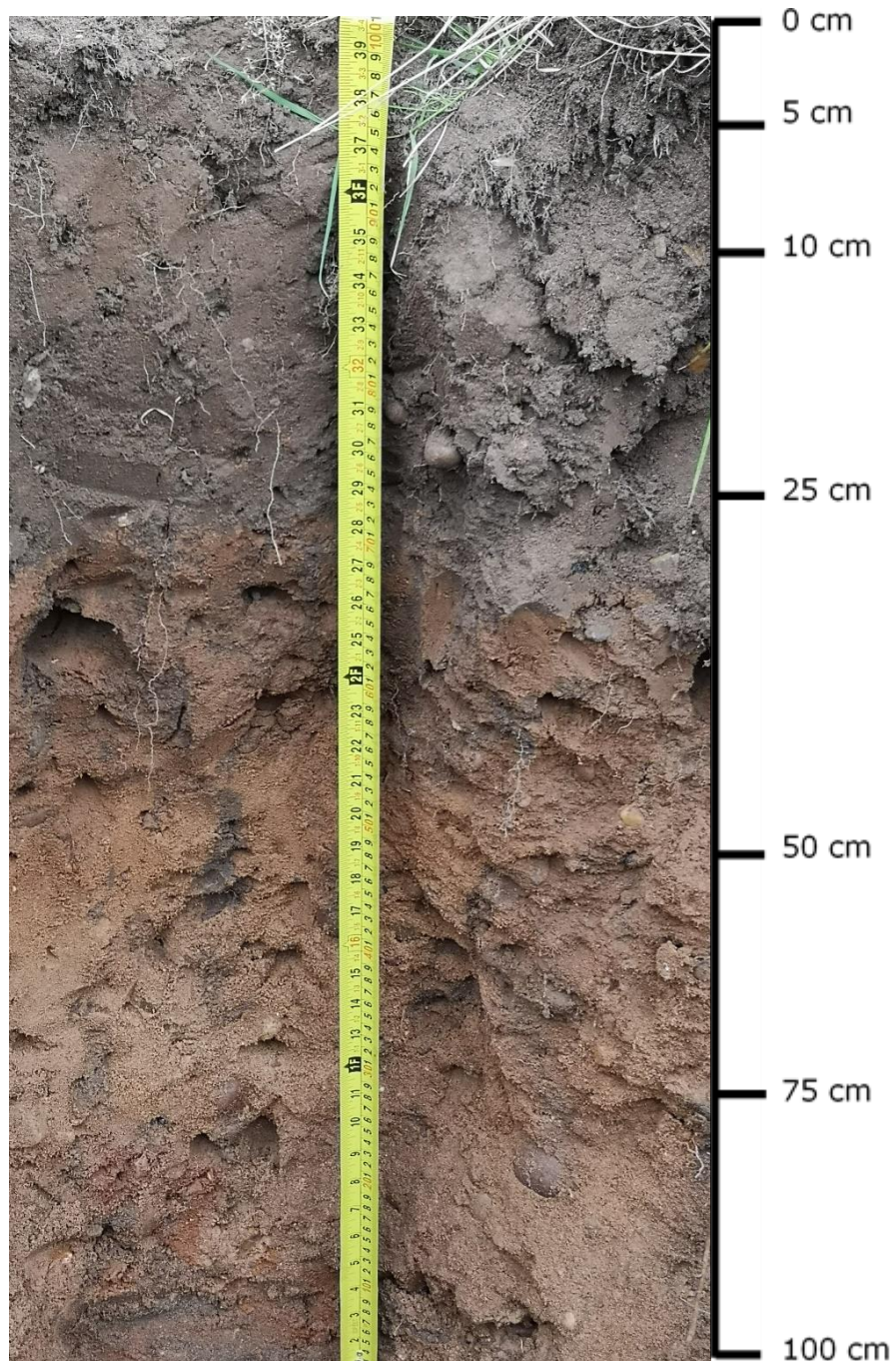


Figure 28: Soil profile of sampled area. Sites of large inclusions are evident around 40 cm depth.

All cores were the same in appearance: surface soil was dry sandy loam, progressing to a saturated sand around 50 cm depth. From 20–60 cm depth, several small gravel inclusions were present.

Table 6: Example of randomised sampling locations: six soil cores taken from the ex-ASGARD site, using the centre of the sampling array as a reference point.

| <i>Sample number</i> | <i>Bearing / °</i> | <i>Distance from sampling array / m</i> |
|----------------------|--------------------|---|
| 1 | 160 | 2.8 |
| 2 | 140 | 2.9 |
| 3 | 5 | 2.9 |
| 4 | 240 | 2.7 |
| 5 | 45 | 2.0 |
| 6 | 350 | 2.8 |

Additional soil cores were taken in July 2019 to complement the existing data (Table 7) and were used to perform soil particle size analysis. These sampling locations were recorded by GPS.

Table 7: Final three soil core sampling locations (ex-ASGARD site).

| <i>Sample number</i> | <i>N</i> | <i>W</i> |
|----------------------|-------------|------------|
| 7 | 52.833185 ° | 1.249655 ° |
| 8 | 52.833402 ° | 1.249469 ° |
| 9 | 52.833260 ° | 1.249109 ° |

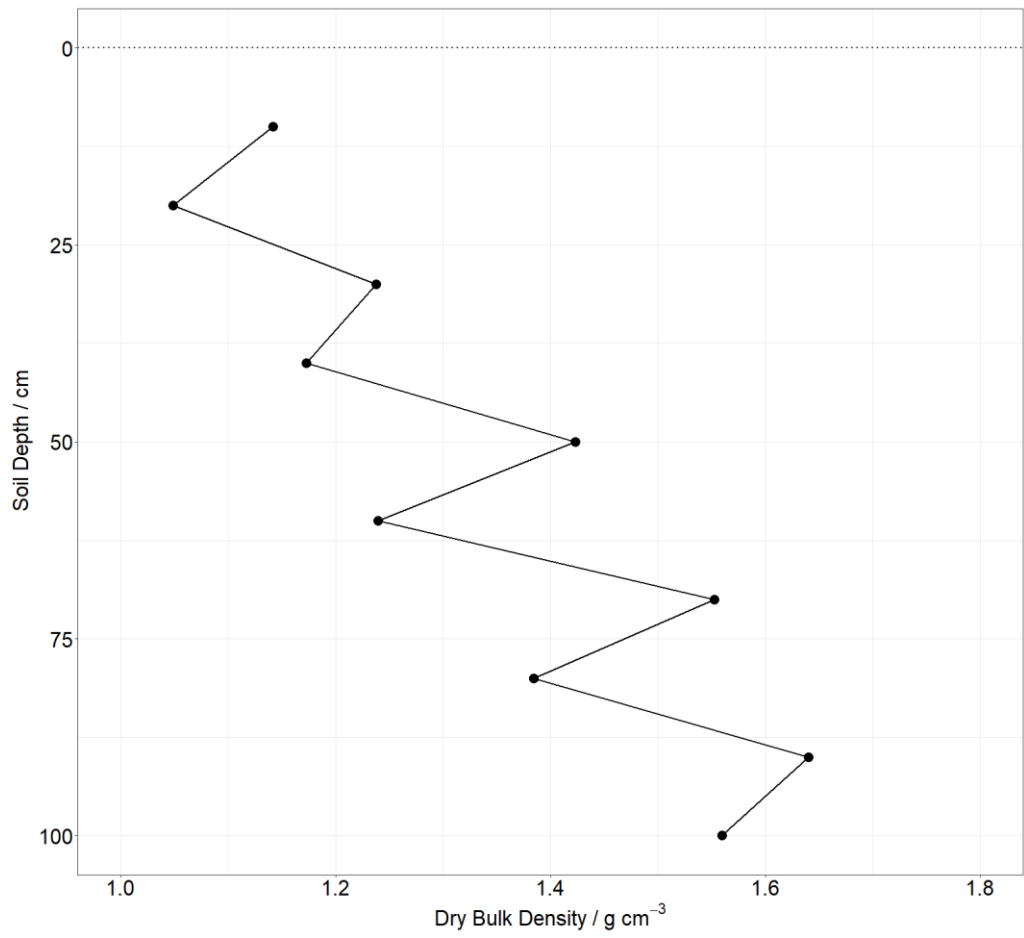


Figure 29 Results of soil bulk density analysis. Dotted line represents soil surface.

Table 8: Particle size distribution in three separate soil cores (Ex-ASGARD site).

| <i>Depth</i> <i>/ cm</i> | <i>Clay Content</i> <i>/ %</i> | <i>Silt</i> <i>Content /</i> <i>%</i> | <i>Sand</i> <i>Content /</i> <i>%</i> | <i>Total</i> <i>/ %</i> |
|-------------------------------|-----------------------------------|---|---|----------------------------|
| 10 | 11.2 | 17.8 | 70.6 | 99.7 |
| 20 | 11.4 | 18.6 | 69.4 | 99.3 |
| 30 | 12.4 | 20.3 | 63.4 | 96.1 |
| 40 | 8.9 | 15.8 | 73.6 | 98.2 |
| 50 | 8.2 | 15.4 | 75.4 | 99.0 |
| 60 | 7.1 | 12.4 | 80.0 | 99.6 |
| 70 | 7.5 | 12.7 | 79.4 | 99.6 |
| 80 | 7.6 | 12.2 | 79.3 | 99.1 |
| 90 | 7.4 | 12.1 | 79.5 | 99.1 |
| 100 | 7.5 | 12.1 | 79.8 | 99.4 |
| 110 | 6.0 | 10.0 | 83.6 | 99.7 |
| 120 | 5.3 | 8.1 | 86.3 | 99.7 |
| <i>Site</i> <i>Average</i> | 8.4 | 14.0 | 76.7 | 99.0 |

Soil penetration resistance was measured on two dates, once during the drought period (July 2018) and once again during a relatively wetter period (May 2019) (Table 9, Figure 30). The relationships between soil penetration resistance and both soil bulk density and soil gas radon activity concentration were made by calculating the mean soil penetration resistance for 10 cm sections of the profile. No significant correlation was found between soil penetration resistance and either soil bulk density or soil gas radon activity concentration, however, the marked

effect of changes in the soil moisture content between the two measurement times are visible in the plotted data (Figure 30).

Table 9: Soil penetration resistance measurement locations (ex-ASGARD site).

| <i>Sample Number</i> | <i>Date obtained</i> | <i>Location /° N</i> | <i>Location /° W</i> |
|----------------------|----------------------|----------------------|----------------------|
| 1 | Jul 2018 | 52.833352 | 1.250121 |
| 2 | Jul 2018 | 52.833340 | 1.250090 |
| 3 | Jul 2018 | 52.833380 | 1.250049 |
| 4 | Jul 2018 | 52.833425 | 1.250084 |
| 5 | May 2019 | 52.833345 | 1.250113 |
| 6 | May 2019 | 52.833350 | 1.250074 |
| 7 | May 2019 | 52.833380 | 1.250061 |
| 8 | May 2019 | 52.833400 | 1.250062 |
| 9 | May 2019 | 52.833405 | 1.250110 |
| 10 | May 2019 | 52.833383 | 1.250134 |

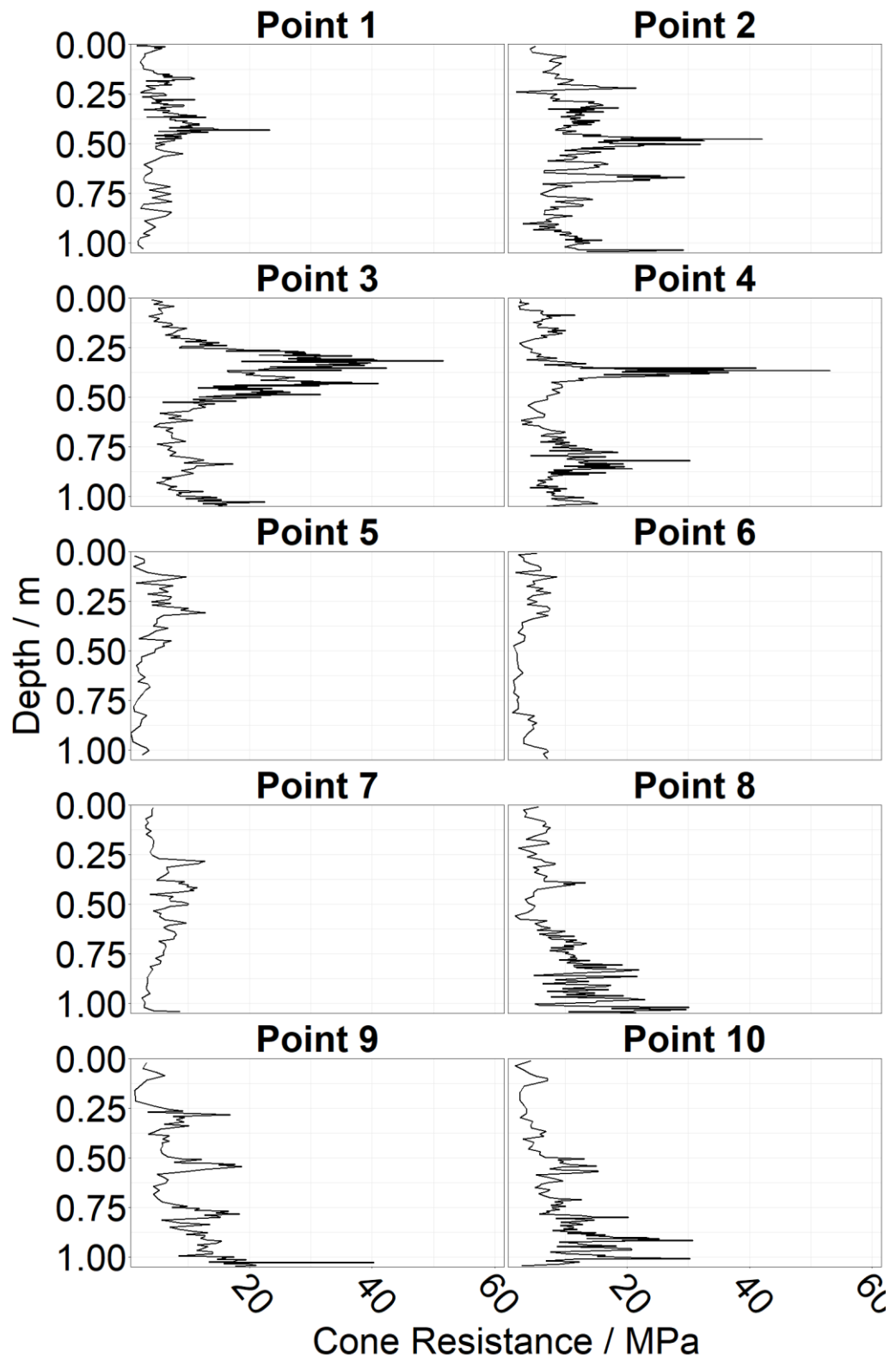


Figure 30 Soil penetration resistance for 10 locations on the ex-ASGARD site, in drought conditions (July 2018, 1-4) and non-drought conditions (May 2019, 5-10).

4.2 Subsurface soil gas recharge rate

The time taken for redistribution of soil gas post-sampling will vary according to the radon production rate and diffusion coefficient of the soil and so be largely dependent on texture. In order to test the recharge rate of a specific site, the assumption must first be made that temporal variations in subsurface radon concentration are negligible.

A single sampler was installed on the ex-ASGARD site at depth 50 cm. From the sampler an initial soil gas sample was taken by the standard method. Subsequent samples were then taken after set time periods: 1 hour, 30 minutes, 15 minutes, 10 minutes, 5 minutes. The order of sampling is necessitated as "build-up" of required recharge may occur when beginning with the smaller time steps.

When measured radon concentrations are statistically different from one another, the time gap preceding that measurement may be deemed too short for the site. The smallest time gap after which measured radon concentrations are equal will be used in future experiments as the maximum temporal resolution. For the ex-ASGARD site (Section 4.1) maximum temporal resolution was deemed to be <5 min.

The process of estimating subsurface recharge rate should be repeated in any soil in which more than one set of samples will be collected, in order to determine whether there are differences in recharge times for soils with different diffusive properties.

The total time for the experiment was ~2 h in field, with another 2 h for preparation of the final samples for LSC. The exercise was performed on 26th November 2018.

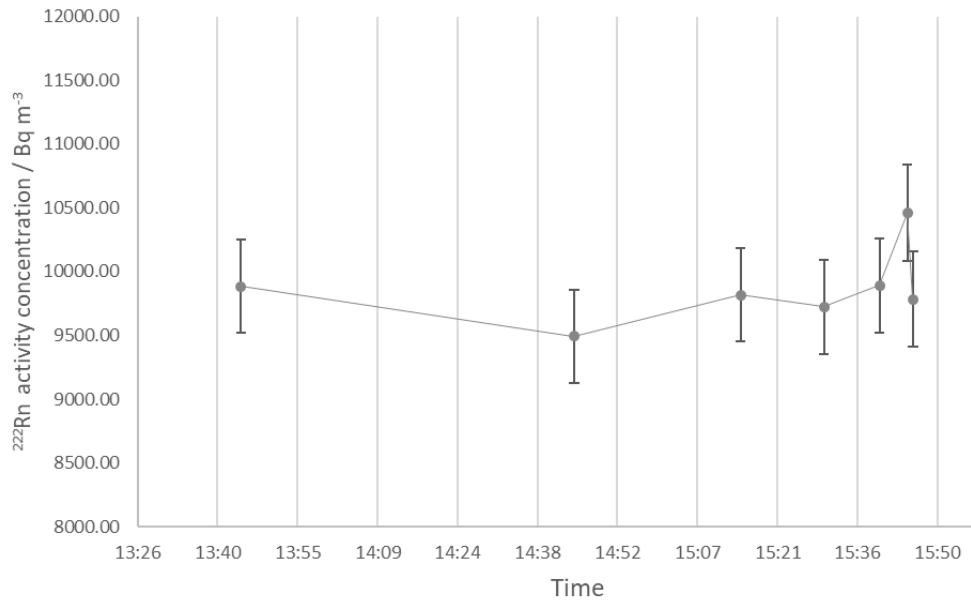


Figure 31 First sampling exercise with decreasing inter-sampling time.

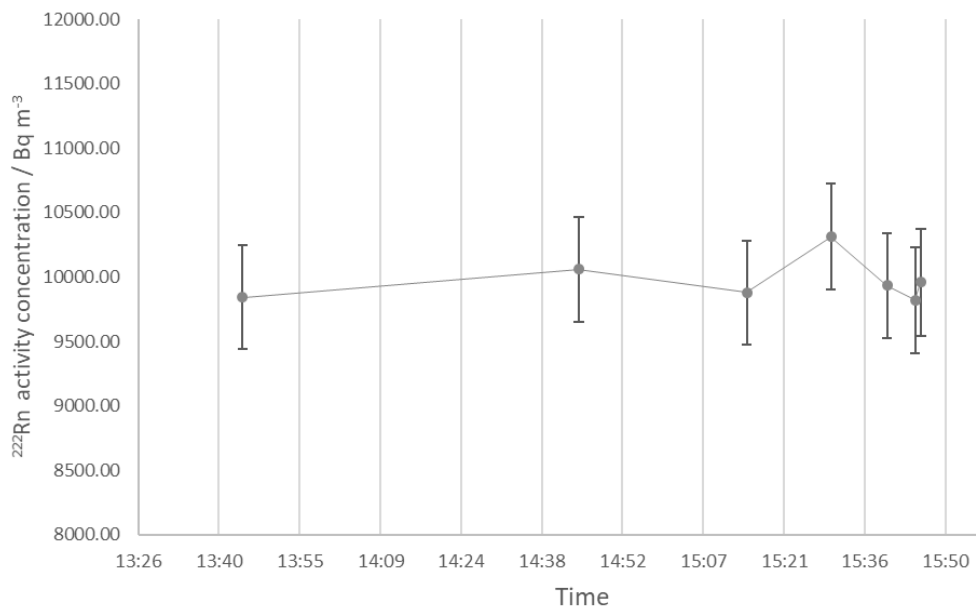


Figure 32 Second sampling exercise with decreasing inter-sampling time.

From these data the recharge rate of soil gas in relatively dry, sandy soil is extremely high. Variations are seen at ~ 1 min however these vary with recounts on the same samples (Figure 31, Figure 32).

For future exercises on the ex-ASGARD site, temporal resolution can be increased as-needed and as-possible, with the latter likely affecting any eventual decision.

The temporal resolution of the main experiments was found to be much greater than what was physically possible with manual sampling, and therefore in all field sampling efforts the belowground soil gas equilibration was assumed effectively instantaneous.

4.3 Annual variation in soil gas concentrations

4.3.1 Annual variation findings

Soil gas radon activity concentrations varied over the 18 months of the monitoring period (Figure 33): at a depth of 10 cm activity concentration varied from 776 to 5730 Bq m⁻³, or 639 %, and at a depth of 1 m activity concentration varied from 9320 to 22900 Bq m⁻³, or 146 %. Soil gas radon activity concentrations were consistently higher in winter months and lower in summer months.

Soil greenhouse gas (GHG) concentrations were also measured throughout the monitoring period (Figure 35–Figure 37). Over the course of the monitoring period concentrations of greenhouse gases varied but with little to no pattern.

The first date of gas extraction from 0.75 m depth was 17/05/2018 on which date soil moisture content of approximately 33.5 % was recorded. The first gas extraction from 1 m depth was 21/06/2018 on which date the soil moisture content was approximately 32.8 %. Tracking of the water table depth was not initially considered part of the current research but proved effective in the monitoring and quality control of the soil moisture data. As the drought of summer 2018 progressed, large changes in soil moisture content became apparent in both sampling locations (Figure 34).

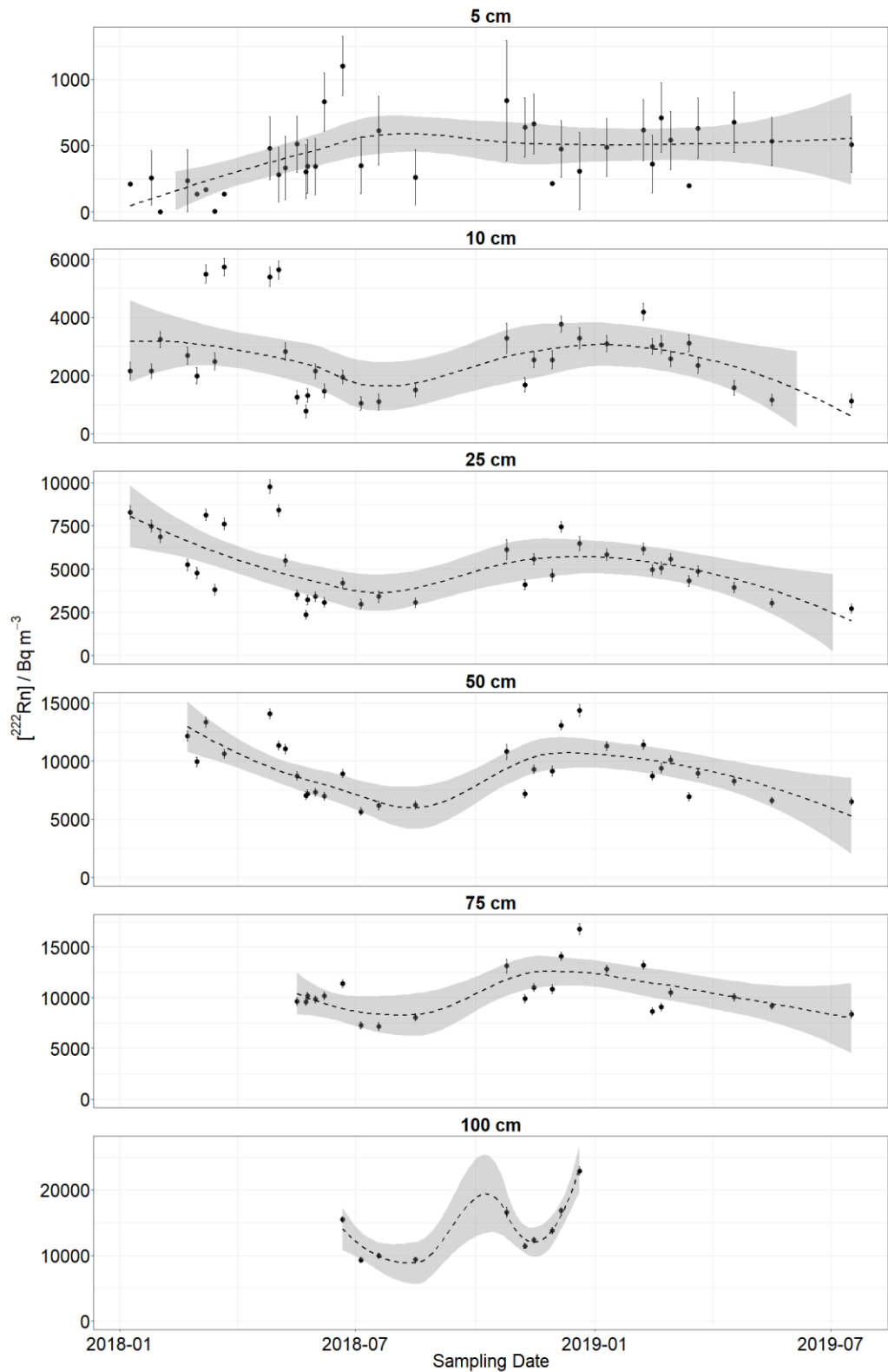


Figure 33: Long-term soil radon activity concentrations at six depths. Smaller sample sizes at depth reduce confidence in trend. Shading represents a fitted 95 % confidence interval for trend illustration.

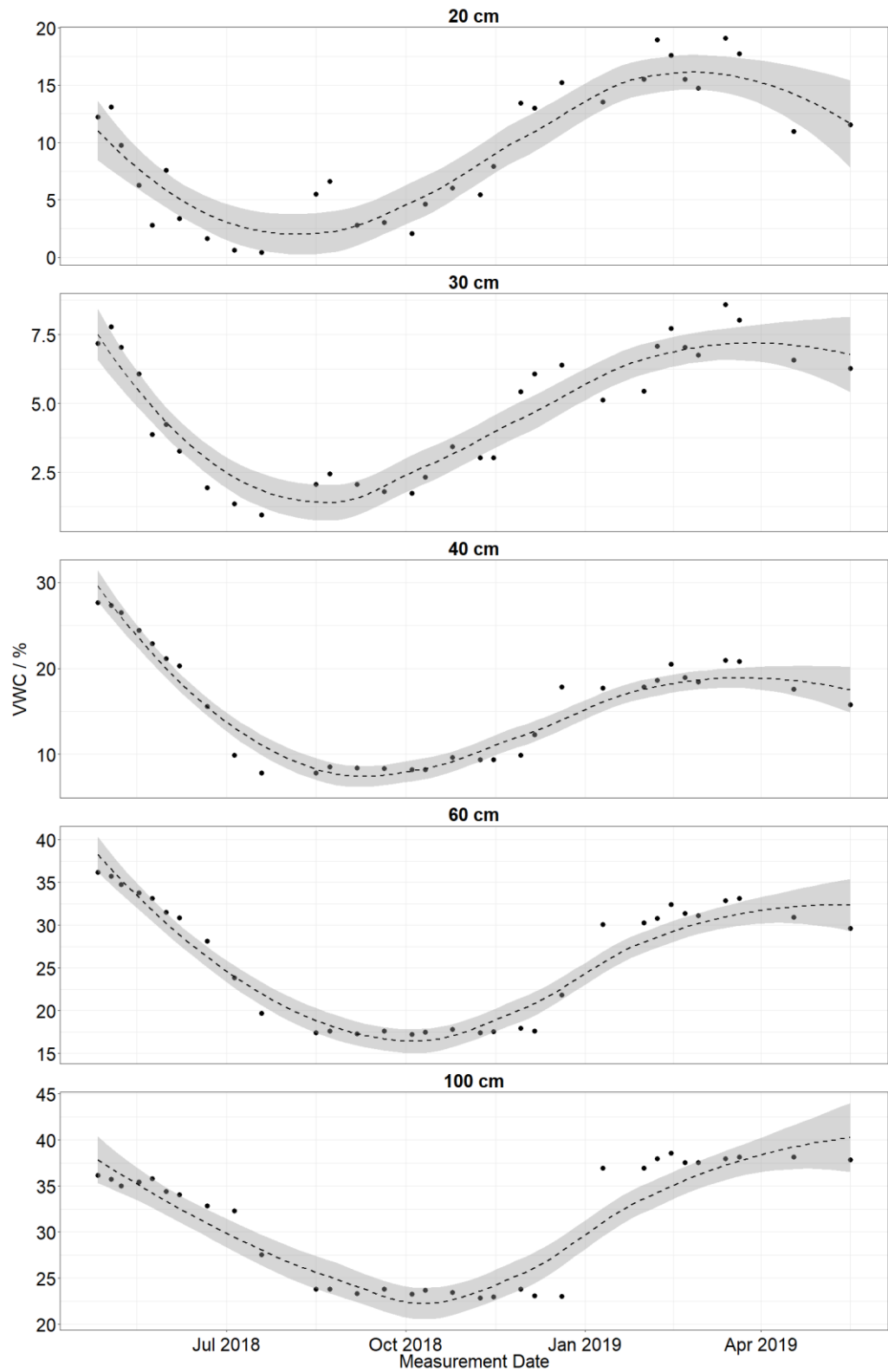


Figure 34: Long-term soil volumetric water contents at five depths. Shading represents a fitted 95 % confidence interval for trend illustration.

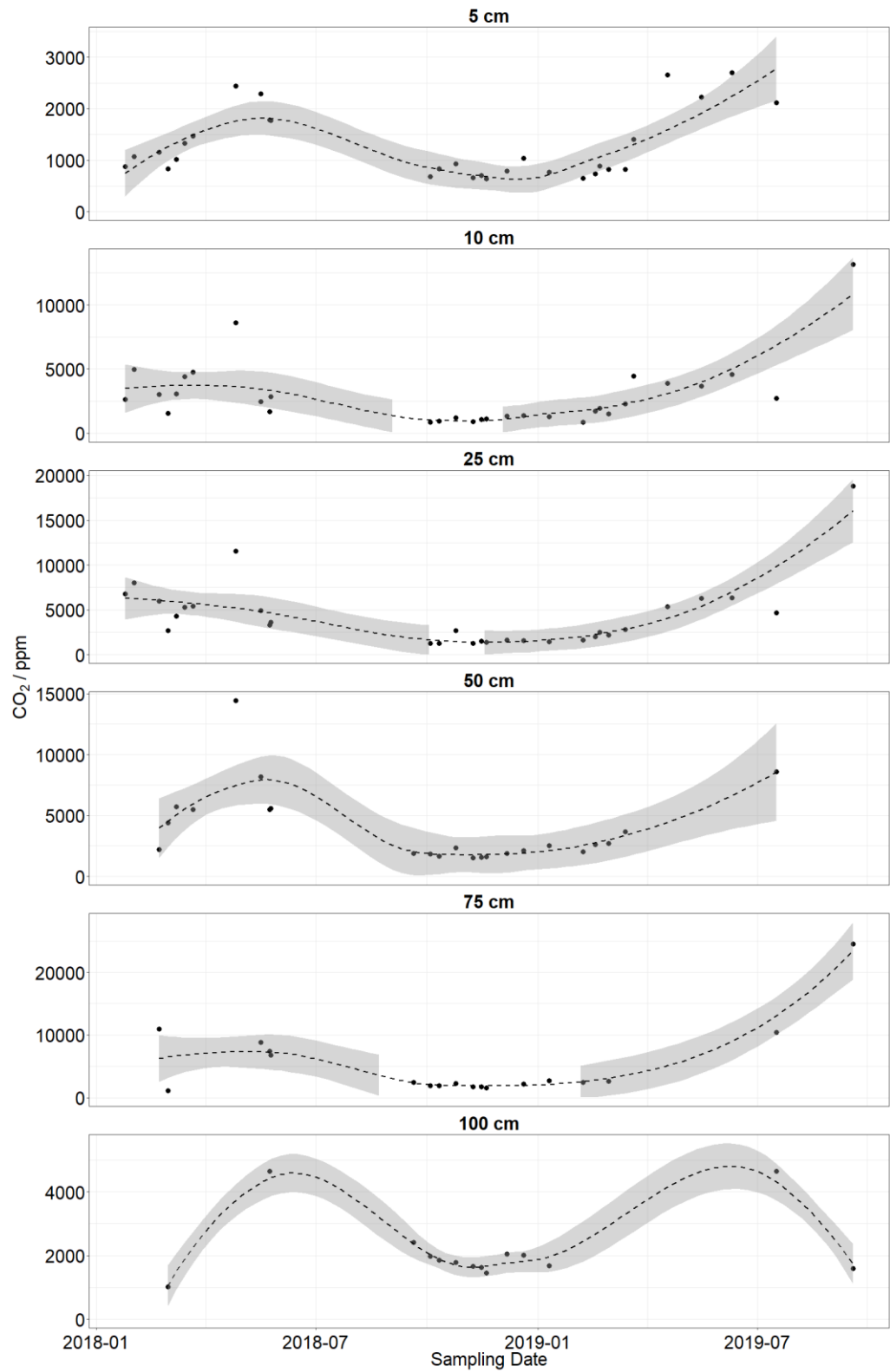


Figure 35: Long-term measurements of soil carbon dioxide concentrations at six depths. Shading represents a fitted 95 % confidence interval for trend illustration.

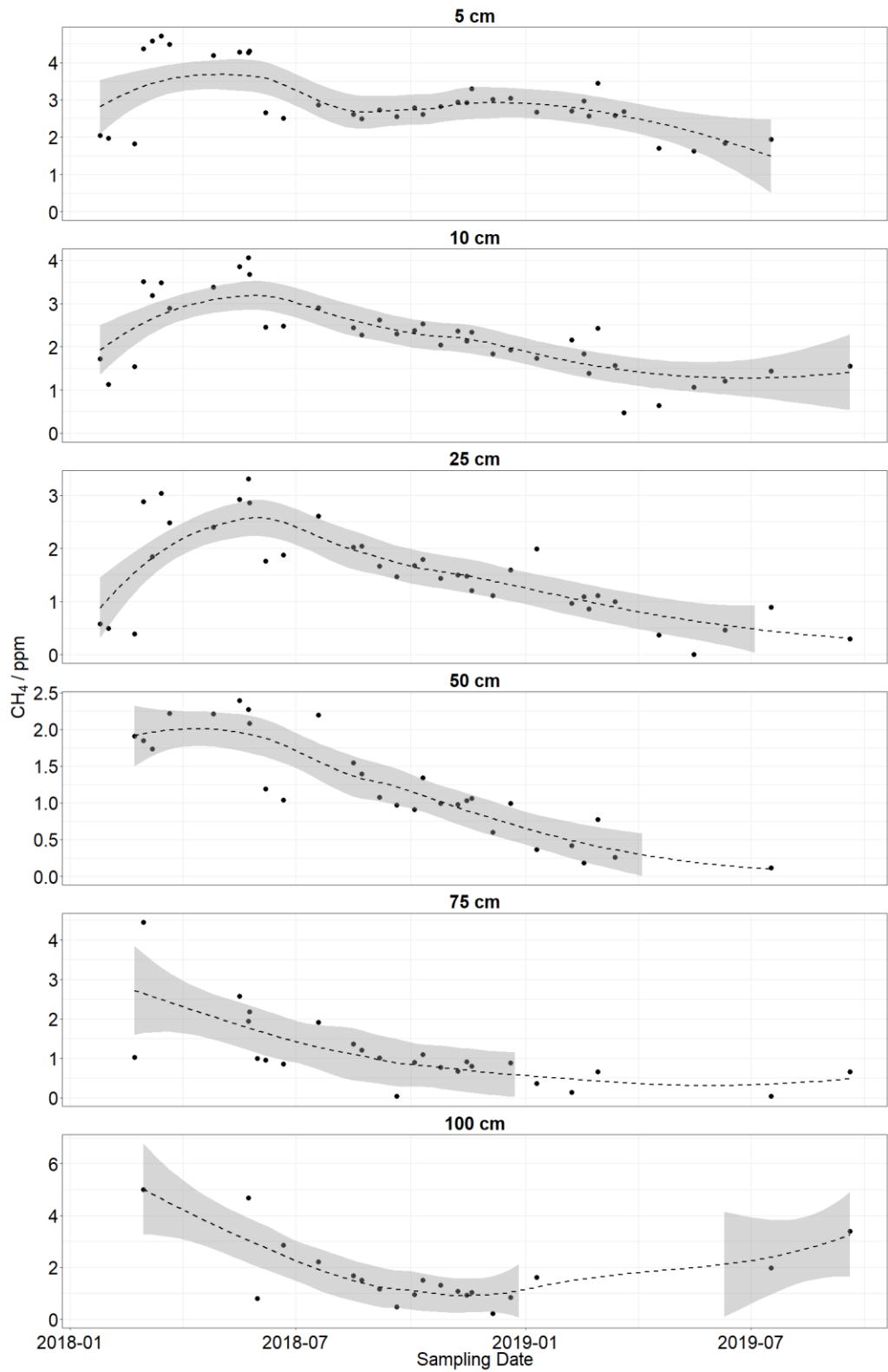


Figure 36: Long-term measurement of soil methane concentrations at six depths. Shading represents a fitted 95 % confidence interval for trend illustration.

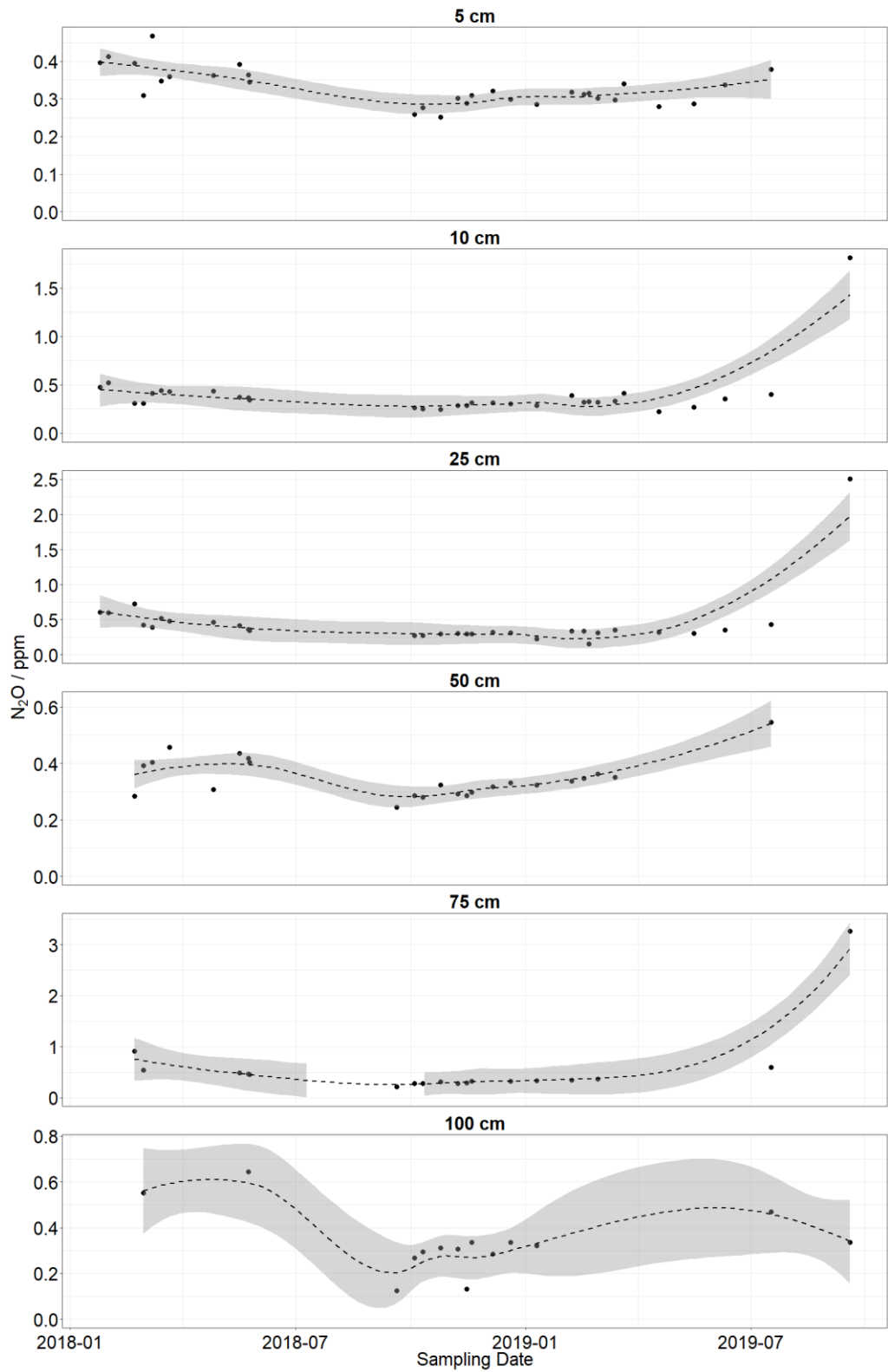


Figure 37: Long-term measurements of soil nitrous oxide concentrations at six depths. Shading represents a fitted 95 % confidence interval for trend illustration.

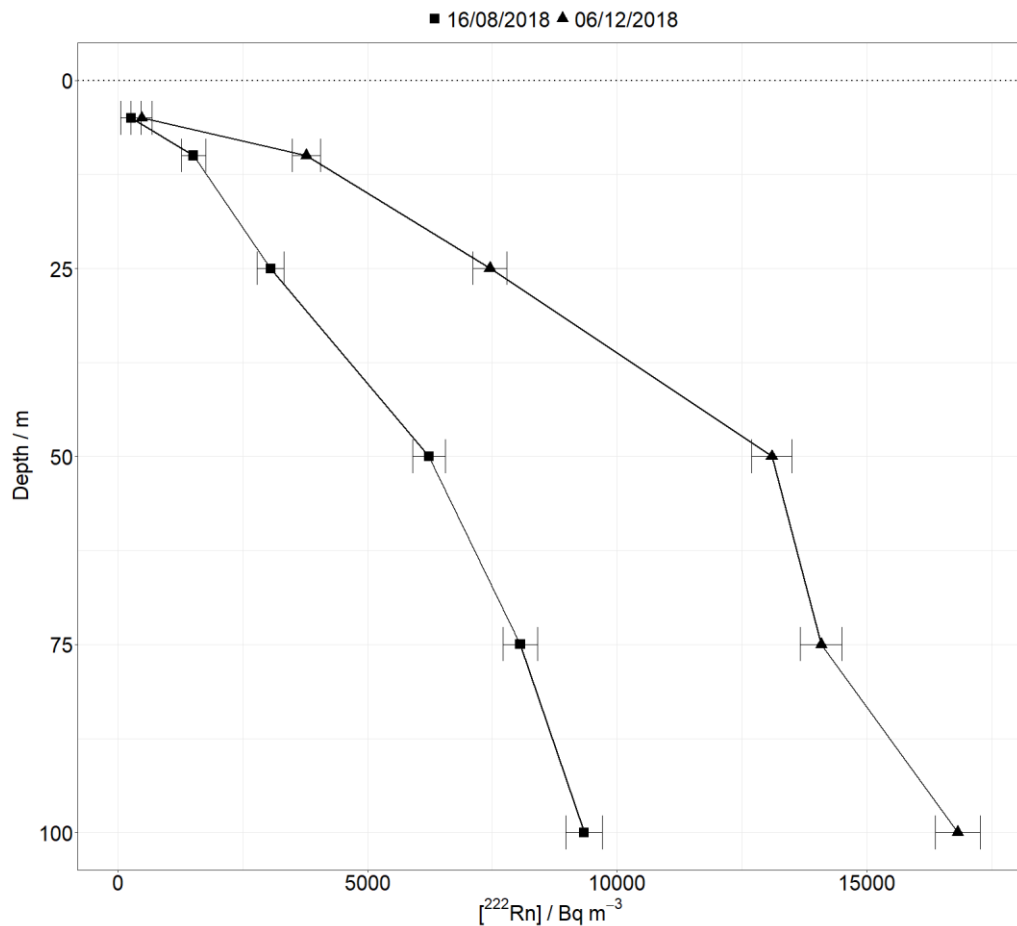


Figure 38: Individual soil gas radon activity concentration profiles with depth in summer and winter. Dotted line represents soil surface.

Soil air-filled porosity was calculated from measured volumetric water content using the soil dry bulk density data collected during September 2019. The relationship between soil gas radon activity concentration and air-filled porosity is shown in Figure 39. The overall negative correlation (-0.77) between these two parameters is significant ($F_{(1,107)} = 156.7, p \ll .005$), $r^2 = 0.5943$.

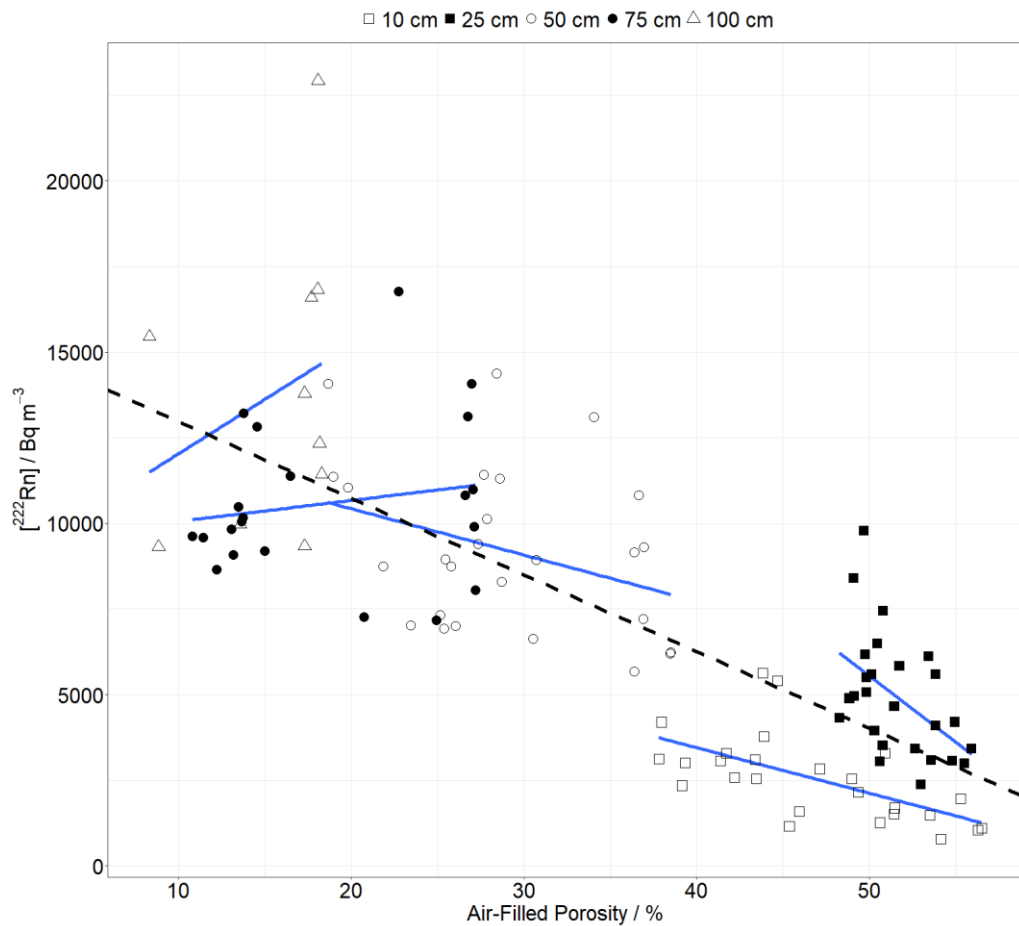


Figure 39: Overall regression (dashed) shows a significant relationship between soil gas radon activity concentration and soil air-filled porosity. Regressions at individual soil depths are shown by solid lines.

At individual time points, soil gas radon activity concentration did not show any correlation with measured soil penetration resistance, taking the soil penetration resistance as an average over the sphere of influence of the sampling point (Figure 6). Soil penetration resistance was also not found to display a significant relationship with measured dry bulk density.

Water table depth, measured from the soil surface, on the site ranged from >101 cm in summer months to 26–49 cm in winter, evidenced by the depths at which soil gas could no longer be

retrieved. The 2018 United Kingdom heatwave from June to August saw soil volumetric water content fall by ~10 % within 1 m of the surface; volumetric water content in the upper 20 cm fell below the detection limits of the Delta-T soil moisture probe. In contrast, the first three months of 2019 were an extremely wet period. Soil volumetric water content during the monitoring period effectively doubled (from 2.5 % to 5 % at 20 cm and from 20 % to 40 % at 1 m); low and high values of volumetric soil moisture content mirrored values of soil gas ^{222}Rn activity concentration.

4.3.2 Annual variation discussion

Soil air-filled porosity displays a strong negative correlation with measured radon activity concentration (Figure 39). Slight heteroskedasticity of the dataset can be accounted for by applying individual regressions to data from individual soil depths, although splitting the dataset in such a fashion significantly reduces sample size per factor, particularly at 75 and 100 cm. Individual regressions show that the relationship between soil air-filled porosity and radon activity concentration ceases to be visible below 50 cm depth. A likely explanation of the breakdown in the relationship between soil air-filled porosity and radon activity concentration is the increased tortuosity of the soil pore network due to proximity to the saturated zone; observed changes in soil texture may also contribute to increased soil pore network tortuosity at depth. The increase in soil pore network tortuosity could result in much more highly

varying soil gas radon concentrations laterally at depth and should be borne in mind when employing the presented method.

The lack of significant relationships between soil bulk density and both soil penetration resistance and soil radon activity concentration may be due in part to the extreme weather conditions present during the monitoring period; a large effect of severe drought at 0–40 cm and then soil saturation at 70–100 cm can be seen between soil penetration resistance measurements (Figure 30).

Two main patterns are observable from the soil gas radon concentration profiles individually (Figure 38): as time passes from winter to summer, concentration profiles display smaller differences in activity concentration with depth, and concentrations themselves also reduce. Secondly, gas is extractable from greater depth in the summer months, due to lowering of the water table between April and August (Figure 34). The variable water table depth is also the reason for smaller sample sizes at depth.

The soil gas radon activity concentrations (Figure 33) show a clear trend over time: data from 5 cm depth, the shallowest sampling depth, differ markedly from the other depths, possibly due to variable vegetation cover and proximity to the atmosphere. Disturbance of the soil during sampling is also more likely with a sampler installed to a shallower depth, and so samples from 5 cm depth may have been subject to preferential flow pathway formation along the body of the sampler as it is moved. The 5 cm sampling depth is extremely close to the soil-atmosphere boundary, and it is possible that any trend is masked, as atmospheric draw-down of gas (i.e. sample dilution) is both likely and variable with the soil air-filled porosity at 5 cm depth. A theoretical sampling radius of 10 cm

(an effective porosity ~ 0.2 as per Figure 6) results in a 5 cm sampling point as the limit of spatial resolution close to the soil surface. Soils with higher porosities may provide the option of a greater spatial resolution to explore the soil-atmosphere boundary without unduly increasing the depth of influence of factors such as wind (Fukuda, 1954).

Soil gas radon activity concentrations in the upper 1 m of the soil varied in the order of 300 % from January 2018 to August 2019. At a depth of 1 m radon activity concentrations varied from $\sim 9,300 \text{ Bq m}^{-3}$ in the summer months to $\sim 23,000 \text{ Bq m}^{-3}$ in the winter months. The annual trend in radon concentrations followed that of soil volumetric water content (Figure 34). The correlation with soil volumetric water content is probably secondary: as gas concentration within the soil pore space is determined by the available interstitial volume, soil radon activity concentration is directly driven by available pore space given the radon production rate and atmospheric pressure are constant. Whilst pressure-driven changes in soil radon flux have been reported (Clements and Wilkening, 1974), such changes occur over hours to days and not annually. There was a clear seasonal pattern to the radon concentrations at all depths sampled. Higher radon concentrations were evident in the winter months. Lower radon concentrations were recorded in spring and summer, increasing again with the onset of autumn and winter. These patterns are clear at all sampling depths but more pronounced in the shallower samples, particularly those taken from 10 cm depth.

Radon activity concentrations measured at a depth of 5 cm were subject to larger errors than those measured below 5 cm depth. The variation in soil gas radon concentration is much larger near the surface of the soil than at depth. Whilst the variability in soil

gas radon activity concentration at 5 cm depth could be attributed to slightly lower bulk densities observed near the surface (leading to larger variation in pore network volume), care should be taken due to the restrictions on sample availability close to the saturated zone in most soils.

There are fewer time points measured at depth than from shallower soils: as a result of fluctuating water table depth, samples at depths 75 cm and 100 cm were not obtainable from January to May 2018; at 100 cm depth, samples were not obtainable in February 2019. Samples from all depths were not analysed in September and October 2018 due to equipment failure.

4.4 Diurnal variation in soil gas concentrations

Two sampling exercises were carried out in order to establish the limit of temporal resolution, the shortest possible time in between samples that would not begin to cause enough mass flow of soil gas to affect measured concentrations substantially. Establishment of the limit of temporal resolution was achieved by systematically shortening sampling intervals for the same sampling point. Appreciable variation in radon activity concentrations only began at a 15 min interval. On this basis, a minimum time interval of 1 h between samples was selected.

In order to test whether diurnal variations in soil gas radon activity concentration are detectable by the method used in the present study, dates were selected close to the winter and summer seasons when, theoretically the minimal and maximal diurnal temperature variations would be encountered, with

periods of anticyclonic (high pressure) weather also preferred to reduce the chances of pressure fronts and rain events which may influence soil gas behaviour. The total number of complete samples analysed by LSC was 73 including an initial blank for a 24 h period. Since the blank sample counting can be started before sampling commences (and all samples are counted for 60 min, and approximately 30 s is required for automatic sample changing), the total time for counting was just over 73 hours, keeping all samples within one half-life of ^{222}Rn (~ 91.75 hours).

4.4.1 Diurnal variation findings

Anomalous data points have all been included in plots and consist of five samples of zero concentration during the late summer sampling; initially low concentrations in the first three samples of the winter sampling period (~ 30 % lower than others, not present in the shallowest samples); and a similar drop by 60 % in a single sample from intermediate depth in the early summer sampling.

4.4.1.1 Diurnal variation in summer

Summer samples were taken hourly between 11:00 on 2nd September and 10:00 on 3rd September 2018 (Figure 40). Samples were collected from 10, 50, 75 cm depth; soil gas could not be sampled from 100 cm depth due to soil saturation. The

overall monitoring duration was 24 hours and final sample preparation for LSC analysis took an extra 2 h.

Soil gas radon activity concentrations displayed little to no trend over the sampling period. Concentrations ranged from 1327–2022 Bq m⁻³ at 10 cm depth, 8117–9251 Bq m⁻³ at 50 cm depth, and 11096–12530 Bq m⁻³ at 100 cm depth, excluding anomalies.

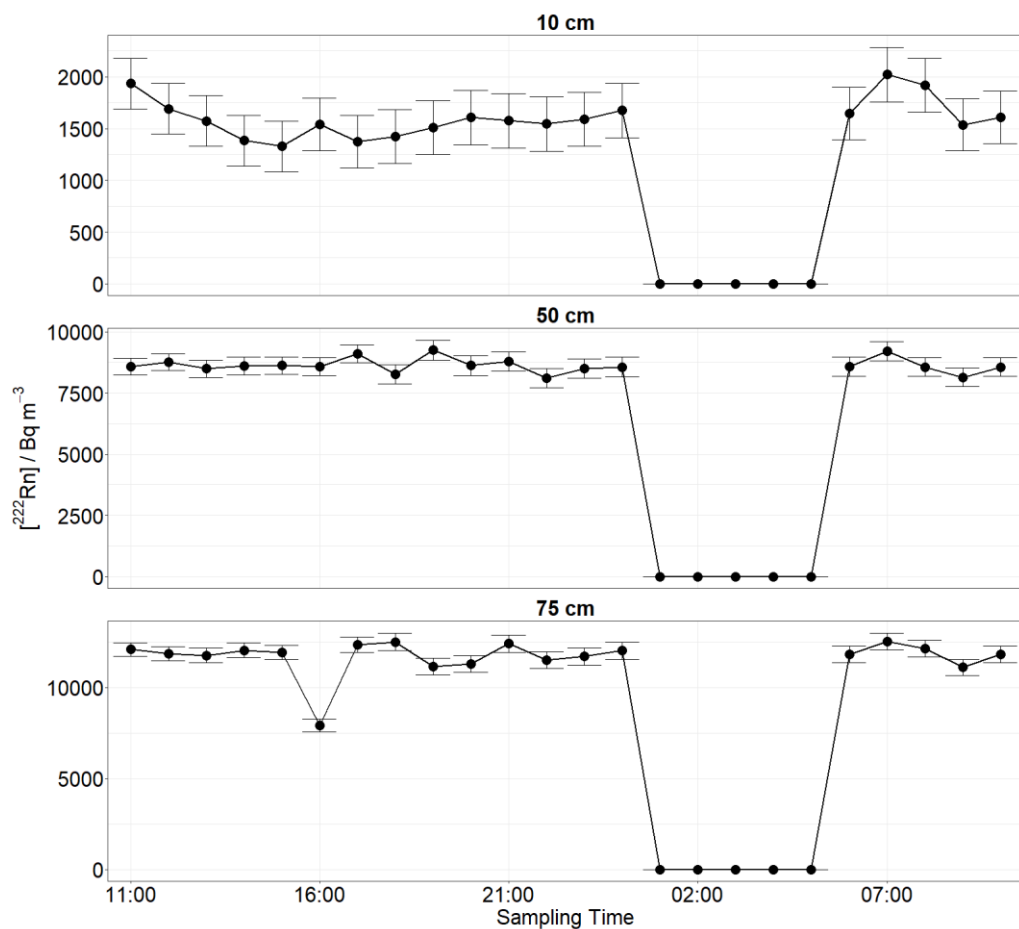


Figure 40: Soil gas radon activity concentrations at three depths over 24 h. 02–03/09/2019. Samples from 01:00–05:00 showed zero activity concentration.

During the night of 2nd–3rd September 2018, skies were clear but became overcast. No rain was observed. Overcast conditions continued until ~10:00. Meteorological conditions were stable throughout the experiment: atmospheric pressure remained between 1014–1016 hPa (Figure 41), air temperature varied between 13.6–19.2 °C, soil temperatures varied from 15.5–19.9 °C at the surface (10 cm) and 17.8–18.1 °C at depth (100 cm), and wind speed varied from 2.52–5.03 m s⁻¹. No rainfall occurred (Figure 41).

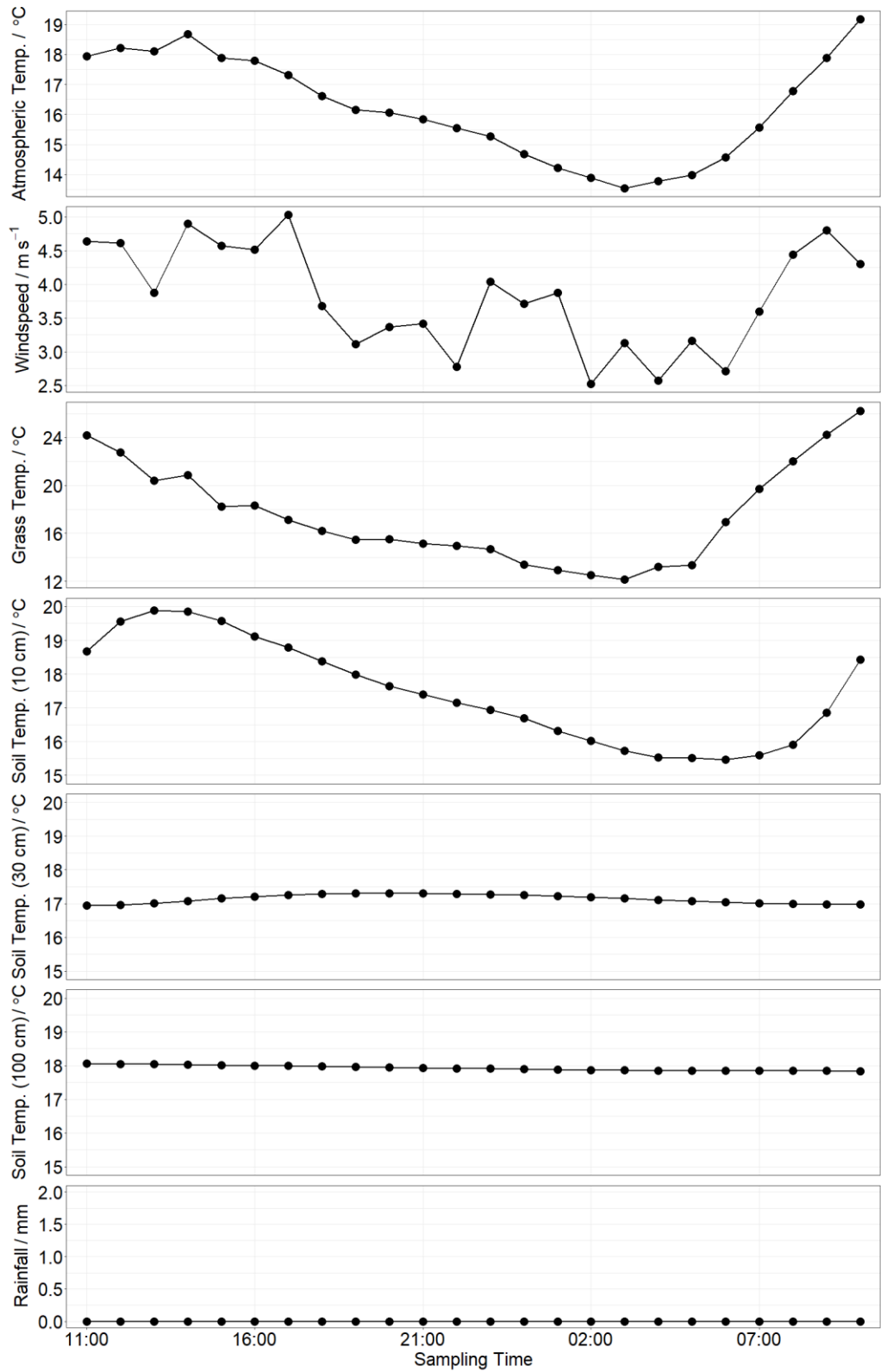


Figure 41: Environmental conditions during the sampling period, 02–03/09/2019. Atmospheric Pressure data from COSMOS station.

4.4.1.2 Diurnal variation in winter

Winter samples were taken hourly over a 24-hour period: from 15:00 on 19th December to 14:00 on 20th December, 2018 (Figure 42). Samples were collected from 10, 50, and 100 cm depth. The overall monitoring duration was 24 hours and final sample preparation for LSC analysis took an extra 2 h.

Soil gas radon activity concentrations displayed little to no trend over the sampling period aside from anomalous points at the beginning of the 50 cm and 100 cm depth datasets. Concentrations ranged from 3265–4380 Bq m⁻³ at 10 cm depth, 13610–15550 Bq m⁻³ at 50 cm depth, and 20310–23580 Bq m⁻³ at 100 cm depth excluding anomalies

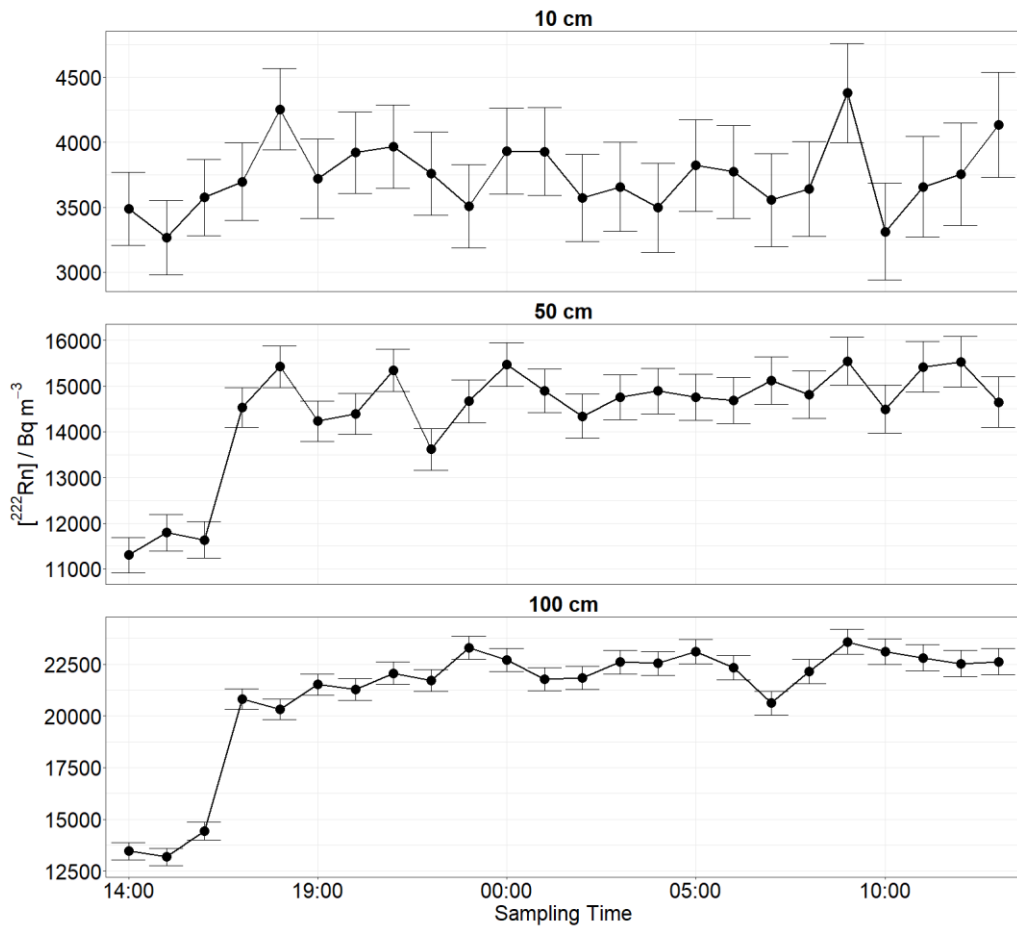


Figure 42: Soil gas radon activity concentrations at three depths over 24 h. 19–20/12/2018.

During the night of 19th–20th December 2018, skies were mostly clear. Light rain was observed at 03:30 and 09:00. Clear, sunny skies presented from 09:30 until 10:30. Remaining periods of the day saw calm, overcast weather. Meteorological conditions were stable throughout the experiment: atmospheric pressure remained between 994–998 hPa, air temperature varied between 5.72–8.75 °C, soil temperatures varied from 4.21–6.74 °C at the surface (10 cm) and 7.32–7.40 °C at depth (100 cm), and wind speed varied from 3.05–4.89 m s⁻¹. Rainfall of 0.8 mm occurred between 02:00 and 03:00 (Figure 43).

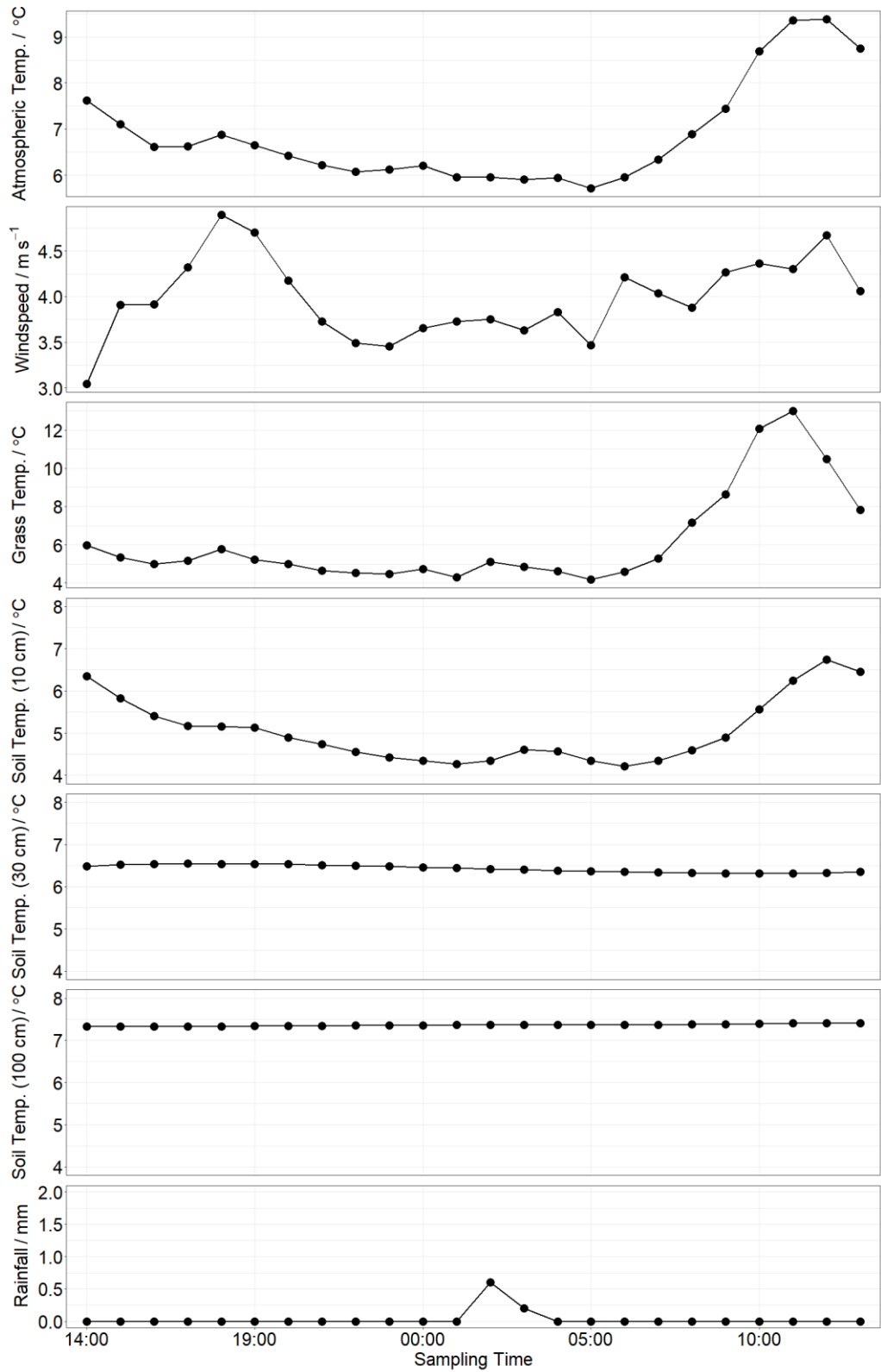


Figure 43: Environmental conditions during the sampling period, 19–20/12/2018. Atmospheric Pressure data from COSMOS station.

A six-hour monitoring period (Figure 44) was undertaken on 10th June 2019, from 12:00–18:00, for the purpose of assessing two anomalies in the December 2018 dataset. Samples were collected from 10, 50, 75 cm depth; soil gas could not be sampled from 100 cm depth due to soil saturation. The two anomalies could not be replicated during the June 2018 sampling period.

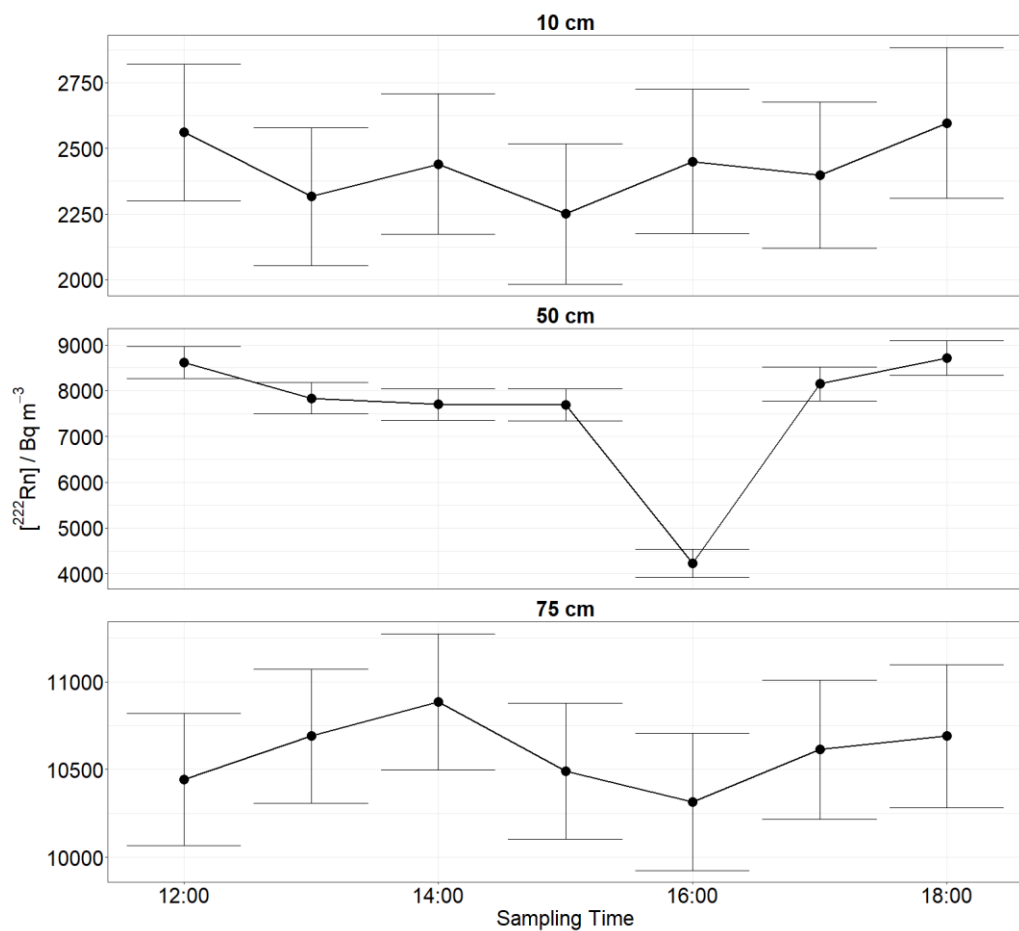


Figure 44: Soil gas radon activity concentrations at three depths over 6 h. 10/06/2019.

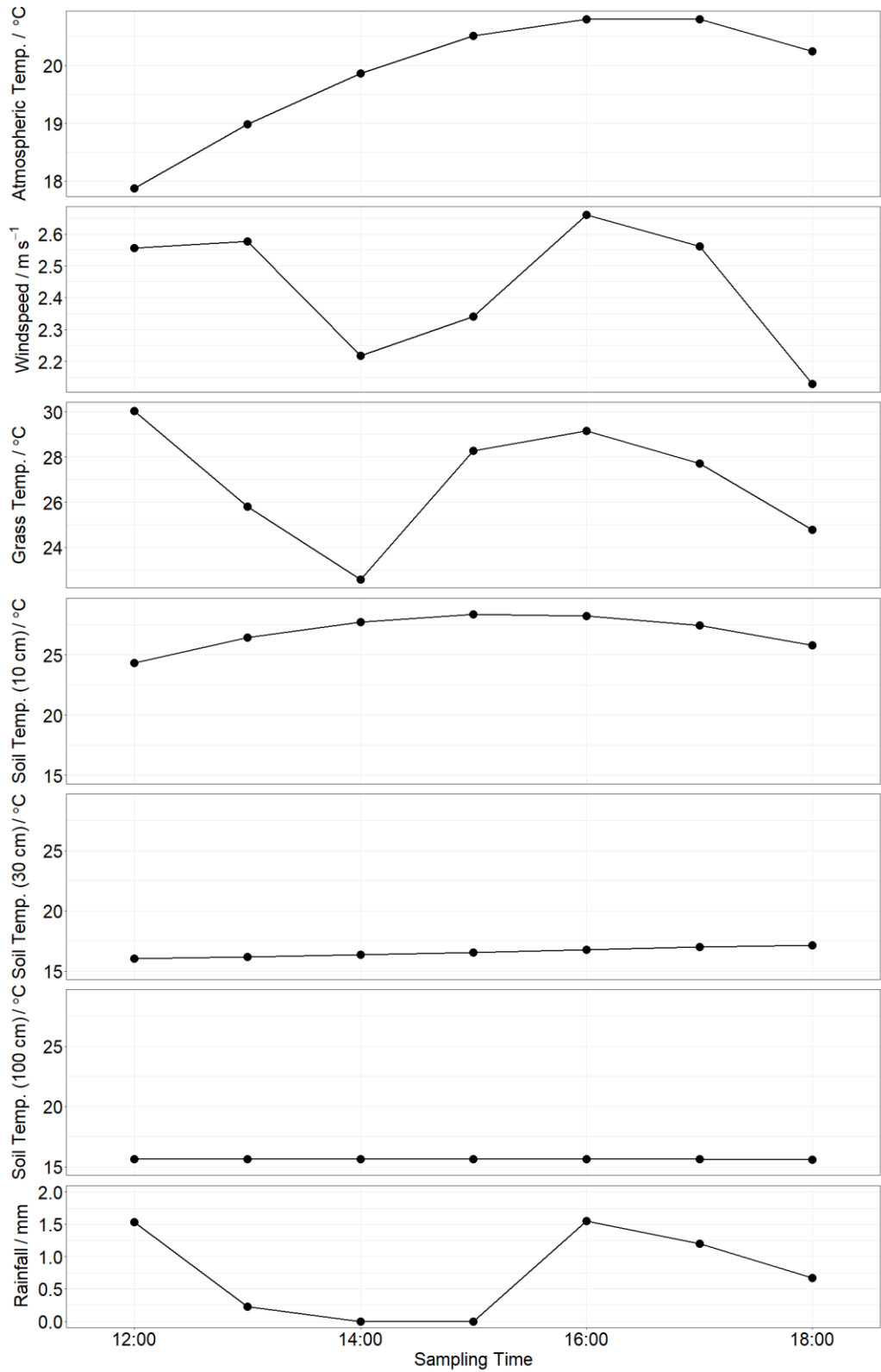


Figure 45: Environmental conditions during the sampling period, 10/06/2019. Atmospheric Pressure data from COSMOS station.

4.5 Discussion: ex-ASGARD site soil gas

While no observable diurnal pattern in soil gas radon activity concentrations is present in the winter data (Figure 42), no pattern is observable in other monitoring periods either (Figure 40). It is possible either that no diurnal variation occurred or that the method used in the presented study had insufficient temporal resolution to reveal small fluctuations in soil gas radon activity concentrations with time. Surface soil radon activity concentrations in summer may show weak variation, although missing values make interpretation difficult. The main drivers of a thermal inversion, surface irradiation and air temperature (Figure 46), do not appear to have been as high as in the previous year, so it may be that the day selected simply did not experience enough of a temperature inversion at the soil surface to effect advective flow of soil gas. Given that diurnal variations can be observed in atmospheric samples but only under drier conditions (Victor et al., 2019), it is likely that environmental conditions present during the sampling periods suppressed any major variations in soil gas transport behaviour.

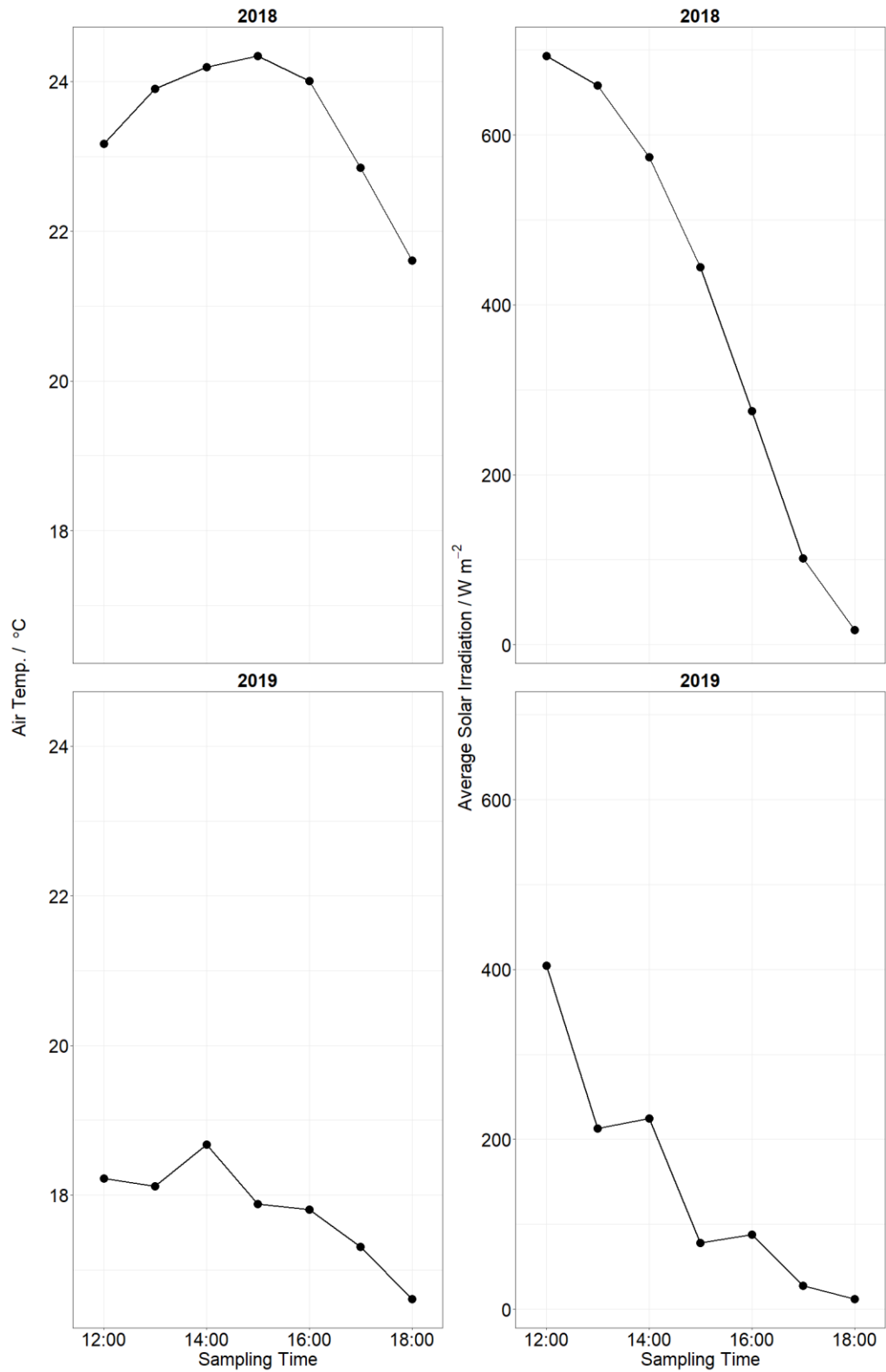


Figure 46: Air temperature during the sampling period, 02–03/09/2019, with previous year for comparison [met. station].

As rainfall was observed during two of the monitoring periods, and the subsequent hours showed no change in soil gas radon activity concentration, it is concluded that rainfall events less than or equal to 1 mm h^{-1} do not have an observable effect on the method used and temporal resolution.

The anomalies of the first three time points in Figure 42 were not present in either of the other time series measured in the current work (Figure 40, Figure 44). Insufficient belowground recharge would probably result in lower measured soil gas radon activity as atmospheric air would be drawn into the system; however, the phenomenon of atmospheric dilution would be present at least at shallower depths and not just in deeper soil. It would also probably be observed at all points as sampling progressed. Preliminary exercises had shown that a time interval of 1 hour between sampling events was ample for belowground recharge (Section 4.2).

The samples of zero measured concentration between 01:00 and 05:00 on 03/09/2019 (Figure 40) may be explained by human error: the sampling equipment for the time points in question were prepared shortly before sampling ($\sim 00:45$) and may not have been sealed to the required degree, allowing sampled soil gas to escape over the sample preparation period, being replaced with atmospheric air which has negligible radon activity concentration.

The anomalous measurements from 100 cm depth at 14:00, 15:00, 16:00 on 19/12/2018 (Figure 42), as well as 16:00 on 10/06/2019 (Figure 44) could possibly be explained by failure to withdraw or include the required $3 \times 15 \text{ mL}$ soil gas during sampling: measurement of only 15 or 30 mL soil gas rather than the prescribed 45 mL would effectively reduce measured concentration by one-third or two-thirds as has been observed.

In the laboratory it was noted that some scintillation cocktail was lost from the sample taken from 100 cm depth at 10:00 on 20/12/2018 (Figure 42); however, no effect on the overall trend seen in the data can be observed.

5 Results: radon measurements in sites with varying soil textures and treatments

5.1 Overview

The sandy soil of the ex-ASGARD site, described in the previous chapter, is close to ideal for soil gas sampling; the soils have high porosity and samplers are easily inserted. Other soils of differing textures and subject to different treatments, including agricultural practices, may not be as readily sampled. In order to explore the applicability of the sampling and analytical method used to determine soil radon activity concentrations in the study, several sites with varied characteristics were selected and sampling of soil gas profiles was carried out.

5.2 Kingston field site (sandy farmed soils)

5.2.1 Site description: Kingston

The Kingston site is located adjacent to the University of Nottingham Farm: 52.84126 °N, 1.25442 °W ("Ki", Figure 4). The experiment was established to examine the effects of crop type and tillage treatment on soil structure. Soil gas samples were taken in November 2018. The soils across the Kingston site are sandy loam and display broadly the same texture distribution as the ex-ASGARD site (Section 4.1). Soil gas sampling was conducted over the existing experimental design

(Figure 47), taking advantage of the different soil treatment types applied:

Kingston site existing experimental design:

Split plot (Figure 47) divided into 4 blocks, each with the same tillage management history.

Each block is divided into 2 plots which are then divided into 3 subplots.

Plots were 12 m long and 9.6 m wide, with a gap of 2.4 m between them. The 'discard' area between each block was 12 m.

In each block, wheat straw was removed from one of the main plots, chopped and added to the other, before treatment:

- *"Ploughed": conventional ploughing to a depth of 30 cm.*
- *"Minimum tillage": cultivated to a depth of 10 cm.*
- *"Zero tillage": soil surface not cultivated.*

Treatments began in September 2014, and in subsequent Septembers all cultivation practices were carried out: drilling of crop seeds took place, followed by rolling. The wheat is naturally irrigated by rainwater and stubble is left at the soil surface after harvesting.

The site was unexpectedly disturbed in September 2018, two months before the reported soil gas sampling, when all plots at the Kingston site were ploughed. It is possible that the disturbance caused by ploughing of the zero tillage and minimum tillage plots served to reduce any changes in soil gas

behaviour that had occurred during the four years of soil treatment.

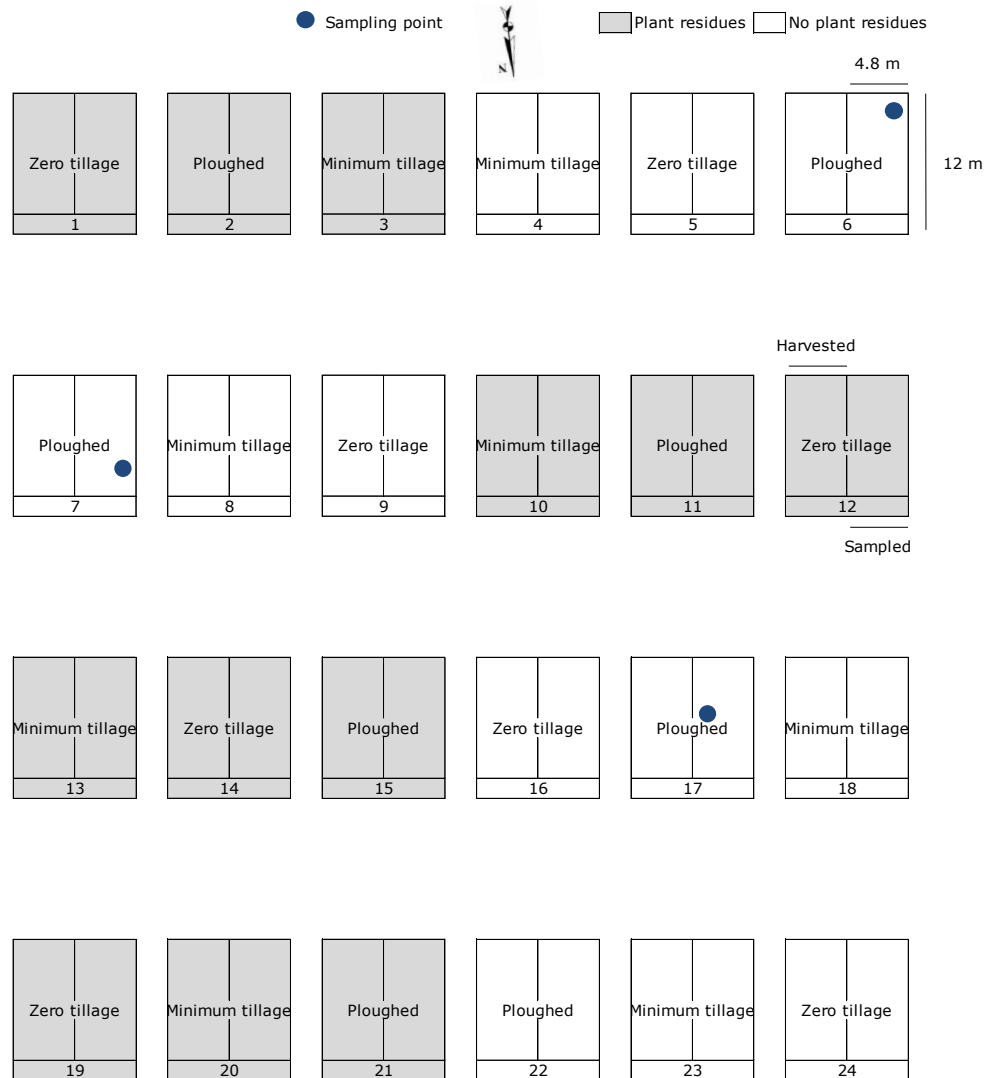


Figure 47: Layout of the Kingston experimental tillage plots

5.2.2 Findings

Of the section of plot from which gas samples were taken (Figure 47), an edge and distance along that edge were randomly generated by computer for the sample point. Sampling was possible on ploughed plots with plant residue treatment; however, the soils in all other treatments were too resistant to insert gas samplers successfully.

Table 10: Locations of successful measurements at Kingston site

| <i>Plot Number</i> | <i>Side / NESW</i> | <i>Clockwise direction / m</i> | <i>Soil treatment</i> |
|--------------------|--------------------|--------------------------------|-----------------------|
| 6 | W | 0.8 | Ploughed |
| 7 | W | 9.3 | Ploughed |
| 17 | E | 7.6 | Ploughed |

An initial point Ki-1 was sampled from a ploughed area of the site (not part of the experimental plan in Figure 47) on 20/11/2018 (Figure 48). The sampled point was within the field but not within the experimental plots. A maximum depth of 38 cm was reached with the soil gas sampler; soil gas was sampled at 10, 20, 30 cm. The method employed was deemed suitable for the site and radon activity concentrations were within detection range.

Attempts were made to sample all plots on 07/12/2018. Sampling depths below 20 cm could not be reached in all but three plots: 6 (Ki-2), 7 (Ki-3) and 17 (Ki-4) (Figure 48).

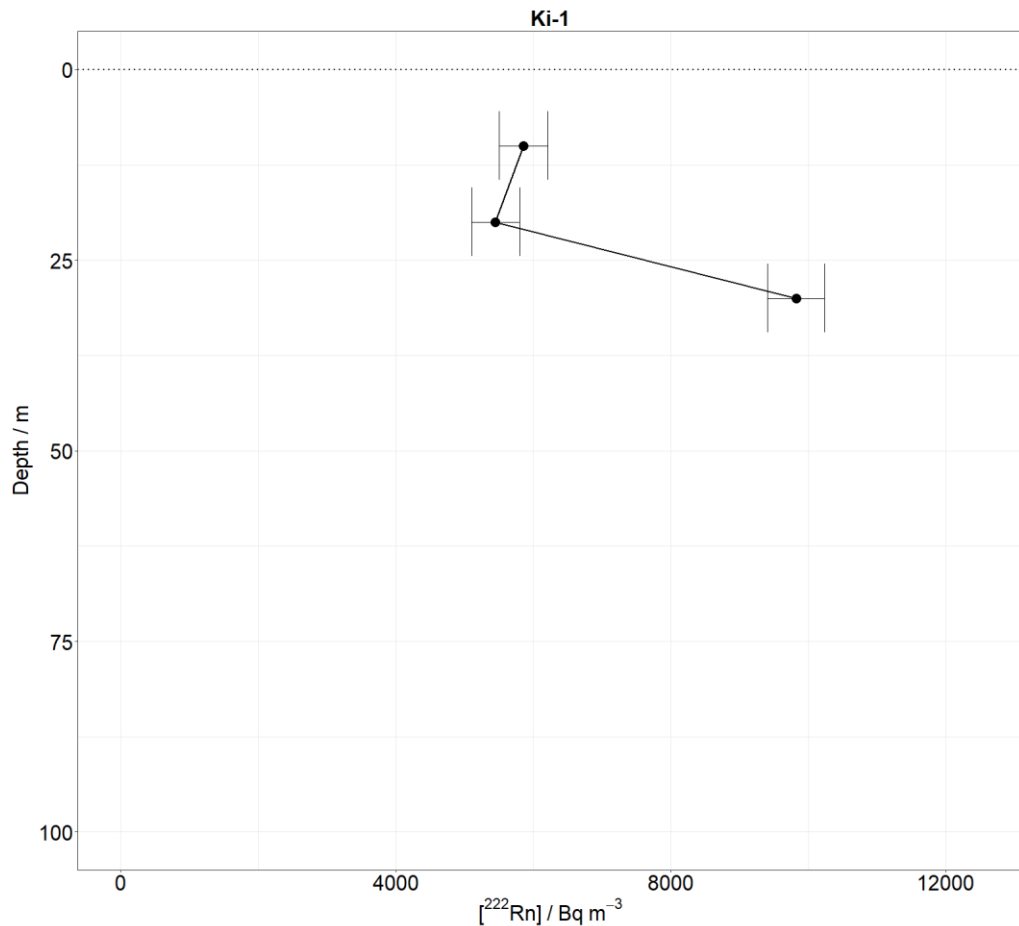


Figure 48: Kingston soil gas radon activity concentration profile Ki-1: Initial sample (ploughed) (Ki-2,3,4 in plots 6,7,17, all ploughed, were below detection limit).

Radon activity concentrations in Ki-2, 3 and 4 were below detection limit or very low in comparison to Ki-1. It is likely that due to the excessive force required to insert the sampler, a channel was created along the sampler body which allowed preferential flow of atmospheric air when pressure difference

was applied using the sampling syringe. Dilution of the sample was the result.

After several attempts it was clear that the soil treatments were the likely cause of the high degree of penetration resistance experienced; a slide hammer attachment was devised to allow force to be applied in-line with the sampler body.

Clear differences could not be discerned between soil treatments from the presented sampling effort. Similarly, regular disturbance of topsoil does not appear to be enough in isolation to allow sampler penetration; some soils still have inclusions (in this case rock fragments) that frustrate sampling efforts.

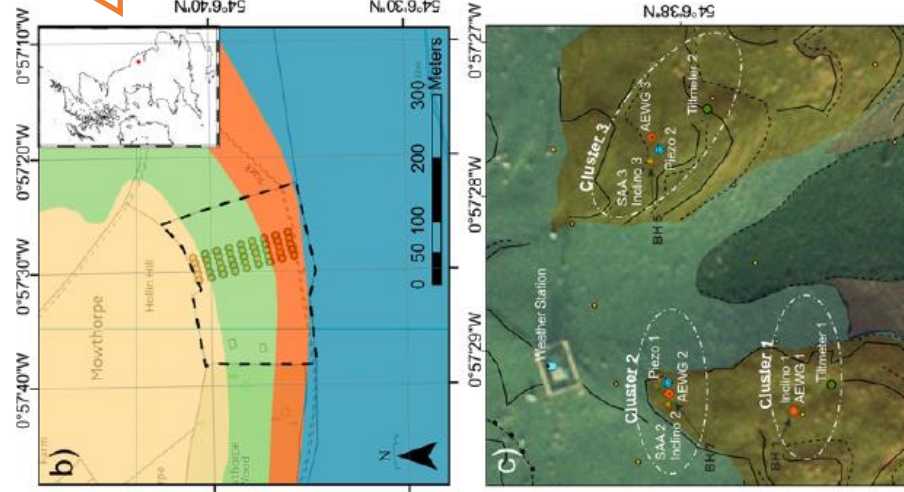
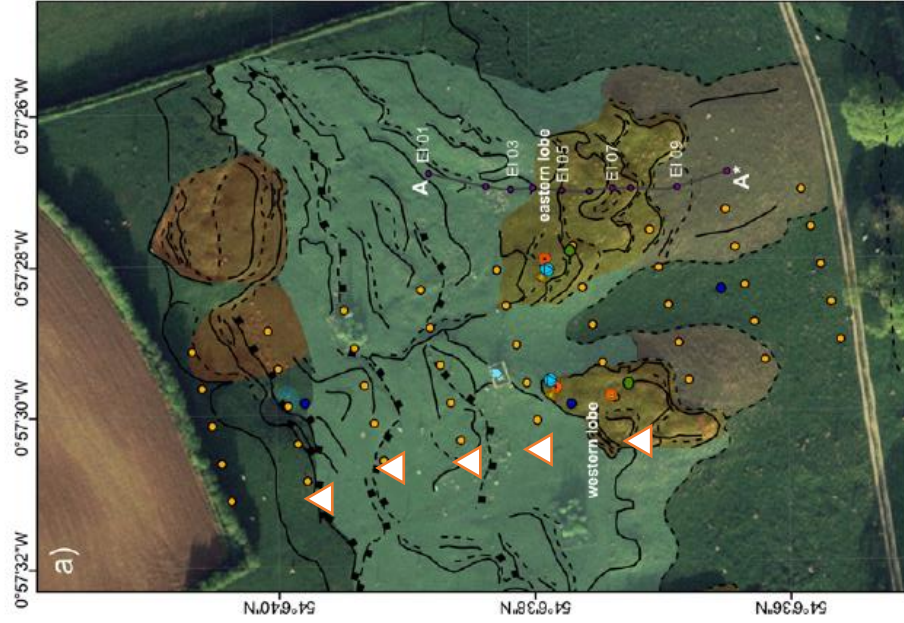
5.3 Hollin Hill field site

5.3.1 Site description: Hollin Hill (slipping clay soils)

The Hollin Hill Landslide Observatory is located in Yorkshire, UK: 54.11073 °N, 0.96027 °W ("HH", Figure 4) and is a "slow-moving earth slide-earth flow" in the Lower Jurassic (Liassic) rocks of the Cleveland Basin, UK (Chambers et al., 2011, Figure 49). Deeply weathered and poorly consolidated Whitby mudstone forms a poorly draining clay soil at the surface. Underlying the soil is Staithes sandstone, the main reason for slippage. Soils at the Hollin Hill site feature narrow intervals of saturation in the top 5 m and maximum movement rate is $\sim 2 \text{ m y}^{-1}$ (based on GPS measurements), usually in winter when the slopes are wettest, but movements are sporadic (Uhlemann

et al., 2017). The site is heavily instrumented and features a COSMOS meteorological station (Section 3.5).

- Legend**
- Geotechnical Sensors**
 - Temperature/GMC/JEC
 - Acoustic Emission Monitoring
 - Inclinometer
 - Tiltmeter
 - ▲ Shape Acceleration Array
 - GPS marker
 - Environmental Sensors**
 - ⊕ Weather Station
 - Piezometer
 - Geology**
 - Dogger Formation
 - Whitby Mudstone
 - Stalthes Sandstone
 - Redcar Mudstone
 - Geomorphology**
 - Landslide Extent
 - Rotational Failure
 - Recent landslide deposit
 - Relict landslide deposit
 - Sag Pond
 - Main Scarp
 - - - Secondary Scarp
 - Breaks in slope
 - Positive
 - - - Negative



Soil gas sampling points HH-1—5 (in order downslope, from the north).

Figure 49: Map showing the landslide observatory at Hollin Hill and its underlying geology (Uhlemann et al., 2016). Sampling points are indicated.

5.3.2 Findings

The sampling locations at Hollin Hill were evenly-spaced downslope over one of the main slippage lobes (Figure 49). A total of five ^{222}Rn concentration profiles were sampled on 14/06/2018. HH-1, 2 and 4 (Figure 50) are presented separately to HH-3 (Figure 51) as HH-3 shows the maximum sampling depth achieved (170 cm), and the highest radon activity concentration measured ($\sim 40,000 \text{ Bq m}^{-3}$) during the current research. Soil gas radon activity concentrations in Profile HH-5 were below detection limit. Low measured activity concentration was initially thought to be due to internal damage to the sampler. The same could be the cause of apparent reductions in radon activity concentrations toward the bottom of each profile, although it could also be due to different soil characteristics.

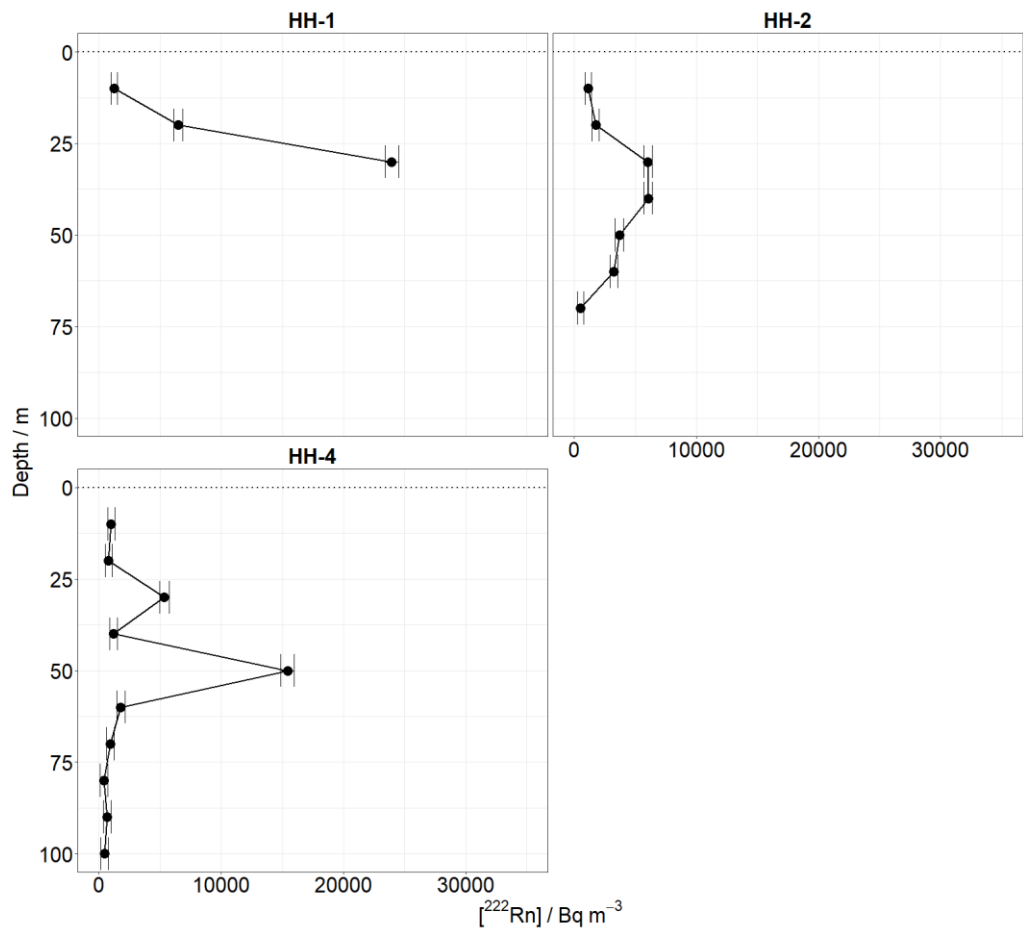


Figure 50: Hollin Hill soil gas radon activity concentration profiles HH-1,2 and 4.

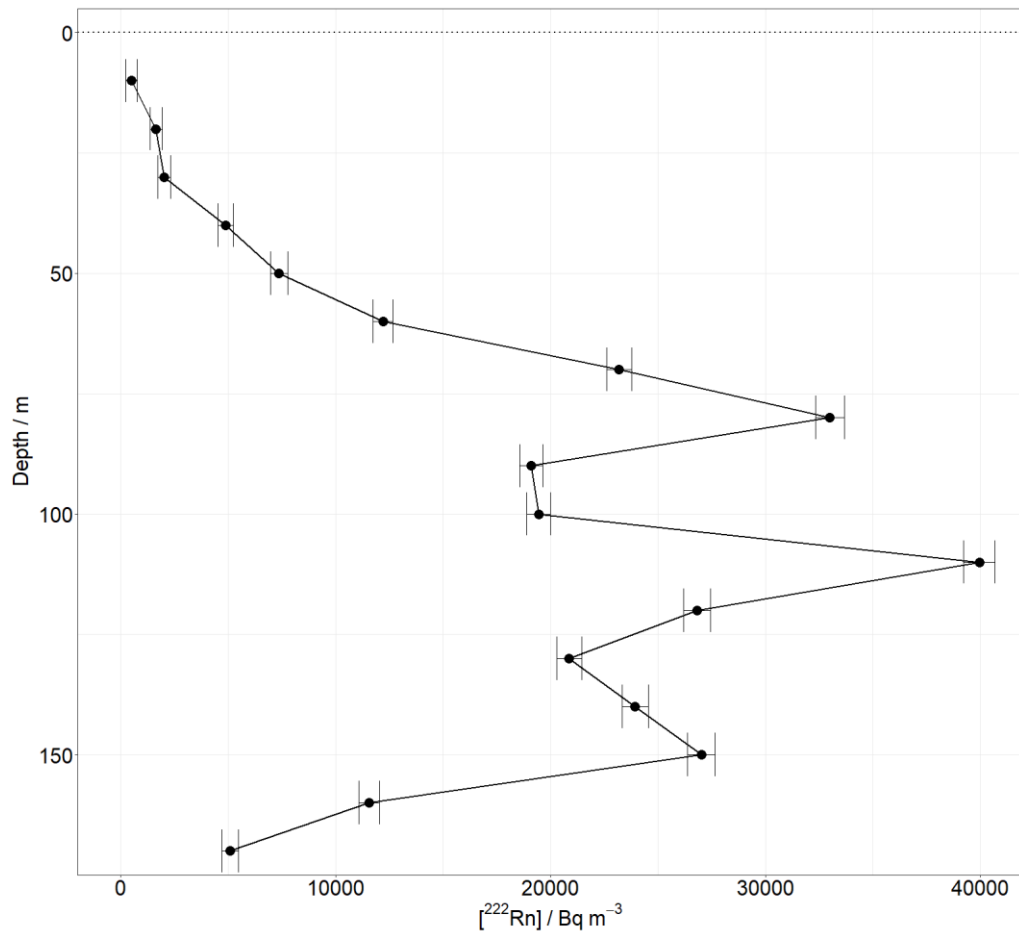


Figure 51: Hollin Hill HH-3 soil gas radon activity concentration profile.

Profile HH-1 (Figure 50) consists of only three measurement points. Profiles with few points are less likely to represent the soil sampled and bring less confidence to any prediction of soil physical properties. Profile HH-2 was sampled to a depth of 70 cm but the deepest sample can probably be discounted as it is below detection limit. HH-3 follows the expected curve (cf. Figure 4) until a depth of ~45 cm at which point the activity concentrations fall below detection limit. Profile HH-4 displays a highly unusual increase in concentration at 50 cm depth, possibly due to extreme lithological conditions, as it was established that atmospheric air did not enter the sample by

damaged equipment. Concentrations below detection limit even at depths of 90 cm suggest dilution of soil gas with atmospheric air.

Profile HH-3 (Figure 51) was taken to a depth of 170 cm, the deepest profile attained over the course of the research. The shallow samples of the curve observed in HH-2 are again displaying a much smaller increase in concentration with depth than expected. Only small increases in soil gas concentrations may be due to topography and/or the extreme winds experienced on the day of sampling. At depth, radon concentrations reduce rapidly, probably due to preferential flow as, at depth, soils become both increasingly resistant to penetration and less porous (the site here being underlain by clays). The required 15 mL of gas therefore may draw a larger percentage from the atmosphere.

The soils of Hollin Hill are known to be moving laterally at a variable rate throughout the year, making the site very different to others studied as part of the presented research. Attention must be paid to the spatial resolution of monitoring techniques when a field site is dynamic in this respect. In the case of Hollin Hill, spatial variability on a sub-10 cm scale would not be visible from the current data regardless of measurement quality, as the maximum resolution sampled was 10 cm. The profiles obtained from soils at Hollin Hill are highly variable due to the nature of the site.

Whilst samplers are more easily inserted into the disturbed ground, clay soils are more difficult to extract gas from (more time is required as porosity is much lower). Clay soils also have displayed a much larger radon generating capability as evidenced from the concentrations $\sim 40,000$ Bq (Figure 51). The profiles from Hollin Hill clearly do not conform to theoretical gas

diffusion behaviour assuming a single diffusion coefficient (Figure 3), most likely due to the highly variable soil textural profile and topography; no other observed conditions were markedly different to other studied sites.

5.4 Bagworth Heath field site (reclaimed colliery soils)

5.4.1 Site description: Bagworth Heath

Bagworth Heath is a reclaimed colliery site in Leicestershire, UK (52.6559 °N, 1.32438 °W) ("BH", Figure 4) which has previously been described by Willoughby et al. (2004). The site comprises a relatively steep dome (~12.5 ° in places), peaking at 170 m above sea level. Annual rainfall is 750 mm y⁻¹ and restricted drainage has resulted in ponding of water in the low-lying areas of the site. To form the site, approximately 13 ha of restored colliery spoil (which had been subjected to enhanced coal-recovery methods) was covered with clean topsoil to a depth of between 15 and 40 cm then fertilised with 600 kg ha⁻¹ NPK and triple super phosphate. A grass mixture was then sown (160 kg ha⁻¹). Contour ripping (50 cm depth every 115 cm) was employed to increase slope stability and mix topsoil with underlying spoil. The spoil is high in iron pyrites and so addition of coarse limestone at 12 tonnes ha⁻¹ was employed in order to buffer acidity as iron leached from the spoil.

Some areas of the site were left to grassland whilst others were seeded with trees (Figure 52) including *Pinus sylvestris* (surface) and *Quercus petraea* (5–7 cm depth), both at a rate of 10⁵ viable seeds per hectare. Seeding took place in late April

1994 and many trees appear to have self-set around the edges of the site since.

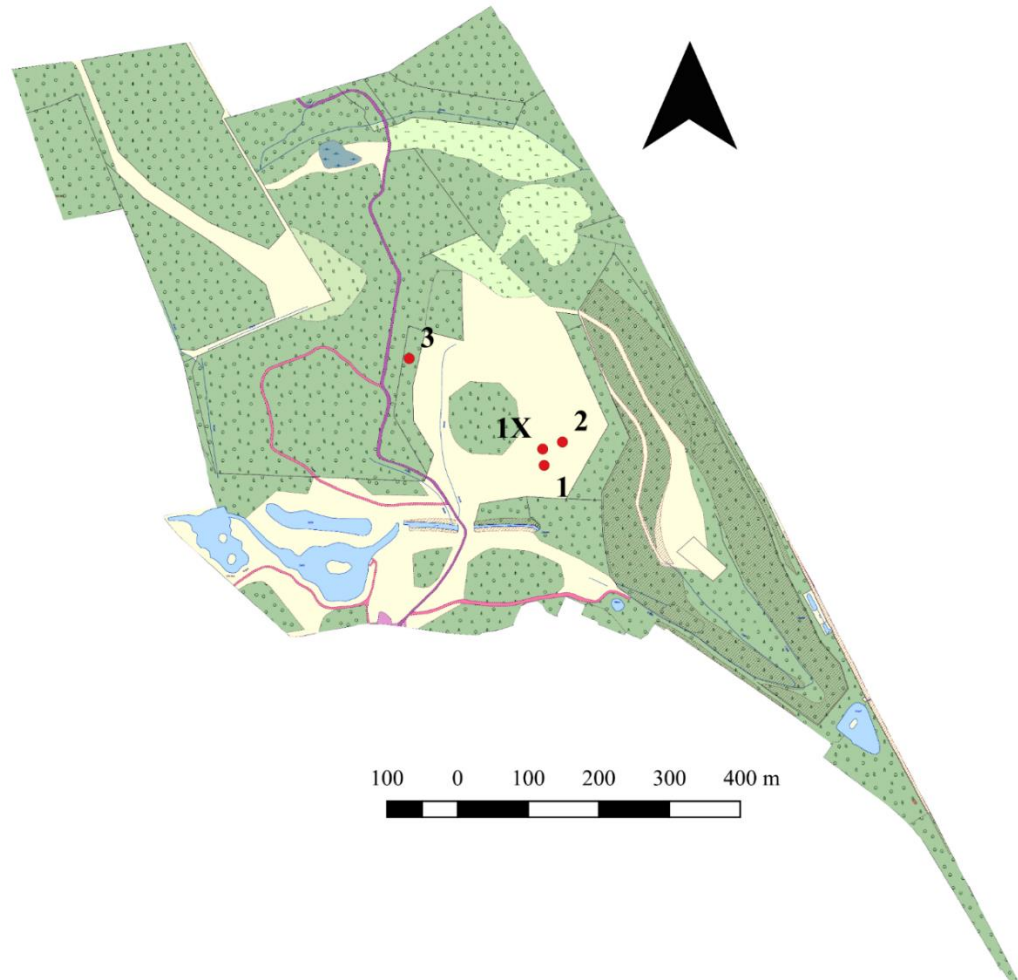


Figure 52: Bagworth Heath site with sampling points indicated. Trees are present in the green areas.

5.4.2 Findings

5.4.2.1 Soil radon emanation estimation

On 27/06/2018 samples of shale and topsoil were collected (no soil coring was carried out due to the artificial nature of the site). Collected soil and shale samples were analysed for ^{226}Ra activity concentration by standard methods (Section 3.3.1).

5.4.2.2 Soil gas measurements

A total of three ^{222}Rn activity concentration profiles were measured (Figure 52) and sampling was also undertaken for greenhouse gases (CO_2 and CH_4). The wooded area of the site contains a high density of vegetation including shallow tree roots. Use of the soil gas profile sampling equipment was made very difficult by the vegetation present, and as such measurement profiles were obtained to a depth of only 20 cm.

5.4.2.2.1 Radon

Soil gas radon activity concentrations were below detection limits at many points.

Position BH-1 (Figure 52) was located next to a drainage lagoon which, due to antecedent weather conditions, was almost completely dry. Surface vegetation was withered or dead due to

the lack of antecedent rainfall and high temperatures. The gas sample from 20 cm depth contained a small activity of radon, but much lower than that from other soils sampled. All other samples to a depth of 70 cm contained no detectable radon gas. Profile BH-2 (Figure 52) was taken on the other side of the lagoon in a patch which was noticeably wetter (vegetation was much greener and showed signs of recent growth). Samples were taken to a depth of 50 cm; however, once again no radon was detected. Profile 3 (Figure 53) was taken to a depth of 20 cm. The woodland site, compact and dry soil made sampler insertion very difficult. Root density was also very high.

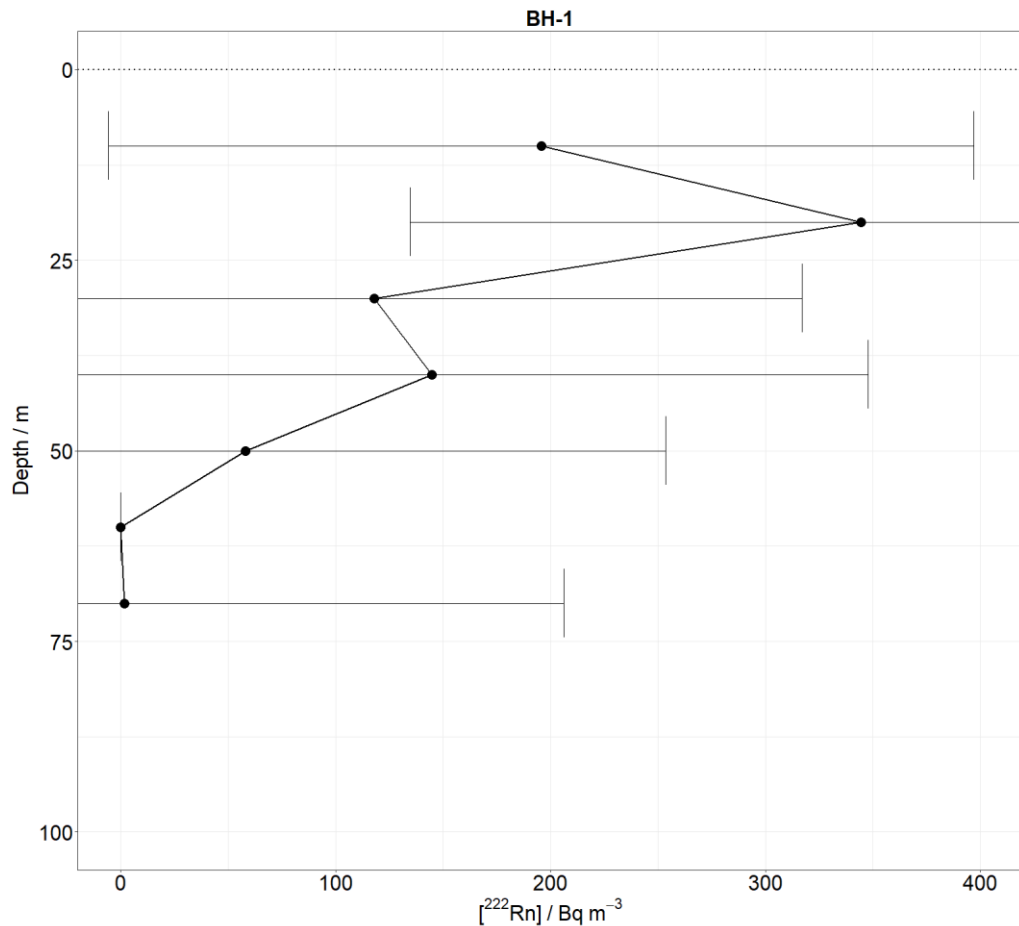


Figure 53: Bagworth Heath soil gas radon activity concentration profile BH-1 (adjacent to drainage lagoon). Profiles BH-2 (drainage lagoon edge) and BH-3 (highground wooded area) below detection limit.

A possible explanation for the low soil gas radon activity (Figure 53) could be the relatively thin topsoil cap which is permeable enough to not allow sufficient build-up of soil gases beneath it, exaggerated by high air-filled porosity due to dry weather in the lead-up to sampling. At the sampled points the radon method did not enable quantification of soil gas movement due to very low natural concentrations of radon gas. As radon was below detection limit, it is not possible to discern what was observed as a well-defined textural change in the subsurface.

5.4.2.2.2 Carbon dioxide

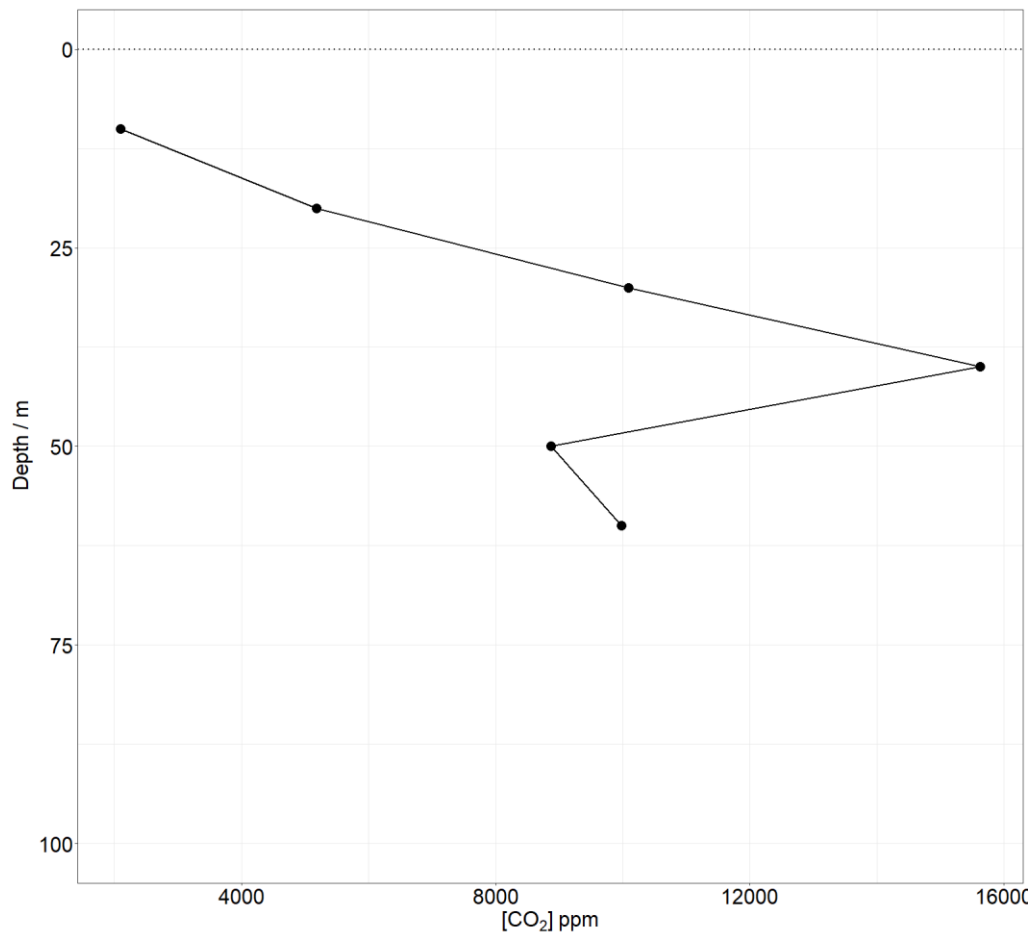


Figure 54: Carbon dioxide concentration profile from location BH-1 (samples from BH-2 and BH-3 were below detection limit).

Only one concentration profile of CO₂ was above detection limit, location BH-1 (Figure 54). It is unlikely that CO₂ concentrations below detection limit were due to a lack of biological activity in those soils or too thin a topsoil layer, as profile BH-1 (Figure 54) was taken from the basin of the drainage lagoon itself, which possessed no topsoil. As with radon at the Kingston site (Section 5.2) the insertion of the soil gas sampler probably created preferential flow pathways which allowed atmosphere draw-down and resulted in heavily diluted samples. The presence of

detectable CO₂ at all depths at BH-1 whilst radon activity concentrations are close to or below detection limit may indicate different production behaviour for the two gases, though detection limits of the two employed instruments are different. The similar shapes of the CO₂ and ²²²Rn profiles (Figure 53, Figure 54) do indicate that both gases are subject to similar subsurface transport behaviour, and also probably subject to the same sampling error (dilution with atmospheric air).

5.5 Allerton Project field site (farmed clay soils)

5.5.1 Site description: Allerton Project

The Allerton Project is in the village of Loddington, Leicestershire, UK: 52.6096 °N, 0.83214 °W ("AP", Figure 4). Soils at the site are clay loam. The experimental plot of interest concerns the effect of tillage reduction on soil health. In the experiment, conducted since 2010, three crops are rotated through a blocked design in which standard tillage is compared with zero tillage (Figure 55). The plots run along the length of the field and consist of four treatments: the two main treatments are "direct drill" and "plough and drill" i.e. zero-till and conventional tillage.

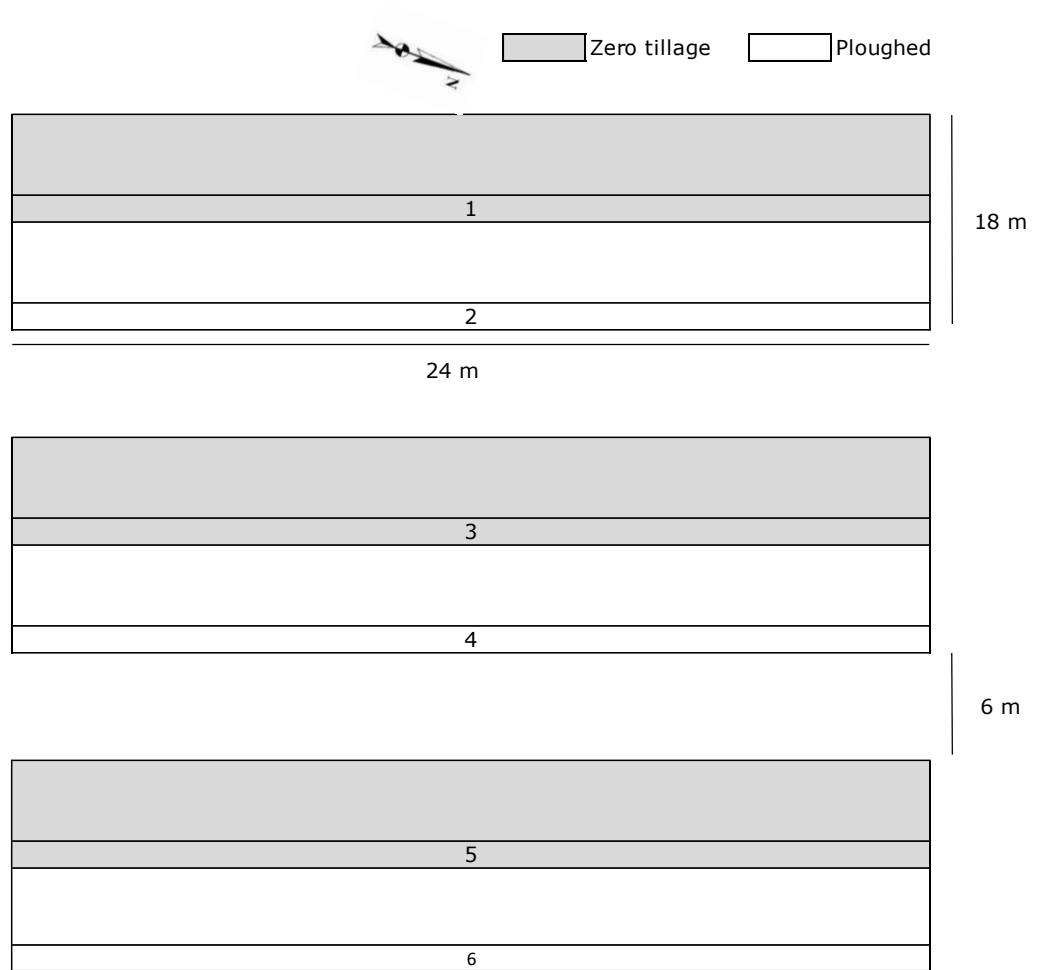


Figure 55: Allerton Project experimental plot design. Block design fully randomised.

5.5.2 Findings

Sampling was carried out on all six plots on 16/11/2018. Sampler insertion required less force than at the sites previously sampled (Sections 5.2, 5.3) and depths of 1 m were reached.

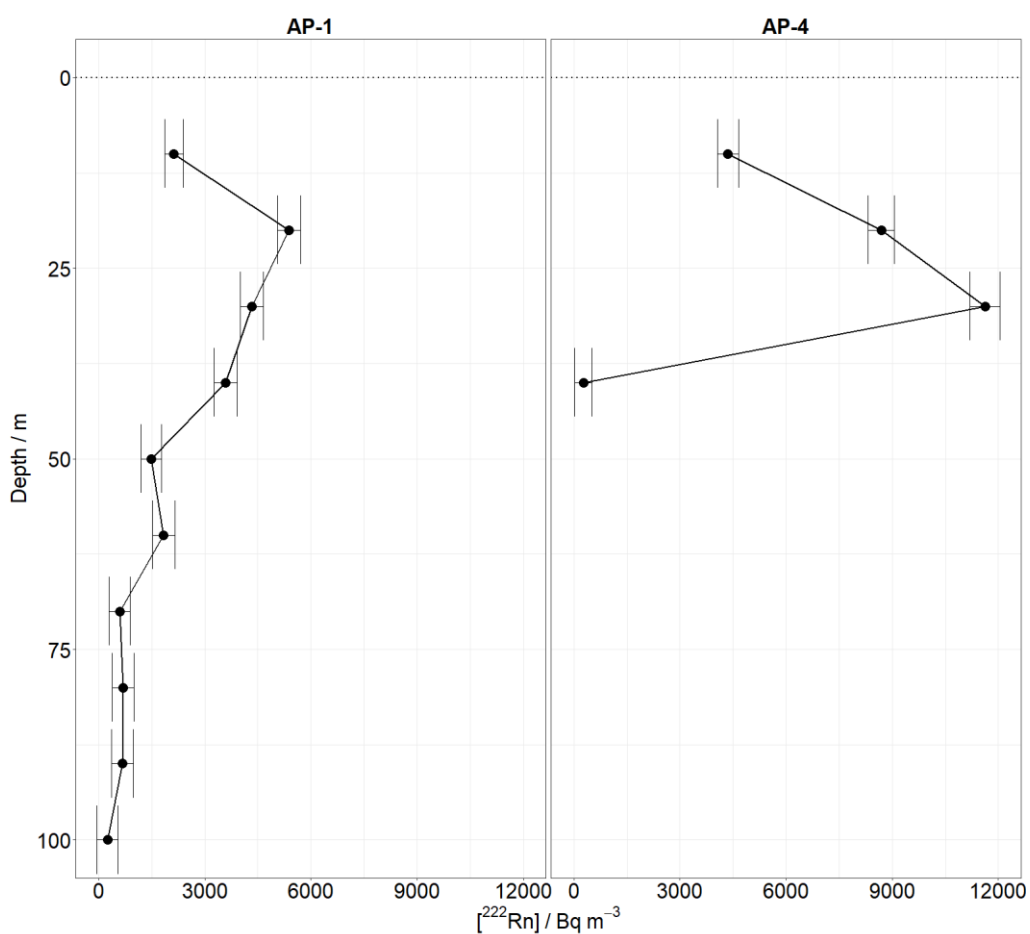


Figure 56: Allerton project soil gas radon activity concentration profiles. AP-1: zero-till treatment, AP-4: ploughed treatment (AP-2, 3, 5 and 6 were below detection limit).

The measured soil gas radon activity concentration profile from plot AP-1 (Figure 56) does not follow the curve predicted by theory (Figure 3). In light of the dissimilarity between the

measurements and gas diffusion theory, two interpretations are possible: a surface layer of soil with higher radon production rate is underlain by a subsoil low in radium; or more likely a "standard" soil profile is present at the site, as evidenced by the 10 cm and 20 cm points, but the deeper samples have been diluted by draw-down of atmospheric air along a preferential flow pathway between the sampler tube and the soil. Whilst the slide hammer attachment was used and a noticeably smaller amount of force was required for sampler insertion than at previous sites (Sections 5.2, 5.3), the tendency of clay soils to retain shape once deformed coupled with the lower porosity of clay soils probably leads to the same effect; atmospheric air dilutes samples, particularly at depth when the risk of preferential flow pathway formation is largest. Radon concentrations are still within detection limits due to the relatively large concentrations present within the soil gas ($\sim 5300 \text{ Bq m}^{-3}$ at 20 cm depth).

The likelihood of spatial variation in the soil radium concentration or otherwise being a factor in other profiles being below detection limit is remote as all soil on the site is of the same parent material. Particularly in the clay soils of the Allerton Project site, preventing the formation of pathways to atmosphere in the soil surrounding the sampler was difficult.

Of the ploughed plots sampled, only the profile obtained from plot AP-4 (Figure 56) possessed activity concentrations above detection limit at all depths sampled: soil gas samples down to 30 cm depth displayed the expected increase in radon activity concentration with depth. The sample from 40 cm however probably suffered from atmospheric dilution along with the remaining two profiles AP-5 and AP-6, in which all soil gas samples possessed radon concentrations below detection limits.

5.6 Boundary Plantation field site (Sherwood Forest soils)

5.6.1 Site description: Boundary Plantation

Boundary Plantation lies on the north side of Sherwood Forest in Nottinghamshire, UK: 53.21512 °N, 1.09919 °W ("SF", Figure 4). The plantation used sampled consists of a stand of Corsican pine trees (*Pinus nigra* var. *laricio*) covering ~3.39 ha, with a standing crop of around 283 m³ ha⁻¹ (Forestry Commission 2013, private communication).

Boundary Plantation has been previously sampled for surface soil and leaf litter, for the purpose of measuring historic radioactive fallout; measurements of uranium concentrations have also been made (Itthipoonthankorn 2017). Based on previous measurements the surface soil can be described as an uncompacted sandy loam with ~55% organic matter in the upper 5 cm (Figure 57).

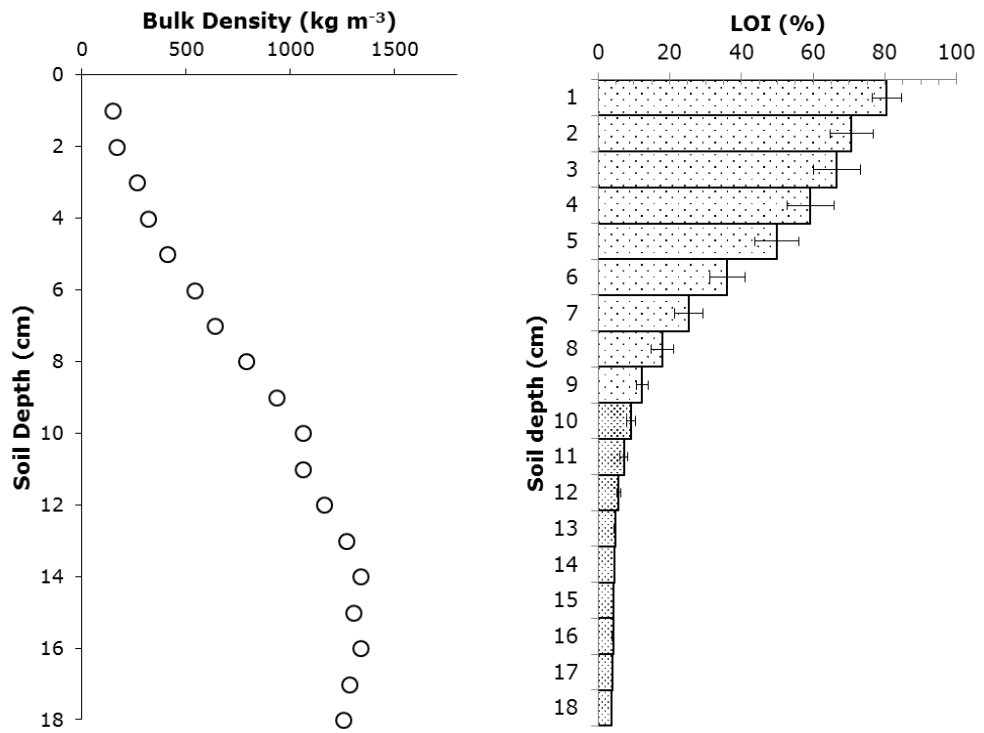


Figure 57: Bulk density and gross organic matter (LOI) profiles in the soil underlying Sherwood Forest Boundary Plantation (from Itthipoonthankorn, 2018).

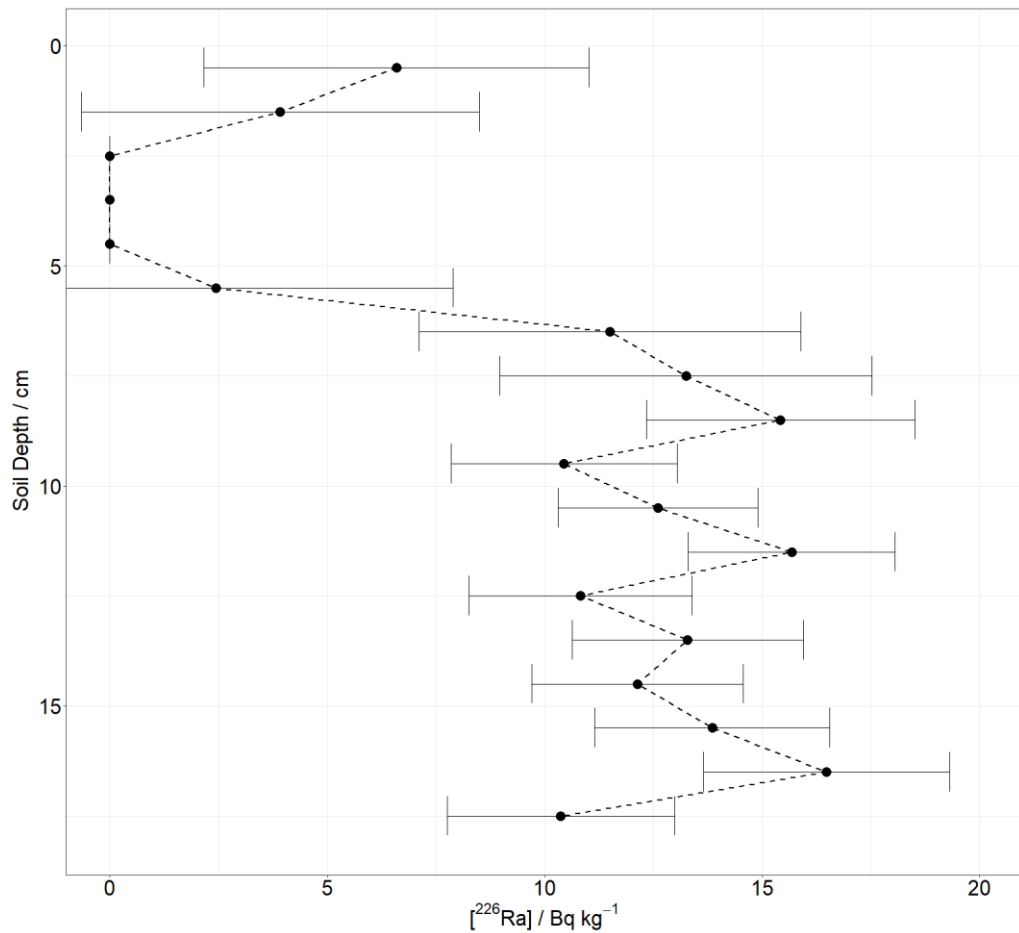


Figure 58 ²²⁶Ra activity concentration profile in the soil underlying Sherwood Forest Boundary Plantation (calculated from Itthipoonthankorn, 2018) data.

5.6.2 Findings

Three soil cores were collected and six ²²²Rn activity concentration profiles were measured on 09/05/2019. At each of the three sampling sites (1, 2, and 3,

) two soil gas profiles were sampled before the extraction of a single soil core of length 90 cm.

As previously described, the soil at the site comprises a sandy loam overlying sand. On the forest floor there is a well-developed layer of partially decomposed organic matter and significant understorey vegetation.

Table 11: Sherwood Forest sampling locations.

| <i>Location</i> | Profile designations | °N | °W |
|-----------------|-------------------------|----------|---------|
| <i>1</i> | SF-1, SF-2 | 53.21476 | 1.09797 |
| <i>2</i> | SF-3, SF-4 | 53.21452 | 1.09882 |
| <i>3</i> | SF-5, SF-6 | 53.21498 | 1.09740 |

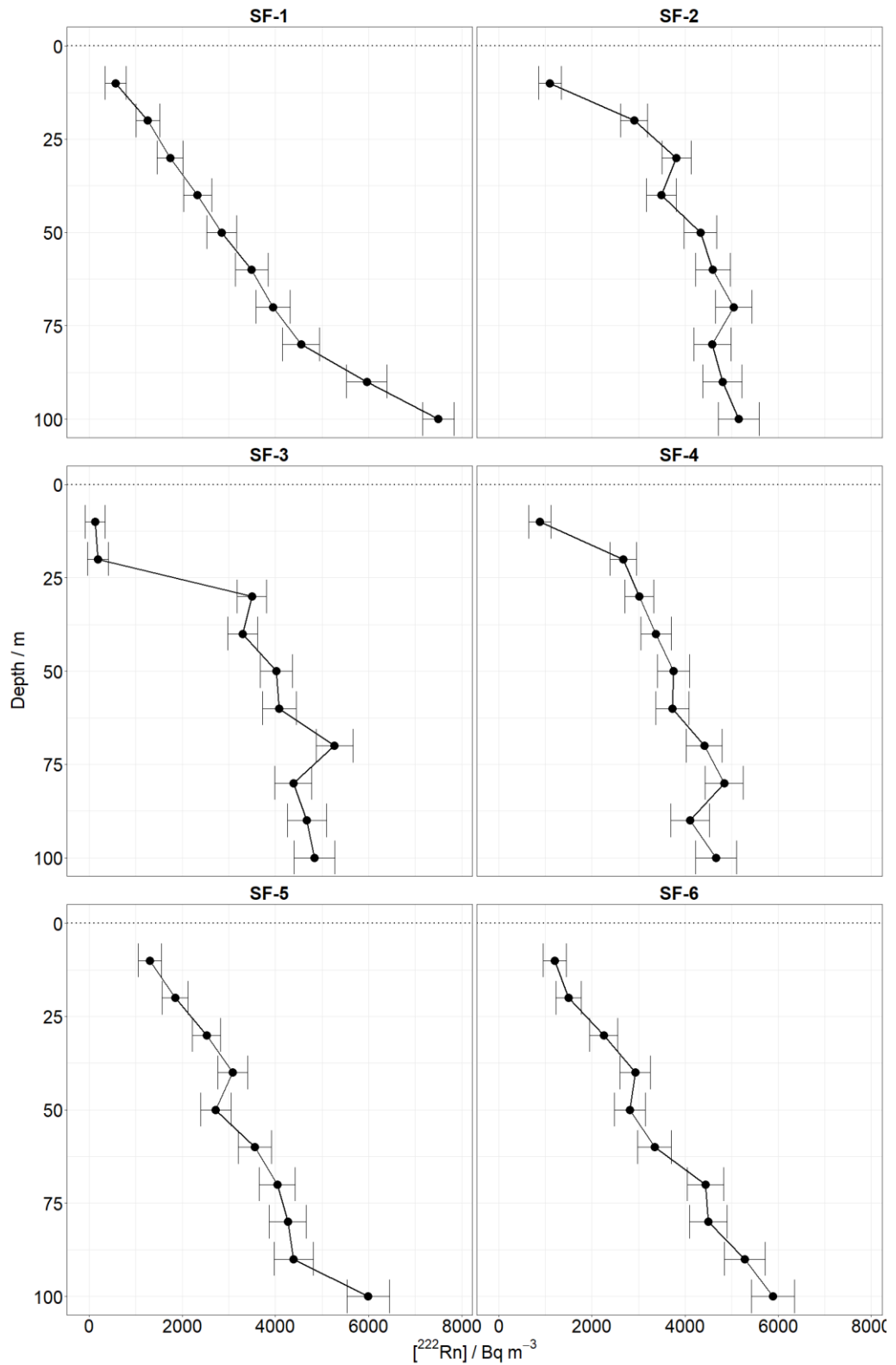


Figure 59: Soil gas radon activity concentration profiles from Boundary Plantation. Each row is a separate location within the compartment (cf.

).

Within location 1 (

), profile SF-1 displays a much more uniform increase in radon activity concentration with depth than profile SF-2 (Figure 59), with a further increase at depth that is beyond that which would be seen in a soil with constant production rate and single diffusion coefficient (as exemplified in Figure 3). A possible explanation is that a localised feature such as an iron pan is restricting gas transport and causing an area of localised radon build-up.

Profiles SF-3 and SF-4 (Figure 59) are much like profile SF-2 albeit with much lower activity concentrations towards the surface. Low activity concentration is probably due to the lower bulk density and radon production rate in the organic layer of the soil. Whilst theory (Figure 3) suggests a decrease to zero at the surface of the soil due to an upper boundary (atmospheric) radon activity concentration approaching zero, organic layers and vegetation serve to act as a boundary. Inclusion of varying radon production rate in computer models is possible, however, specifications must be set per soil. The sampling resolution of 10 cm make the analysis of radon distribution and behaviour within these layers difficult to characterise.

Profiles SF-5 and SF-6 (Figure 59) did not display such low activity concentrations towards the surface, but still exhibited behaviour expected of such soils, supporting the theory that surface behaviour varies in a way that is specific to a measured point, even within one sampling area. The variability of gas diffusion in soils is therefore at least as great as the variability of the soil surface vegetation and litter.

The rapid decrease in radon activity concentrations towards the surface of the soil is not only due to the diffusion process itself at Boundary Plantation, but also due to the lack of parent material (and so minimal radon production) in the organic surface layers (Figure 58).

5.7 Discussion: field section

At a range of field sites with quite different physical characteristics various physical anomalies made sampler insertion and/or removal difficult, ranging from simple stony soils at Kingston (Section 5.2.1), to clayey soils at Hollin Hill and Allerton (Sections 5.5.1, 5.3.1), to extreme soil compaction and tree roots at Bagworth Heath (Section 5.4.1).

Most study sites displayed variable vegetation cover. As at the ex-ASGARD site (Section 4.1) vegetation cover varied through the monitoring period and may have influenced soil gas transport in a similar fashion to periodic snow cover (Fujiyoshi et al., 2010).

Numerous samples were to contain no measurable radon activity concentrations, even though it is known that all geological materials have some degree of radon production potential. The most plausible explanation for samples with radon activity concentrations below detection limit is preferential flow along the body of the sampler, resulting in dilution of samples with air from the free atmosphere above the soil, regardless of the amount of care taken on insertion.

With variation seeming to occur on a spatial scale much smaller than the maximum 10 cm sampling resolution Hollin Hill, modelling of gas diffusion at the discussed sites cannot be reasonably modelled using the employed method; however, the soils at the ex-ASGARD site and Boundary Plantation (Sherwood Forest) appear to conform to expected theoretical diffusion behaviour (Section 2.6). Estimations of the soil gas radon diffusion coefficient D_s have thus been made for the ex-ASGARD site over time, and Boundary Plantation over space.

6 Results: computational soil gas modelling

Fitted values of D_s as resolved by the model are presented in this section. Models were run using $dx = 0.01\text{ m}$, $dt = 800\text{ s}$, and radon emanation as calculated from (3.16) and (3.17). An analysis of the sensitivity of the model to the radon emanation rate is provided in Section 7.2.5.1.

Some radon activity concentration profiles do not exhibit the same characteristic shape as is expected from theory (Figure 3). The reason for this is unknown but might be due to highly localised inclusions / soil layers. The presence of macropore features and fractures due to physical or biological action may also play a role.

When the characteristic shape of the radon activity concentration profile is observed, close model fits can be obtained without the addition of extra variables. Close fits to data by a simple model of diffusion supports the hypothesis that the movement of radon (and other gases) in soils is primarily by diffusion.

The diffusion model described in Section 3.6 and provided in Appendix has been fitted to the observed radon concentration profiles from the ex-ASGARD site and from Boundary Plantation (Sections 4.3.1, 5.6.2). Fitting was achieved by calculation of the radon production rate in each layer of the soil, using measured ^{226}Ra parent material concentration data as well as soil moisture content data where available, followed by adjustment of the diffusion coefficient D_s . The model yields D_s estimates for each measured profile over the course of the monitoring period considering the soil physical characteristics,

including (in the case of the ex-ASGARD site) the observed variation in soil moisture with time (Figure 34).

6.1 Temporal variability of gas diffusion in soil (ex-ASGARD site)

Computed values for soil gas radon activity measurements over the sampling period are displayed in Figure 60. Diffusion coefficient were highest in spring and summer: values as high as $2.46 \times 10^{-6} \text{ m}^2 \text{ s}^{-1}$ were computed (literature values are as high as $8.5 \times 10^{-6} \text{ m}^2 \text{ s}^{-1}$). In autumn and winter, diffusion coefficients were lower: values as low as $1.99 \times 10^{-7} \text{ m}^2 \text{ s}^{-1}$ were computed (literature values for sandy soils are as low as $2 \times 10^{-7} \text{ m}^2 \text{ s}^{-1}$).

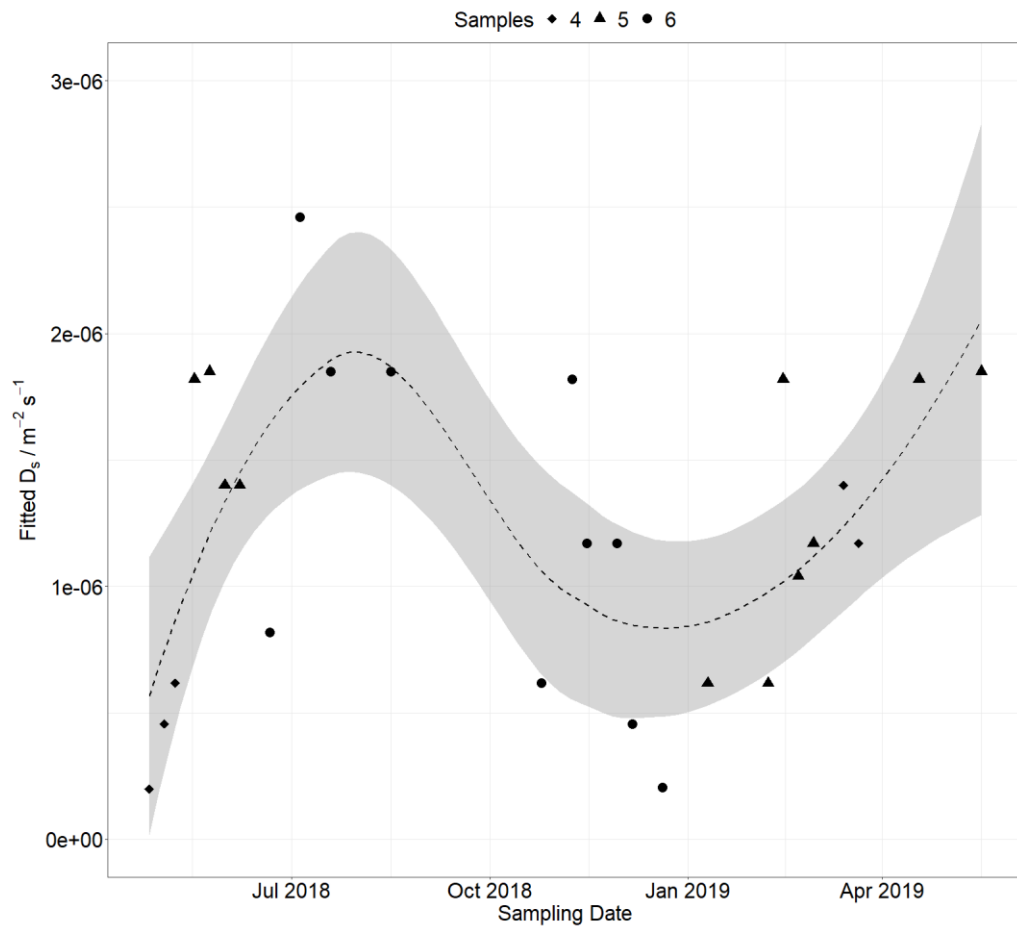


Figure 60: Fitted diffusion coefficients vs. sampling date. Profiles with maximum depth 50 cm, 75 cm and 100 cm are shown by squares, circles and triangles, respectively. Shading represents a fitted 95 % confidence interval for trend illustration.

In both the spring/summer periods studied, March to August 2018 and March to June 2019, fitted D_s values increased by a factor of 2, as soils dried resulting in decreasing pore network tortuosity; gas movement became less restricted in the ex-ASGARD soil over the spring to summer months. The period from September 2018 to January 2019 saw D_s decrease by a factor of 2, as soils became wetter and pore network tortuosity

increased; gas movement became increasingly impeded over the autumn to winter months.

The number of depth measurements in a sampled profile varied between sampling points because the water table depth varied throughout the monitoring period, causing some samplers to be surrounded by saturated soil.

Profiles were fitted using soil volumetric water content where possible to estimate radon emanation with depth (Section 3.13.2.1). Where soil VWC was used, goodness of fit ranged $0.848 < r^2 < 0.990$ with critical values from $p < 0.01$ to $p < 0.1$. Excluded from Figure 60 are cases where soil radon emanation was assumed to be constant. In these nine cases goodness of fit ranged $0.817 < r^2 < 0.959$ with critical values from $p < 0.01$ and four fits not statistically significant according to the employed method ($p > 0.1$).

Figures 46–50 show measured radon activity concentrations (plotted as points) with accompanying modelled data represented by dashed lines. The horizontal dotted line represents the soil surface. Statistics to represent goodness of fit are sometimes included in literature and so are displayed on each model-data plot here for reference. Goodness of fit for each individual plot can be assessed visually.

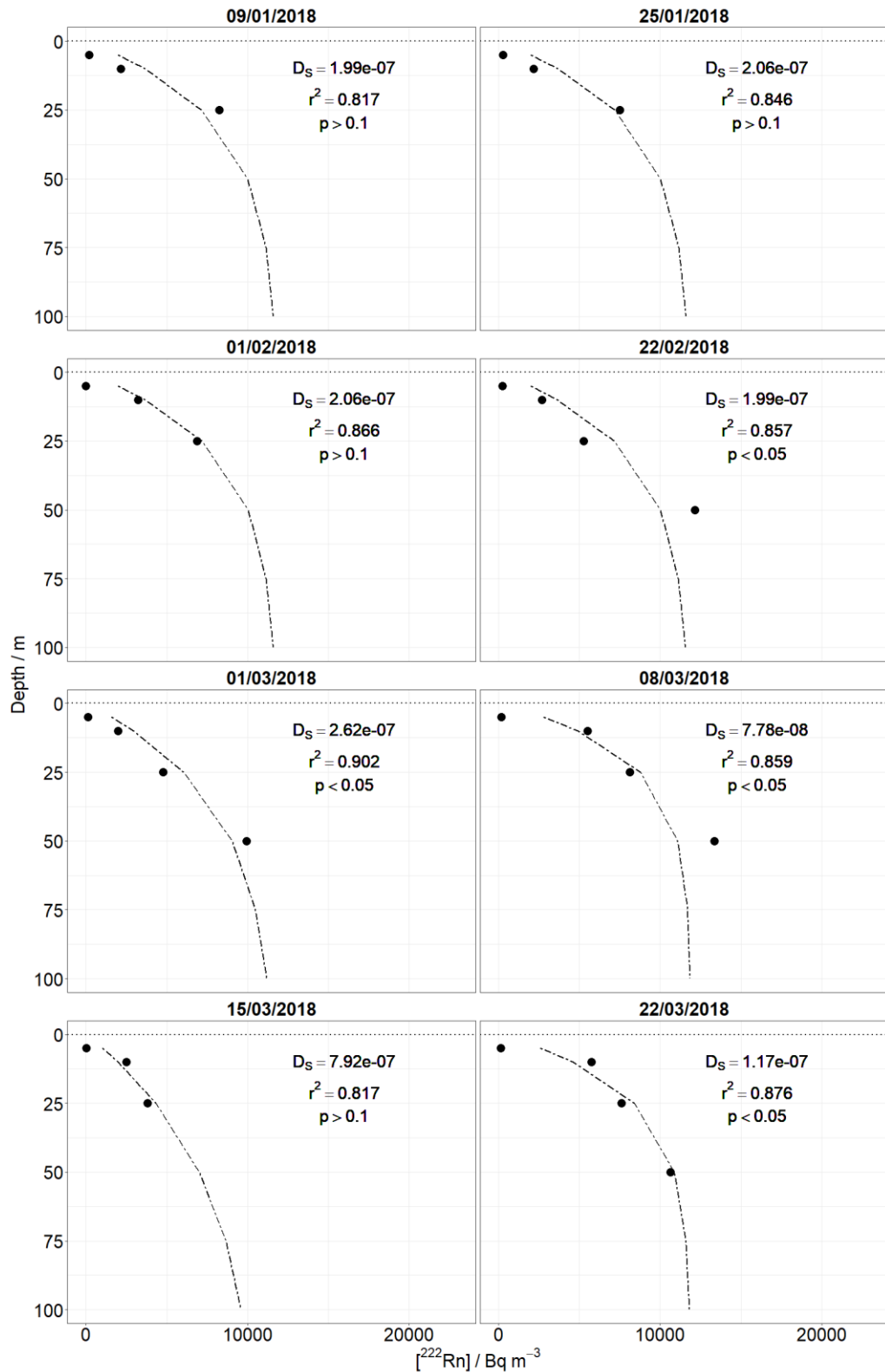


Figure 61: Measured soil gas radon activity concentration data with fitted profiles, January to March 2018. Fitting involved an assumed fixed radon emanation rate.

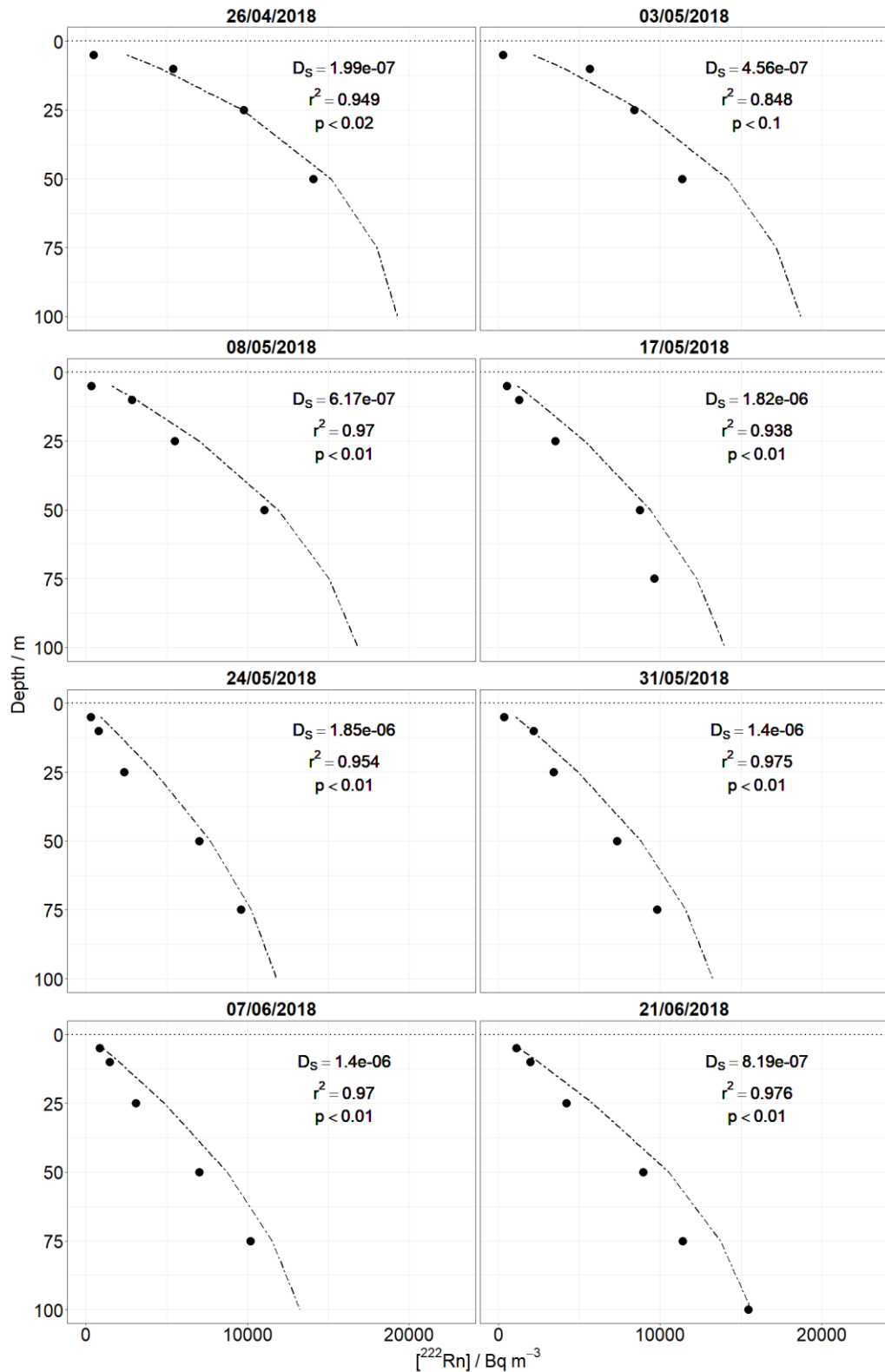


Figure 62: Measured soil gas radon activity concentration data with fitted profiles, April to June 2018.

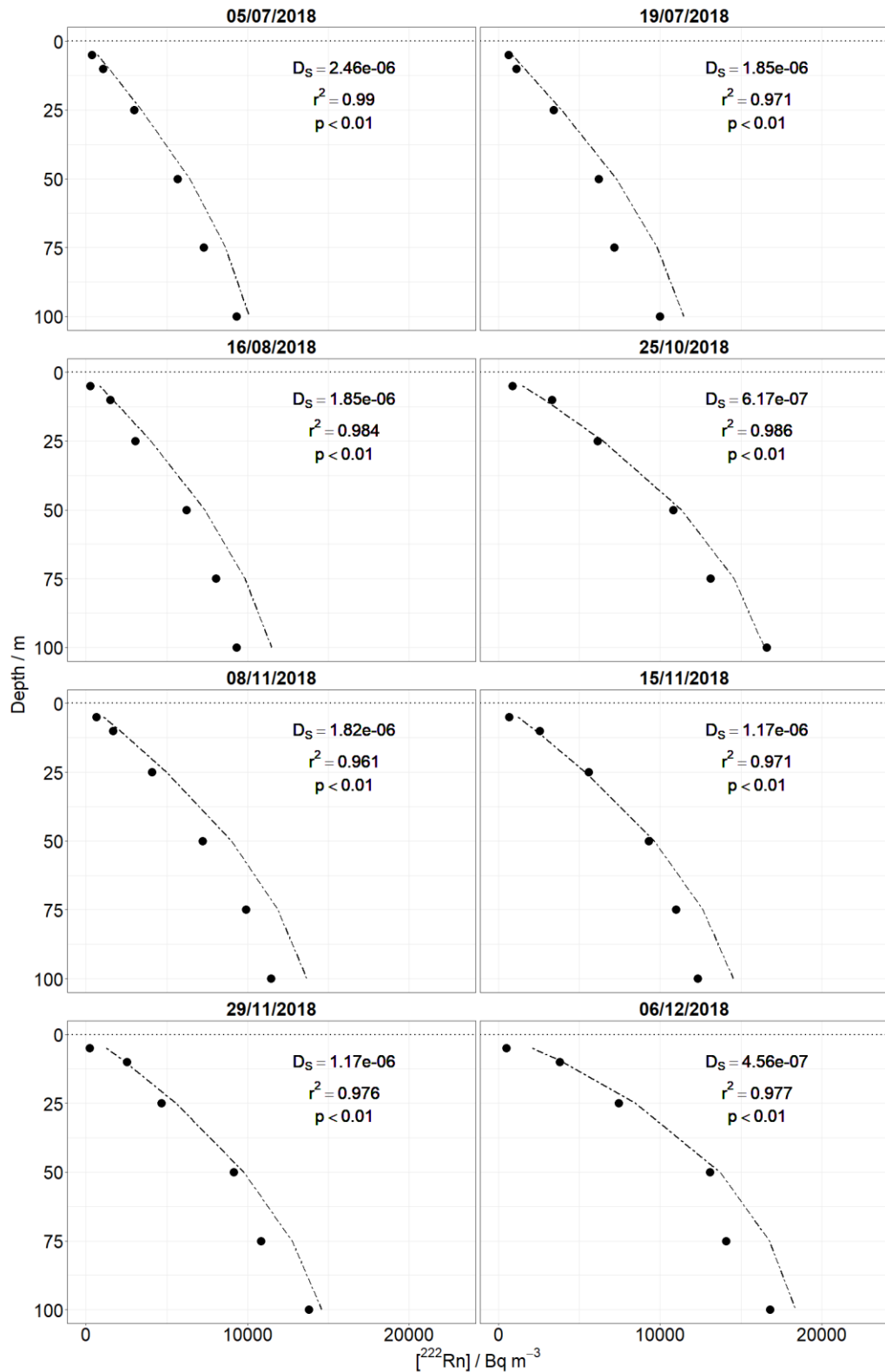


Figure 63 Measured soil gas radon activity concentration data with fitted profiles, July to December 2018.

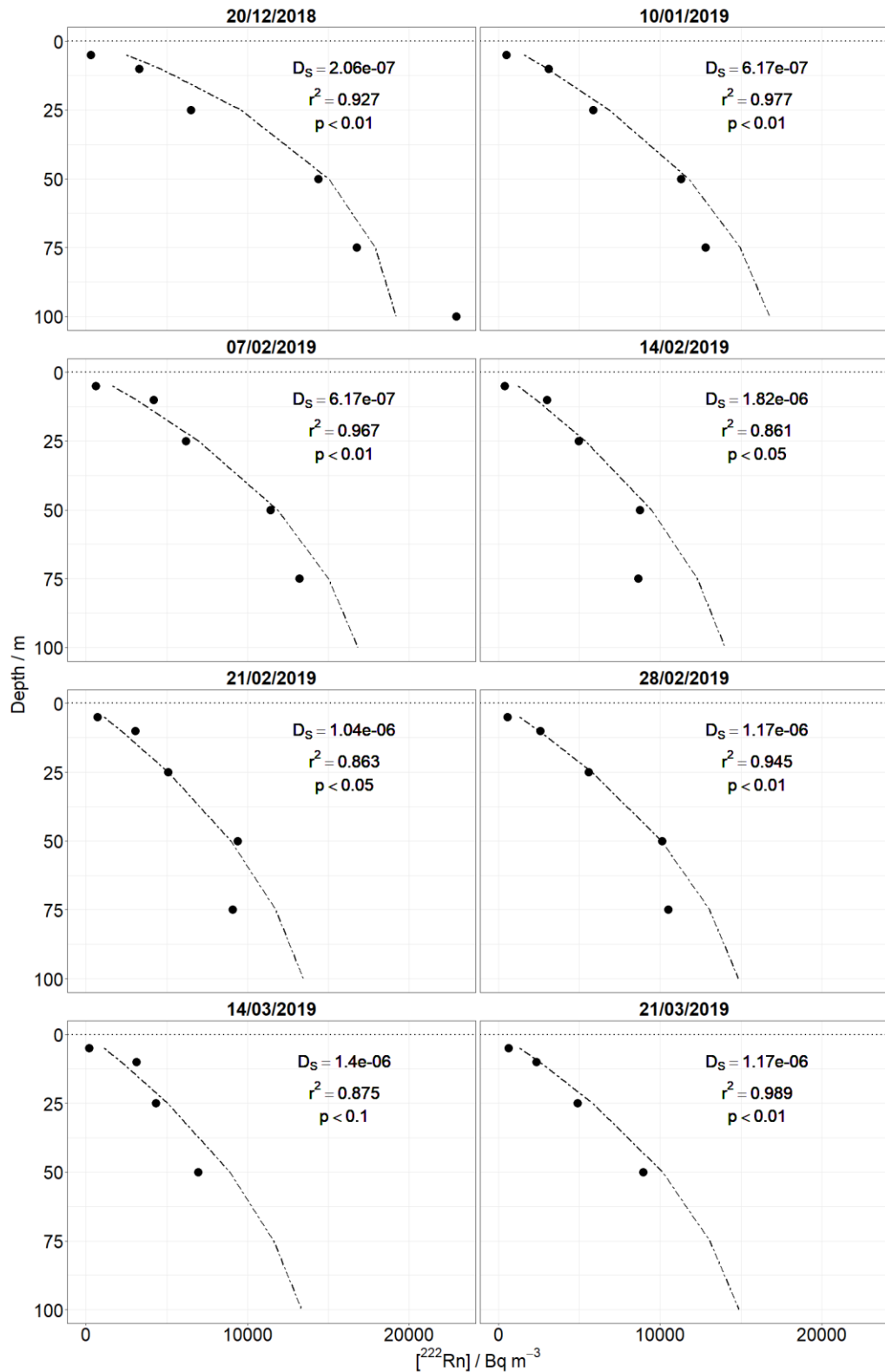


Figure 64: Measured soil gas radon activity concentration data with fitted profiles, December 2018 to March 2019.

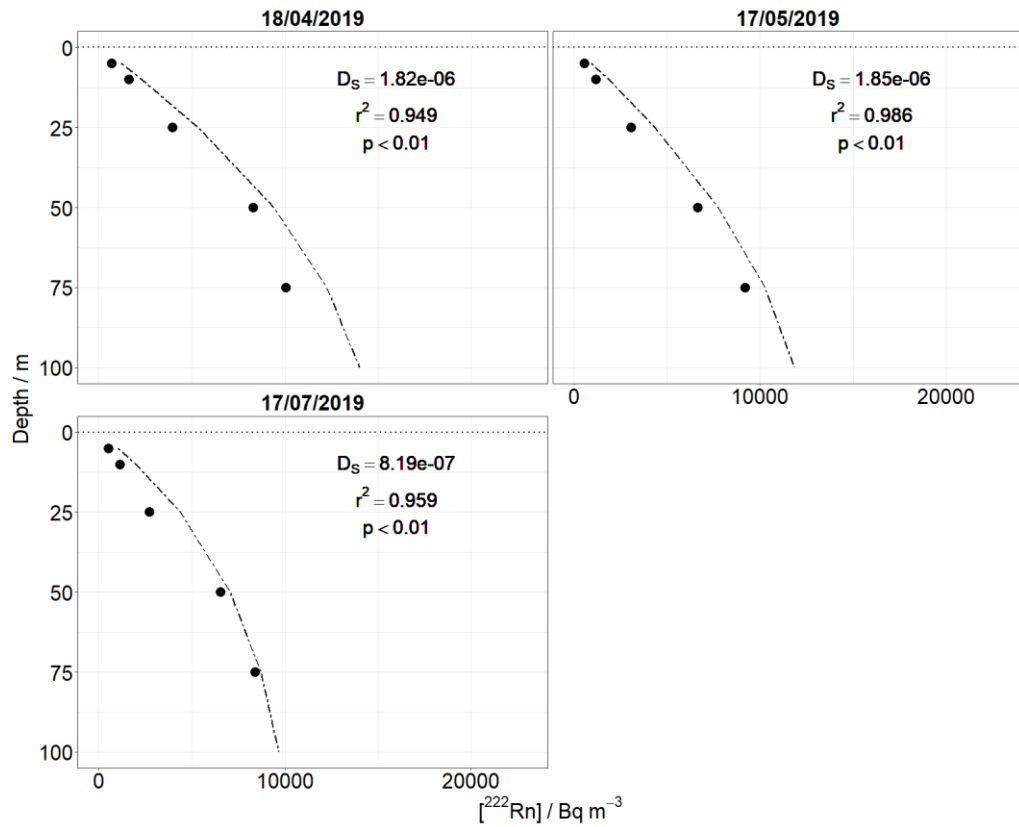


Figure 65: Measured soil gas radon activity concentration data with fitted profiles, April to July 2019. Fitting of profile 17/07/2019 involved an assumed fixed radon emanation rate

6.2 Spatial variability of gas diffusion in soil (Boundary Plantation, Sherwood Forest).

In cases where a field site is visited only occasionally, single concentration profiles can be analysed as shown previously. Measured soil gas radon activity concentrations from Boundary Plantation (Section 5.6.1) appeared to broadly follow the expected theoretical monotonic increase with depth (Figure 66). For fitting, radon emanation was assigned a constant value of $0.025 \text{ Bq m}^{-3} \text{ s}^{-1}$ as soil physical characterisation was not carried out to the same level of detail as for the ex-ASGARD site. Due to the $\sim 55\%$ organic material content (Figure 57) and sections of low or zero ^{226}Ra parent material activity (Figure 58), a value of 0.014 Bq s^{-1} was employed for the initial 10 cm. The estimated radon emanation coefficient was within the range used for the sandy soils of the ex-ASGARD site (Section 3.13.2.1).

Comparisons of modelled and measured radon activity concentrations for Boundary Plantation are displayed in Figure 66. Based on the model fits, radon diffusion coefficients were estimated to lie between $2.20 \times 10^{-6} \text{ m}^2 \text{ s}^{-1}$ and $2.83 \times 10^{-6} \text{ m}^2 \text{ s}^{-1}$, which are within the literature range for a sandy soil (Table 2). Goodness of fit ranged $0.678 < r^2 < 0.932$. All fits are statistically significant to $p < 0.05$ with five of the six fits being significant to $p < 0.01$ according to the method employed.

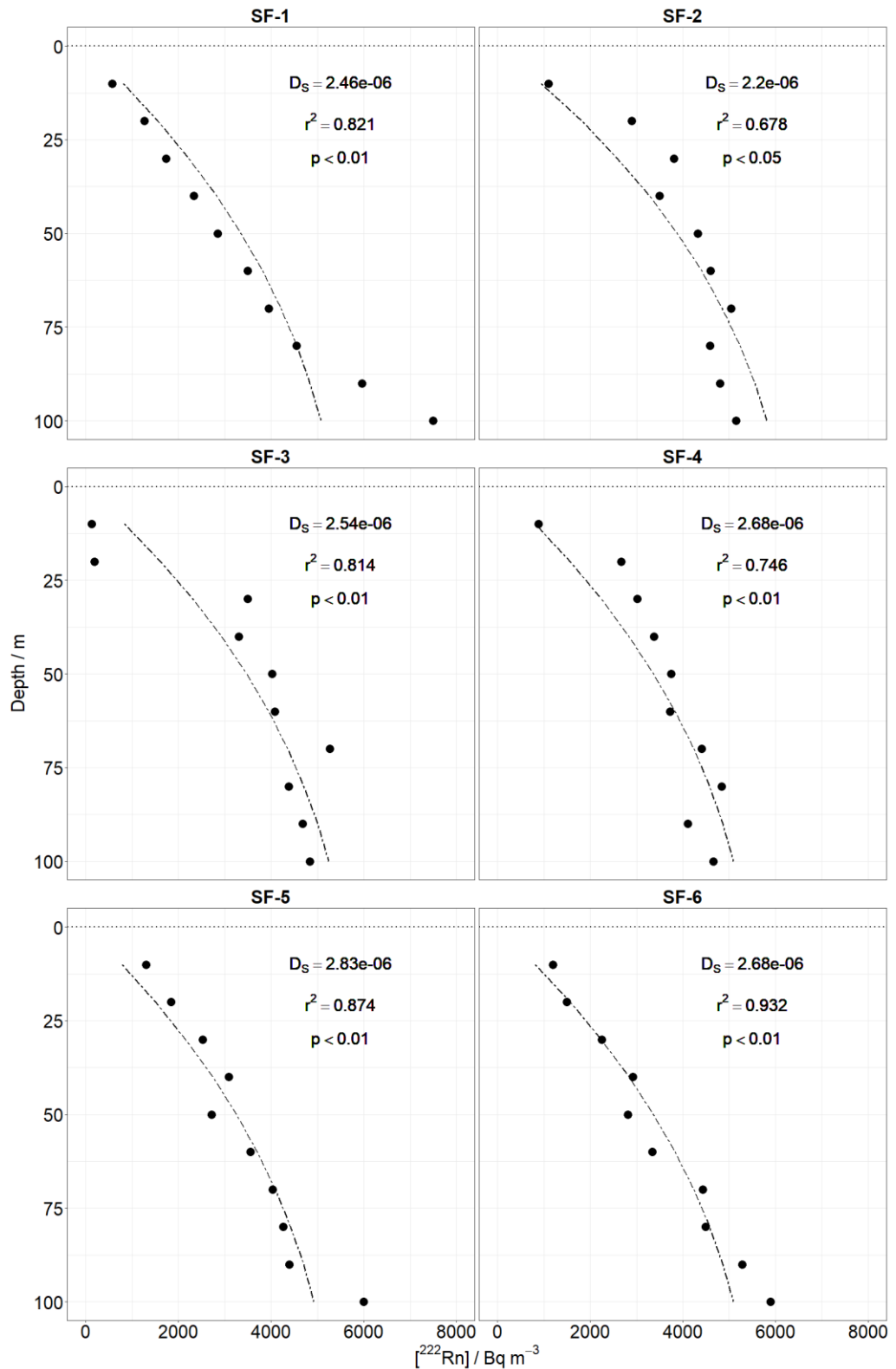


Figure 66: Measured soil gas radon activity concentration data with fitted profiles for Boundary Plantation. Fitting involved an assumed fixed radon emanation rate.

6.3 Discussion: modelling soil gas dynamics

The computational algorithm devised and employed in the present study has allowed the quantification and visualisation of soil gas transport characteristics for a time period spanning several seasons during which extreme wet and dry periods were encountered.

All fitted profiles have provided estimates of the effective diffusion coefficient for radon within literature ranges for their soil types; diffusion coefficients for loamy soils are typically within one order of magnitude and values for wet clay soils are several orders of magnitude smaller still (Table 2).

Within the monitoring period there was a period of extremely dry weather followed by very wet conditions. The observed initial increase in D_S (Figure 60) covers the drought conditions during the 2018 British Isles heatwave (from June to August). The drought saw a sustained decline in soil volumetric water content of the ex-ASGARD site from 12 % to 0 % at the surface, and 35 % to 25 % at 1 m depth (Figure 34). As shown earlier (3.17), below a value of 0.1, soil volumetric water content affects soil radon emanation and so incorporation of soil volumetric water content into the model was necessary.

Single visits to field sites do not allow for the detailed analysis of soil physical characteristics required for estimation of the soil radon production rate, so fitted profiles are a general indication of soil texture variation with depth (goodness of fit), and general soil texture (order of magnitude of D_S). Comparisons of D_S value between spatial points at a site are possible; however, inter-site comparison is less certain. Nonetheless, the fitted D_S values for Boundary Plantation soils are in the order 2.5×10^{-6} , much

higher than for the ex-ASGARD site at a corresponding time of year ($6.17 \times 10^{-7} \text{ m}^2 \text{ s}^{-1}$ the previous day), around the D_s of the ex-ASGARD soil on 05/07/2018 (Figure 63) when soils of the ex-ASGARD site were nearing their driest (Figure 34).

When soil volumetric water content was included in the radon emanation calculation, all fitted profiles were statistically significant to $p < 0.5$. Critical values $p > 0.5$ were obtained by fitting profiles without access to soil volumetric water content data; however, the profile fits in question possess only one degree of freedom ($n = 3$) and so may not be statistically significant even if soil volumetric water content data were available. Future work should attempt to increase the sample number in a soil profile by assessing soil air-filled porosity and decreasing the inter-sample spacing accordingly.

7 General Discussion

The primary objective of the research presented in this thesis was the use of belowground soil gas radon activity concentrations to estimate the soil gas radon diffusion coefficient, by fitting measured data to a bespoke numerical model. A non-invasive method of obtaining estimates of D_s is desirable as methods for characterising soil gas transport behaviour in soils can involve invasive measurement of soil physical characteristics (e.g. Boon et al., 2013). The following sections assess the extent to which this thesis has fulfilled its aim. The outputs obtained will be compared with those that exist in literature and future directions of this work will be discussed.

In addition, as part of the research, the requirement for more comprehensive long-term observations of soil gas radon (Rose et al., 1990) has been addressed, and these observations have been used to visualise the changes in the soil gas transport behaviour over time and space. The soil gas sampling method employed and developed in this research enabled soil gas sampling down to depths of approximately 1 to 1.5 m (1.7 m maximum sampling depth achieved), and effective measurement of radon activity concentrations in gas samples from sandy soils to a depth of approximately 1 m.

Numerical models using Fick's Law have been shown to be a valid approach to approximating soil gas transport characteristics, including surface fluxes in simplified systems and belowground gas concentrations, with representations of soil gas dynamics in the literature correlating with measured datasets both from the laboratory and the field (Maier and Schack-Kirchner, 2014; Hafez and Awad, 2016; Maeng et al.,

2019). Many assumptions have been made in the creation of such models, and some have been challenged. In the following sections some suggestions are made to improve model fitting to data and/or increase the general validity of such approaches, considering recent findings and existing literature.

7.1 Literature estimations of soil gas diffusivity

In the context of determining changes in soil gas transport behaviour over time or space, it has been shown in the present research that temporal changes can be much greater than spatial changes; radon gas activity concentrations in soil have been reported to vary by factors of 1.3 and 4.5 temporally (over one month, Maeng et al., 2019; and over three months, Fujiyoshi et al., 2013); a factor of 5 spatially (at 1 m depth across 400 m, Kunze et al., 2013); and in extreme cases (volcanic soils) increasing from below detection limit to in excess of 150 kBq m^{-3} (Silva et al., 2015). In the present study, soil gas radon activity concentrations varied temporally at ex-ASGARD by a factor of 6 at 10 cm depth and by a factor of 1.5 at 1 m depth over ~ 18 months (Figure 61–Figure 65). Spatially at Boundary Plantation, soil gas radon activity concentrations varied by a factor of 12 at 10 cm depth and by a factor of 1.5 at 1 m depth over ~ 50 m (Figure 66). The large variation in surface activity concentrations may be due to the different vegetation patterns present at field sites across the globe.

Table 12 Summary of literature findings on the variability of soil gas radon activity concentrations

| Study | Variation | Location | Conditions |
|-------------------------------|---|--------------------------------|----------------------------------|
| <i>This study</i> | ×6 (10 cm depth) ×1.5 (100 cm depth) | Single location over 18 months | Sandy loam soil |
| | ×12 (10 cm depth) ×1.5 (100 cm depth) | Locations separated by ~50 m | Sandy loam soil |
| <i>Silva et al., 2015</i> | Increasing from below detection limit to in excess of 150 kBq m ⁻³ (60 cm depth) | Single location over 24 months | Volcanic soils (active) |
| <i>Fujiyoshi et al., 2010</i> | ×4.5 (80 cm depth) | Single location over 3 months | Soil under snowpack |
| <i>Kunze et al., 2013</i> | ×5 (1 m depth) | Locations separated by 400 m | Soil overlying salt dome |
| <i>Maeng et al., 2019</i> | ×1.3 (mean of a 1 m depth profile) | Single location over one month | Soil before and after rain event |

In terms of fitted soil gas radon diffusion coefficients, spatial variation at Boundary Plantation was by a factor of 1.3 over ~50 m, and temporal variation at ex-ASGARD was by a factor of 2 over the course of an annual cycle. Temporal variation in soil gas transport behaviour is likely to be visible regardless of whether atmospheric phenomena are accounted for in the upper 20 cm of modelled systems.

Table 13 Summary literature values on soil gas diffusion variability.

| Study | Data | Model design | Findings |
|--|--|--|--|
| <i>Current study</i> | UK Sandy loam soils Probe method Liquid scintillation counting ^{222}Rn | Single-layer diffusion with diffusion-only boundary condition. | High correlation ($R^2 > 0.677$), between measured data and numerical model. |
| <i>Antonopoulos-Domis et al., 2009</i> | Greece Unknown soil texture Fixed detectors ^{222}Rn | One- and two- layer [soil-soil] 1-D systems, diffusion and diffusion-advection boundary conditions | Diffusion-only boundary is acceptable where non-surface concentrations are concerned |
| <i>Levintal et al., 2019</i> | Laboratory columns Particle size 0.09–4 cm CO_2 | Single-layer diffusion with diffusion only boundary condition | High correlation ($R^2 > 0.977$) between measured data and numerical model |

| | | | |
|-----------------------------|---|---|--|
| <i>Savovic et al., 2011</i> | Laboratory column with separate headspace measurements Unknown soil type Unknown detector ^{222}Rn | Explicit one- and two- layer [soil-air] systems, diffusion only boundary condition | Both systems gave equal estimations for equilibrium conditions |
| <i>Hafez and Awad, 2016</i> | ^{222}Rn data from literature sources including Kunze et al., 2013 | Multi-layer system with diffusion-advection boundary condition | Correlation $R^2 = 0.691$ |
| <i>Fierer et al., 2005</i> | California, USA Grassland loam Permanent probes <i>in situ</i> ^{222}Rn and CO_2 | Fick's Law aggregated model (Davidson and Trumbore, 1995) | "good correlation" |
| <i>Maeng et al., 2019</i> | Korea Unknown soil type Probe (continuous) ^{222}Rn | Single-layer diffusion with diffusion only boundary condition | Visibly strong correlation |

The concept of “enhanced diffusion”, i.e. fluxes greater than expected by diffusion alone and yet not due to advection, has been cited in explanation of the difference between measured and modelled results concerning diffusion in porous media (Levintal et al., 2019 and references therein). The phenomenon is not suggested here due to its presence being reported only in porous media with particle size >2 cm.

7.2 Literature approaches

While the approach of fitting a numerical model to data is practiced in literature (Levintal et al., 2019; Hafez and Awad, 2016) some reports feature only simple polynomial fits to measured data (Fujiyoshi et al., 2013; Nguyen et al., 2018). Simple polynomials are useful in displaying trends; however, the success in the present study of fitting an, albeit relatively simple, 1-D diffusion model to measured soil gas concentration data cannot be ignored and therefore numerical modelling should be employed when assessing soil gas transport characteristics in future, whether it is by way of bespoke computational modelling, as in the current research, or by assessing previously reported representations of the soil gas diffusivity (Table 1; Pingintha et al., 2010).

7.2.1 Fitting method

The fitting method utilised (minimisation of the residual error) has been employed in similar studies (Antonopoulos-Domis et al., 2009; Levintal et al., 2019); however, root-mean square error might be a better indication of fit of the model to the data, as was utilised by Pourbakhtiar et al., (2017) for model fitting. Nonetheless, the fitting method utilised in this work has provided fits to the data that are clearly appropriate and which effectively show the underlying temporal trend(s) in soil gas radon activity concentrations.

Counting error (two-sigma, 95 %) of radon activity concentrations have not been utilised in fitting theoretical activity concentration curves. Model fitting which takes account of measurement errors would involve sampling from a distribution for each measured point and constructing a distribution of fitted D_s values. Calculating theoretical profiles for multiple statistical samples from each measured profile would increase computational time substantially and, therefore, future work considering the analytical error in radon measurement would require computational methods more efficient than those employed in this research. As fitting values of D_s to three significant figures also represents a small range of fits to the data (previously discussed in Section 7.2.1), it is unlikely that inclusion of radon activity counting error will have any effect on the fitted values of the soil gas radon diffusion coefficient.

Many fitted profiles appear to have residuals that are distributed non-normally i.e. more data points lie on one side of the model than the other (profile "17/05/18", Figure 62). This is due to the fact that the grid search method employed (Figure 25)

approaches the data “from one side” and since D_s is only being calculated to a set precision, will often stop at a point where an observer may believe a better fit is possible; such a fit would have the same value of D_s , to the displayed precision.

Advanced fitting methods include Monte Carlo simulations, recently used by Feng et al., (2019) in addition to a probability model for soil pore size, to estimate radon diffusion coefficients in porous media (non-soil) to within 15 % of measured values without using further parameters such as moisture, temperature, or pressure.

7.2.2 Goodness of fit and statistical significance

The results of the current research have shown that calculations based upon Fick’s Law result in models strongly correlating with measured soil gas transport data, as have similar approaches from literature sources (Fierer et al., 2005; Pingintha et al., 2010; Levintal et al., 2019; Hafez and Awad, 2016).

Of the cited literature sources, some have reported r^2 goodness of model fits to data, with or without corresponding critical values (Pingintha et al., 2010). Other studies have presented correlation data without critical values (Levintal et al., 2019; Hafez and Awad, 2016). Both r^2 and p have been included for reference in the current work; however, the relevance of such statistics is questionable, especially concerning nonlinear models. A simpler and more effective solution to correlation statistics would be simply to allow objective goodness of fit to be established by readers in light of theory (Hooper et al., 2008), an approach taken here particularly with discussion

surrounding the effect of surface windspeed on gas transport. In any case where r^2 and p are included with model fits, readers must take care as indices can sometimes indicate good overall fit when specific parts of a model are in fact not providing suitable explanation of the data (Tomarken and Waller, 2003).

7.2.3 General model assumptions

The assumption of steady-state conditions in a soil, particularly at greater temporal resolutions, has been questioned (Maier and Schack-Kirchner, 2014). As an example, in the specific case of soil CO₂, post-rainfall dissolution of the gas dramatically altered measured concentrations. Such behaviour is not observed in the case of radon gas. It has been shown in this work that in a sandy soil the assumption of steady state concentrations holds for intervals >1 h, as measured activity concentrations do not deviate from one another.

Some assumptions made during this research may not be suitable for certain field sites. For example, significant horizonation in soil profiles might allow localised areas of preferential flow or gas build-up in the subsurface soil. It has been shown that D_s values are not static either spatially or temporally. Non-static D_s within a single profile could explain some of the poorer model fits observed in this research, such as profile SF-1 (Figure 66). Some soil gas profiles not displaying the expected activity concentration distribution is unavoidable when measuring environmental variables *in situ*. Elucidating and accounting for such variables is valid and can be worthwhile (Baykut et al., 2010, Silva et al., 2015).

7.2.3.1 Variation in model parameters

Utilising a second medium for the atmosphere when modelling a soil-air system has previously been investigated (Savovic et al., 2011); however, differences between the more complex models and a soil-only system were shown to be near-zero once a model has reached equilibrium. All models in the current research were run to equilibrium. Use of multiple media representations within the soil, however, can clearly be appropriate within numerical models in some cases (Figure 69), despite the increase in model fitting complexity.

7.2.3.1.1 Variability of diffusion coefficient with soil depth

Literature model fits for radon profiles vary in quality but overall correlate well with measured datasets. The model fits from the current work are similar in goodness-of-fit to those of Levintal et al. (2019) and Hafez and Awad (2016) as well as the apparent correlation of Fierer et al. (2005). Many other fitting operations utilise non-static values of D_s with soil depth. It has been shown in the current work that differences in the soil gas transport behaviour over time as well as over space can be visualised without the extra model complexity that comes with a dynamic value of D_s . Taking the fitting by Hafez and Awad (2016) of a numerical model to the data of Kunze et al. (2003) and Antonopoulos-Domis et al. (2009) as examples, multiple values of D_s provide a clear improvement in model fit to data in some soils (Figure 68, Figure 67). In the case of the current research, however, a single value of D_s has appropriately explained the

measured data with profiles such as SF-5 have been adequately explained by a single D_S . Profiles such as SF-1 (Figure 66), however, would clearly benefit from different assumptions being made concerning spatial homogeneity. Therefore, in the case of non-homogeneous soils and soil gas profiles, employment of a variable D_S with depth should be considered in future work in order to maximise correlation in a valid fashion should intra-soil variability be the focus of study.

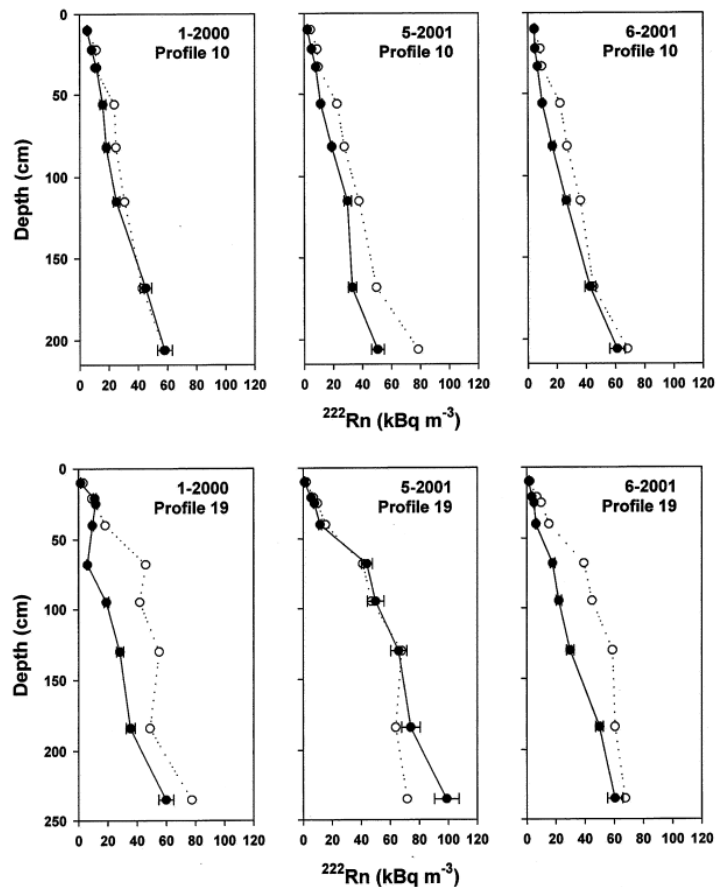


Figure 67 Numerical model fits applied to soil radon activity concentration profiles by Fierer et al. (2005).

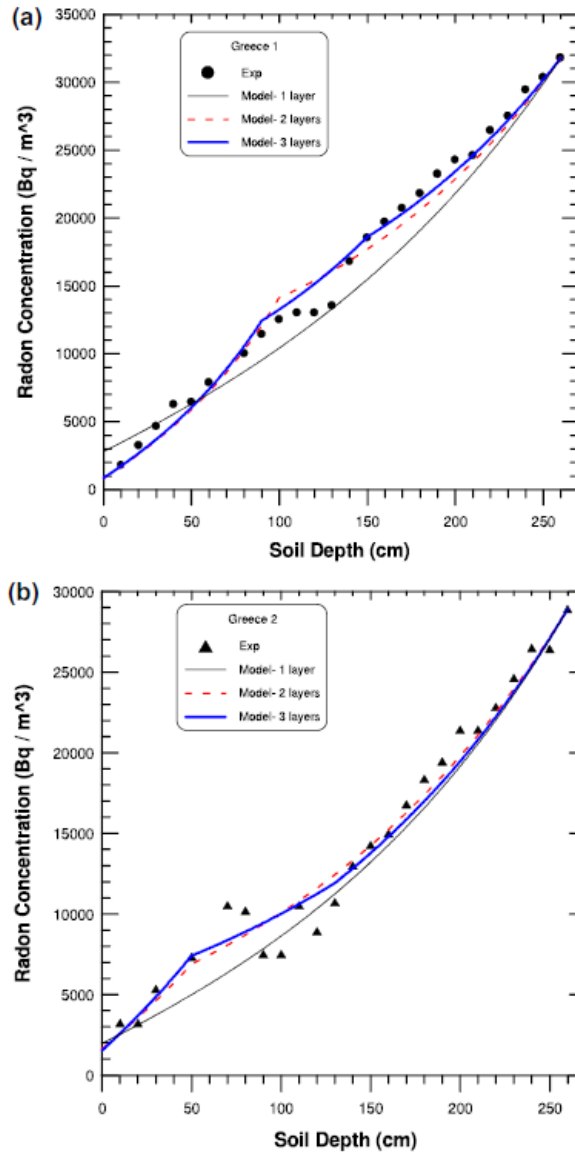


Figure 68 Numerical model fits to Greek soil data (Antonopoulos-Domis et al., 2009) using values of D_s which vary with soil depth. From Hafez and Awad (2016).

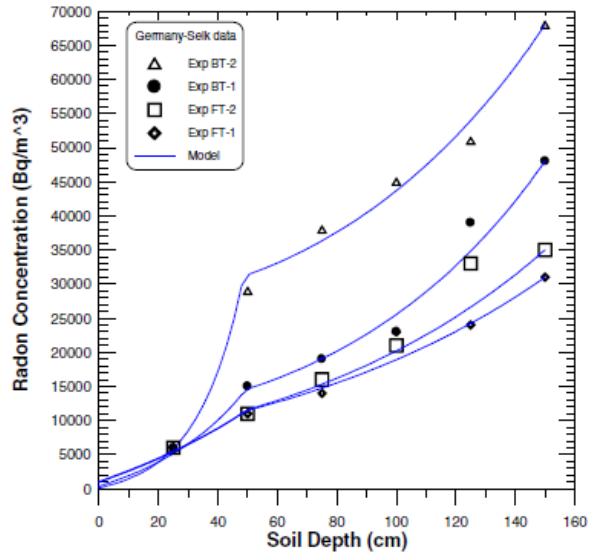


Figure 69 Numerical model fits to German soil data (Kunze et al., 2003) using values of D_s which vary with soil depth. From Hafez and Awad (2016).

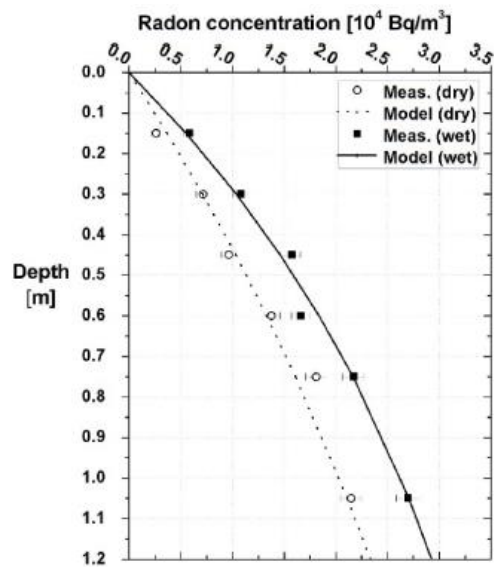


Figure 70 Numerical model fits to Korean soil data (Maeng et al., 2019) using a model of single D_s ; production, diffusion, and decay similar to that developed in the current research.

7.2.3.2 Atmospheric effects on soil gas transport

In the model fits to single profiles at both the ex-ASGARD site (Figure 61–Figure 65) and Boundary Plantation (Figure 66) the shallowest points (5 and 10 cm depths, respectively), often deviate from the fitted curve, suggesting an inadequate model representation of soil gas dynamics at the soil surface. The reason for surface soil disparity could be atmospheric draw-down, although this is only likely when air-filled porosity falls below ~ 0.4 (Figure 6); air filled porosity at 10 cm depth fell below 40 % on only four occasions at the ex-ASGARD site (Figure 39). Secondly, the assumption of an open boundary condition for the atmosphere in the model may underestimate the total gas transport occurring across the interface.

Soil gas diffusion theory suggests a decrease to zero activity concentration of radon at the surface of the soil (Figure 3) due to the presence of negligible radon activity concentration in the free atmosphere; however, organic layers and vegetation could serve to act as a boundary layer, complicating the soil-air interaction in a manner postulated by Laemell et al. (2017). A vegetation layer could be included in a numerical model by treating any suitably dense vegetation layer as an additional “soil” layer with high D_s value. The same may be true of soils with appreciable layers of organic matter which, unlike mineral soils, will not produce any radon gas. The maximum sampling resolution of approximately 10 cm in this study makes the analysis of radon distribution and behaviour within such layers difficult to track using the method employed. That said, fitting of the 1-D diffusion model to the collected data (Figure 61–Figure 66) appears to suggest that, in fact, more radon is being removed from the surface than has been accounted for.

The numerical model of soil gas transport developed over the course of this research does not include a mass flow component, i.e. there is no advection, only diffusion of gas. Open boundary conditions utilising diffusion only have been challenged (Antonopoulos-Domis et al., 2009; Hafez and Awad, 2016). The probe method of sampling soil gas does not shield the soil surface from atmospheric effects, so while the measured soil gas profiles can be considered a closer representation of “natural” conditions within the soil, they may not be adequately described by a soil gas model which lacks an active transport component.

By combining pressure-driven flux with molecular diffusion, Clements and Wilkening (1974) made comparisons of fluxes in soil radon between *in situ* and laboratory column soils. A single atmospheric pressure change is reflected in the soil gas profile after 1–2 days. Since environmental measurements are subject to dynamic pressure changes, some of which are probably muted by dense vegetation at the soil surface, a similar approach is unlikely to be of use for *in situ* soils. Field conditions may not always be well-reproduced in laboratory experiments, however (Laemell et al., 2017). For example, air pressure fluctuation frequency is different when artificially induced in experiments than it is in the environment. The conclusions of laboratory experiments may overemphasise or mask the effect of parameters like air pressure fluctuation on soil gas transport.

Effects of atmospheric parameters such as surface wind speeds on soil gas transport have nonetheless been shown (Laemell et al., 2017; Ye et al., 2019) yet only under certain canopy conditions or volumetric water contents, respectively. The effect of atmospheric radon processes on the surface flux has been calculated to be <1 %, however (Dmitriev 2018), which is much

less than measurement error. For this reason, any deviation from modelled concentrations may simply be due to either canopy conditions allowing for larger-than-normal influence of surface windspeed on soil gas concentrations, or simply radon measurement error and not due to more ubiquitous significant parameters being excluded from the model. That said, effects measuring up to 70 times greater than molecular diffusion alone have been observed in laboratory setups for wind gustiness. These effects influence only the top 20 cm of soil (Pourbakhtiar et al., 2017) and may necessitate inclusion on a per-site basis.

Future work should consider that the presence of vegetation, variable in both space and time, at field sites may affect soil gas dynamics. Advection or other mass transport phenomena may need to be accounted for (Laemmel et al., 2019; Hafez and Awad, 2016), or an 'effective diffusivity' can be employed which encompasses all processes (Antonopoulos-Domis et al., 2009), in a similar fashion to the present research.

7.2.4 Model parameter selection

7.2.4.1 Radon production rate

Radon production is a necessary inclusion in a modelled system and is often assumed to be spatially static (Hafez and Awad, 2016; Fierer et al., 2005). A constant radon emanation is based upon a measured value at "infinite depth", the depth at which it is assumed that diffusional losses of radon can be ignored. In cases of soil moisture content <10 %, however, the production rate is affected (Zhuo et al., 2005). This was the case during

this research and further field work was undertaken to facilitate the estimation of radon production rate. Although radon emanation can be estimated through other environmental parameters as in this work, direct measurement of radon emanation in the laboratory should be attempted as part of any future effort. In individual cases where soil moisture is not extraordinarily low, radon production within a single horizon can be remarkably consistent, within 10 % (Girault and Perrier, 2012; Fierer et al., 2005). When radon production rate is a constant value, the physical characterisation required can be reduced, especially useful when sites which are not going to be studied in the long-term.

Radon emanation rate estimates in modelling during this research were 0.1–0.2 Bq m⁻³ s⁻¹. Reported measured rates in soils of similar texture range from 0.0072–0.022 Bq m⁻³ s⁻¹ (20–60 mBq kg⁻¹ h⁻¹) (Chhangte et al., 2019). Given the different parent materials of the samples cited, the estimated radon emanation rate is considered acceptable.

In order to gain more direct estimates of soil radon production rate than have been made as part of this research, samples of soil can be sealed in glass jars and measured during equilibration (Fierer et al., 2005; Zhang et al., 2012). Whilst the initial field work involved in such characterisation makes any study more difficult from the outset, not to mention the risk of soil disturbance should the sample collection precede gas measurement, it is recommended that radon be estimated using this method in conjunction with the calculation method employed as part of the current research (3.17). Standard laboratory methods for soil analyses such as drying and crushing should be avoided as they risk changing the radon

emanation coefficient from what would be observed *in situ* (Girault and Perrier, 2012).

The same parameters as in this study have been employed to model soil gas radon activity concentrations using a sealed vessel method established in the literature (Ota et al., 2007; Ye et al., 2019) for radon production rate calculation. It was shown in the former that soil moisture content versus soil radon emanation displays a trend initially consistent with the relationship utilised in this work (Zhuo et al., 2005), but with a decrease at soil moisture content values of 0.3 and ~ 0.35 (Figure 71). The decrease in radon emanation rate suggests an effect of saturating soils on their radon production. Decreasing soil radon production at soil moisture contents near saturation is a clear and necessary consideration in future work; however, as experienced in the current study, it becomes increasingly difficult to sample gas from soils as their volumetric water content increases. It is likely that under field conditions the method employed in the current research would not feature data points from the ranges where soil radon production is affected: maximum soil volumetric water contents of $\sim 38\%$ (saturation) were measured in the ex-ASGARD site soil, and soil gas could not be sampled successfully above a value of 30% (Figure 39). The soils in the current study are of different types to those described by Ota et al. (2007) and it is possible that the observed effects are only present in (or exaggerated by) clayey textures. For this reason, the effect of soil water content on radon production rate requires assessment in each soil type studied.

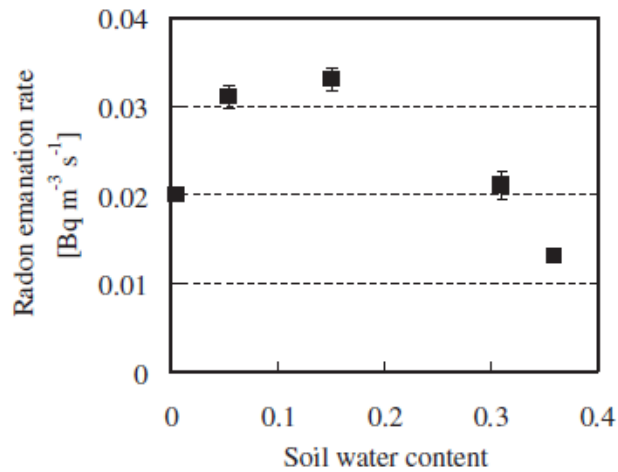


Figure 71 Relationship between soil water content and radon emanation rate. From Ota et al., (2007).

Parameters such as soil temperature are also often included in numerical solutions to the diffusion equation (Ota et al., 2007; Iskandar et al., 2004). The effect of soil temperature on radon production was quantified by Iskandar et al. (2004) (7.1). A change in temperature of 20 °C alters the soil radon emanation power ~15 % to ~20 %.

$$EF = 0.21T + 14.8 \quad (7.1)$$

Dependence of radon emanation factor on soil temperature. From Iskandar et al. (2004).

In the present study, changes in soil temperatures were ~2 °C, in summer and winter, and only noticeable at 10 cm depth, not at 50 cm or 100 cm (Figure 41, Figure 43). Such a change in temperature equates to a difference in *EF* of approximately 0.5 % according to (7.1) and would be present only in the

uppermost sections of the soil gas concentration profile. Since changes in radon emanation are already negligible under most environmental conditions (Zhuo et al., 2005) the small overall effect of soil temperature allows for its exclusion from numerical models concerning daily changes in soil gas transport behaviour; however, lower emanation in surface soils might help to improve model fits to measured data in the upper layers of the soil, which has been observed to be less successful in the model developed during this research.

On an annual scale, temperature differences are greater than observed over an average 24 h period and a difference in radon emanation of $\sim 5\%$ between summer and winter months may prove a useful inclusion in future modelling work, especially in areas of high temperature variation and/or extreme soil moisture contents.

The impact of temperature on soil radon emanation suggests that soil gas should be sampled at the same time of day to minimise error in modelled soil gas radon concentrations.

7.2.4.1.1 Inter-parameter interaction

It has been reported that, in certain datasets, soil temperature explains most of the variability in soil radon concentrations (Silva et al., 2015). However, as with soil moisture content, interactions between parameters may contribute to the strength of this observed relationship; increasing soil temperature may not only be driving increased emanation as the authors suggest, but also driving changes in the soil moisture content (increased evaporation with solar irradiation). Such interactions may

explain the large differences in radon activity concentration observed with temperature such as -20 % with 20 °C (Antonopoulos-Domis et al., 2009), as well as some recently reported relationships between soil moisture content and soil radon emanation which show the opposite trend to that described previously in this section (Zhang et al., 2019). Variation in soil radon emanation and exhalation with temperature remains a complex relationship across soil types and requires individual assessment on a per-site basis.

Silva et al. (2015) showed the complexity of interacting variables on a complex (volcanic) site. Many environmental parameters were identified as being significant, but they varied from site to site and in the effect they were having on radon activity concentrations. Similarly to the highly dynamic soils encountered at Hollin Hill (Section 5.3), high levels of subsurface complexity in a field site render the use of simple numerical models difficult or impossible.

7.2.4.2 Subsurface gas recharge rate

For the study of soil gas transport behaviour over time, the belowground recharge rate requires quantification. Continuous measurements of soil gas radon activity concentrations offer an increased robustness in estimation (Beresford et al., 2012; Silva et al., 2015) and, in the present work, recounting of soil radon samples produced slightly different results (Section 4.2). Repeated soil gas sampling without assessment of belowground recharge rate is not recommended, as any sample dilution due to insufficient belowground recharge would compound natural

statistical variation in radon counting, a theme that has been reported previously (McAlary et al., 2009).

The accuracy of estimated values of diffusion coefficients may be increased by detailed physical characterisation of sites of interest including belowground recharge times for soil gas. For a temporal analysis (longer-term sampling efforts), soil characterisation can be quickly and easily established for many soils. In cases where single sites are being visited for spatial analyses, however, detailed soil physical characterisation may require too much time. Many model parameters involving further physical characterisation of soils, such as soil volumetric water content, should remain optional inclusions in order to keep wide applicability of the method.

7.2.5 Model confirmation and further prediction

7.2.5.1 Sensitivity analysis

A sensitivity analysis of the resolved radon diffusion coefficient D_s to the radon emanation rate showed the model to be sensitive to the radon emanation rate. A decrease in emanation rate by 10 % yielded an increase in the resolved diffusion coefficient by 24 %. Likewise, an increase in emanation rate by 10% yielded a decrease in the resolved diffusion coefficient by 30 % (Table 14).

Table 14 Differences in modelled radon gas concentrations and corresponding diffusion coefficients as the average emanation rate is adjusted by 10 %.

| Fitted D_s / $m^2 s^{-1}$ | Modelled soil gas radon activity concentration / $Bq m^{-3}$ | | | | | | Average source term / $Bq m^{-3} s^{-1}$ |
|--------------------------------|--|-------|-------|-------|-------|--------|--|
| | 5 cm | 10 cm | 25 cm | 50 cm | 75 cm | 100 cm | |
| 1.55×10^{-7} | 2843 | 5193 | 10300 | 15080 | 17400 | 18400 | 0.0315 |
| 2.06×10^{-7} | 2710 | 5014 | 10240 | 15440 | 18110 | 19340 | 0.0350 |
| 2.93×10^{-7} | 2629 | 4908 | 10230 | 15780 | 18760 | 20210 | 0.0385 |

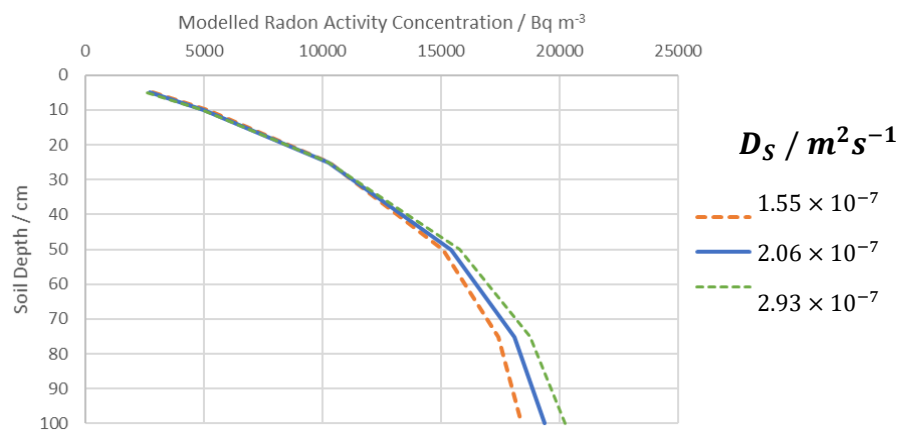


Figure 72 Visualisation of the difference in fitted radon concentration profile with varying diffusion coefficient.

7.2.5.2 Radon observations

Surface soil radon activity concentrations in summer may show weak variation; however, analytical errors are large due to low activity concentrations near the surface. It is also possible that variations cannot be detected on the temporal resolution of the method used in this study; rainfall of <1 mm was observed not to affect measured soil gas radon activity concentration at 10 cm depth or deeper (Figure 43). Since no effect on radon activity concentrations was observed following rainfall or changes in atmospheric pressure it can be assumed that the subtle effects of daily rainfall and barometric pressure fluctuations are unimportant at the temporal resolution of the method used in this study, and subsequent descriptions of soil gas transport behaviour are unaffected.

7.2.5.3 Greenhouse gas observations

Greenhouse gas concentration profiles varied greatly over time (Figure 35–Figure 37) with less clear temporal trends than soil gas radon activity concentrations (Figure 33). Changes in carbon dioxide concentrations can be driven by biological activity or solely by soil physics (Fujiyoshi et al., 2010). The results from this research illustrate the advantage in using radon gas as a tracer rather than one of the more commonly measured greenhouse gases in that radon activity concentration profiles were much closer in appearance to theoretical diffusion behaviour than the equivalent GHG profile (Figure 54). Concurrent measurement of gases other than radon can assist in the deduction of any sample dilution, as well as the evaluation of future methods of soil gas sampling (Section 5.4.2.2.2).

The measurements of soil greenhouse gases can be used for further predictions of soil gas diffusion coefficients (Fierer et al., 2015). In the current study, however, measured greenhouse gas concentrations did not display any trends that would be suitable for such inter-gas comparisons. Fick's Law-based approaches are comparable with surface chamber methods for predicting soil gas fluxes (Maier and Schack-Kirchner, 2014) and so would probably be effective in predicting soil profile concentrations also. The consistent underestimation of soil CO₂ concentrations by the Fick's Law model of Fierer et al. (2015) shows that an inert tracer approach (e.g. radon) is necessary alongside sampling of greenhouse gases in order to provide a reference. Soil CO₂ concentrations measured in the current study are not useful for this purpose, as the small sample size for gas chromatography necessitated by the overall sampling volume may have negatively affected measurement quality in

the case of CO₂, CH₄ and N₂O. In future work it is therefore recommended that separate samples are taken at separate times for soil greenhouse gas analysis; belowground recharge rate can be assessed as not unduly affecting sampling influence volumes (Section 4.2). This approach would be preferable to a separate sampling array, as it has been shown that temporal variation on the scale of hours is relatively small (Section 4.4). The spatial variation in soil gas behaviour is probably much larger and has been shown in this work to be a factor of 1.3 over 50 m, and to be as large as $\pm 11\%$ over 50 cm elsewhere (Antonopoulos-Domis et al., 2009). Despite this, some studies continue to assume spatial homogeneity in sampled soils (Nguyen et al., 2018).

7.2.5.4 Laboratory experiments

The excellent agreement between the model used in the present study and field data for sandy soils suggests that consideration of molecular diffusion and radon production are enough for the prediction of the soil gas diffusion coefficient. Model verification is desirable, however. Use of a laboratory column of the style of Clements and Wilkening (1974) in order to confirm and test the model under more controlled conditions was not possible; nonetheless, soil laboratory columns may prove a useful inclusion to future soil gas modelling work as they can be quickly set up to approximate simple gas transport in the laboratory (Allaire et al., 2008; Hunkeler et al., 1997; Ichedef, 2019; Levintal et al., 2019; Schubert and Schulz, 2002).

7.3 Summary of soil gas sampling

7.3.1 Soil gas samplers

The soil gas samplers developed during the presented research enabled soil gas sampling in a minimally invasive fashion for relatively low cost and with reliability in the field, as was desired. A maximum sampling depth of 1.7 m was achieved using the slide hammer mechanism (Figure 51). Deformation of the sampler body was still a problem in cases when extreme force was needed to insert the sampler, although not on the same scale as with aluminium samplers. Difficulty removing samplers from depths greater than 1 m, especially in clayey soils, was addressed with the design and manufacture of a handle attachment. Over the course of the presented research, development has been made of a method of soil gas sampling that continues to be popular (Buzinny et al., 2009; Holý et al., 2017; Mitev et al., 2018; Elío et al., 2019).

Drawbacks to the design of the tube samplers, noted during sampling efforts, included the tendency for water to collect in taps if they were not positioned facing downwards during long-term installation. In winter months water collection would be compounded by water freezing within the taps, preventing access to the sampling tube.

7.3.2 Soil gas sampling process

Extraction of soil gas samples which are genuinely representative of the belowground environment can be subject to sampling error. Measured values which are anomalous by either 30 % (Figure 40) or 60 % (Figure 44) are indicative of human error during sampling and can be discounted.

7.3.2.1 Effect of soil type on sampling

The sandy soils of the ex-ASGARD, Kingston, and Boundary Plantation sites (Sections 4.1, 5.2.1, 5.6.1,) allowed for a quicker and easier sampling process, although localised features of soils *in situ*, including glacial till, can necessitate several attempts at sampler insertion. Sandier soils complicate soil core extraction, particularly when soil volumetric water content is low, as these soils more readily lose structure when disturbed. More freely-draining sandy soils also tend to have higher observed air-filled porosity (less suction was required for gas extraction), allowing for samples of soil gas to be taken quickly and, theoretically, with a greater spatial precision (Figure 6). The effect of highly porous soils could also be negative, however: in soils with low radon production, a larger pore network volume would result in a low radon activity concentration that could drop below detection limits, especially near the surface.

Atmospheric dilution is also likely when sampler insertion requires repeated impacts, especially in clayey soils like those of Hollin Hill (Section 5.3.1) and the Allerton Project (Section

5.5.1), and when sampler installation is not long-term. Preferential flow pathways are created when the sampler moves laterally, forming gaps between the sampler tube and the soil. The nature of clay soils to retain their shape once deformed exacerbates pathway formation and measurement accuracy is compromised by mixing of atmospheric air and soil gas *via* the void between sampler body and soil. The slide hammer attachment developed for the current study means less force is required for sampler insertion and minimises the formation of preferential flow pathways. Provided suitable care is taken in sampling from preinstalled equipment, the problem of preferential flow pathway formation does not affect long-term sampling of a soil gas profile because soils are dynamic systems and any openings become sealed over time through natural processes.

Other possible explanations for soil gas concentrations deviating from a theoretical curve (Figure 3) include spatially-varying production rate; observed in the profiles of greenhouse gases (Figure 54), the likelihood of spatial variation in the soil radium activity concentration being a factor in varying radon activity concentration in soils is low and was not evident in any of the sites sampled.

Overall, the phenomenon of atmospheric dilution is important to remember, considering data can appear plausible when measured soil gas radon activity concentration profiles remain within detection limits.

7.3.2.2 Effect of field conditions on sampling

Soils containing large numbers of trees and other established plants, as well as agricultural soils subject to zero tillage, displayed high degrees of resistance to sampler insertion, as did frozen or extremely dry soils. Radon activity concentration profiles at several field sites did not conform to the theoretical curve shown in Figure 3 (cf. Figure 51), probably because of changes in soil texture throughout the profile, possibly compounded by non-uniform distribution of radon emanation (especially in the case of Hollin Hill). In future work, high spatial resolution soil gas radon profiles may be useful in indicating or confirming subsurface features without the need for invasive field work, *via* their impedance to soil gas transport.

8 Conclusions

A reliable and robust method of measuring soil radon activity concentrations has been developed and implemented to sample soil gas across temporal scales and at sites with a range of soil characteristics. Using this data, a bespoke computer model of soil gas diffusion has been used to generate estimates of the effective soil gas radon diffusion coefficient D_s both across field sites and, in a single location, over a period of 18 months.

Sampling of several field sites has been carried out and monitoring of soil gas radon activity concentrations has been undertaken *in situ* in several different soil types and treatments. Findings are summarised in Table 15. This research has successfully tracked subsurface changes in the soil gas transport behaviour through annual cycles and enabled reliable determination of a range of values for the soil gas radon diffusion coefficient over a period of one year at a single site (ex-ASGARD, Section 4) and across a limited spatial scale at another site (Boundary Plantation, Section 5.6). Measurements at several other sites with different soil textures have been attempted, although with comparatively poor results.

Table 15 Summary of findings from the presented research

| <i>Study site</i> | Contribution to understanding |
|-----------------------------------|--|
| <i>Kingston</i> (Section 5.2) | Soil compaction and localised inclusions make the probe method less useable. Soil treatment effect on method: only ploughed soils allowed for sampling. |
| <i>Ex-ASGARD</i> (Section 4.1) | <p>Long-term installation of probe soil gas samplers is valid and effective.</p> <p>Soil gas radon diffusion coefficient varied by a factor of 2 over 12 months.</p> <p>At a depth of 10 cm, soil gas radon concentration varied by a factor of 6 over 18 months.</p> <p>At a depth of 100 cm, soil gas radon concentration varied by a factor of 1.5 over 18 months.</p> <p>Diurnal variation in soil gas concentrations may not always be visible.</p> <p>Homogeneous soils conform to theory of diffusive gas transport and can be successfully modelled using Fick's Second Law.</p> <p>Belowground recharge time of soil gas can be quicker than measurement windows.</p> <p>Gas transport by diffusion is better represented by soil gas radon than greenhouse gases.</p> <p>Soil gas concentrations are driven by soil air-filled porosity.</p> |

Bagworth Heath
(Section 5.4)

Soil gas transport data cannot always discern soil textural boundaries.
Plant roots can impede probe sampling.

Allerton Project
(Section 5.5)

Clayey soils can allow for preferential flow pathway formation, aiding atmospheric dilution of sampled soil gas.

Hollin Hill
(Section 5.3)

Different soil textures may necessitate fitting of different soil gas diffusion coefficients.
Recently disturbed soils allow for easier sampler insertion (lower soil penetration resistance).
Cracks in soils make atmospheric dilution of samples more likely.

Boundary Plantation
(Sherwood Forest)
(Section 5.6)

Soil gas diffusion coefficient varied by a factor of 1.3 over 50 m.
Gas transport behaviour in homogeneous soils is approximated well by diffusive theory (Fick's Second Law).
Radon emanation must be accurately measured as it can vary in soils with high organic matter content.

As with many literature conclusions concerning soil gas transport (Sun et al., 2004; Bozkurt et al., 2009) and specifically active soil gas sampling (McAlary et al., 2009), the methods employed in the presented research are best suited to soils of high homogeneity and porosity, e.g. sands, principally due to the large flow rate potential relative to finer-textured soils. High porosity in a soil allows for easy sampler insertion and soil gas extraction. Alternative sampling methods such as passive or continuous active gas sampling (Beresford et al., 2012) can be applied to different soil textures but may require even greater radon production rate than most soils if sampling volume is to be minimised (Chanyotha et al., 2016).

The soil gas sampling apparatus described in this thesis can be used in several ways to suit specific applications: field profiles can be obtained at individual time-points by sampling progressively deeper in the soil, or samplers may be inserted for long-term gas sampling from a single soil profile. Methodology for both scenarios has been developed, key points noted, and further improvements suggested for future use.

The process described could be further optimised to allow for monitoring of changeable sites, where monitoring of the evolution of a soil physical process (such as land slippage) is desired. In sites with high water tables, however, a drastic reduction in samples successfully obtained (and, consequently, statistical power) is inevitable in proximity to the saturated zone of the soil. Soils that regularly reach saturation point reduce the power of statistical analyses that can be performed on subsequent soil gas concentration data, because they restrict the period during which gas can be sampled from them. The result is soil gas profiles with relatively few data points. Future analysis of the belowground soil gas recharge rate may allow

for a larger number of samples to be collected per unit depth. Future long-term sampling efforts using the method described in this thesis should also endeavour to place samplers at the limit of resolution for the chosen soil. Soil air-filled porosity assumes different values at different depths, and so analysis of the soil air-filled porosity and how it is likely to vary over time is required in order to inform sample point spacing in the future.

Quantification of soil radon emanation and exhalation rates, and how these vary spatially, should be a major focus of any future research. Sensitivity analysis of the developed model shows that for accurate resolution of diffusion coefficients, the accurate and precise quantification of the gas production rate is critical. Soil radon emanation rate should not vary with soil volumetric water content, except with values <10 %; however, the potential effects of various other phenomena, particularly atmospheric, require greater investigation.

Soils which display a changeable or erratic increase in soil gas radon activity concentration with depth should have multiple D_s values fitted with depth as part of any future modelling work. In the case of models with multiple parameters, the utilisation of advanced fitting methods could increase precision of results. Use of high-performance computing to incorporate prior knowledge from field expeditions could serve to further reduce computation time and enable increased suitability and accuracy of model fit to the measured data.

9 References

Abjoassim, A. A. (2017) Alpha particles concentrations from some soil samples of Al-Najaf (Iraq). Polish Journal of Soil Science, L/2, 249-164.

Antonopoulos-Domis, M., Xanthos, S., Clouvas, A. and Alifrangis, D. (2009) Experimental and theoretical study of radon distribution in soil. Health Physics, 97(4), 322-331.

Algade Inc. (Online). Available at documentation.algade.fr Accessed 22/10/2016.

Asher-Bolinder, S., Owen, D. E., and Schumann, R. R. (1990) Pedologic and climatic controls on Rn-222 concentrations in soil gas, Denver, Colorado. Geophysical Research Letters, 17(6), 825-828.

AZoNetwork UK Ltd.
<https://www.azom.com/article.aspx?ArticleID=2863>. Last accessed 02/01/2020.

Ball, B. C. (1981). A Laboratory Method to Measure Gas-Diffusion and Flow in Soil and Other Porous Materials. The Journal of Soil Science 32(3), 323. Not available online. Cited in: Moldrup et al., 2000

Baykut, S., Akgul, T., Inan, S. and Seyis, C. (2010) Observation and Removal of Daily Quasi-periodic Components in Soil Radon Data. Radiation Measurements, 45, 872-879.

Bem, H., Gasiorowski, A., and Szajerski, P. (2020) A fast method for the simultaneous determination of soil radon (^{222}Rn) and thoron (^{220}Rn) concentrations by liquid scintillation counting. Science of the Total Environment, 709, 136127.

Beresford, N. A., Barnett, C. L., Vives I Batlle, J., Potter, E. D., Ibrahim, Z.-F., Barlow, T. S., Schieb, C., Jones, D. G., and Copplestone, D. (2012) Exposure of burrowing mammals to ^{222}Rn . *Science of the Total Environment*, 431, 252-261.

Boon, A., Robinson, J. S., Nightingale, P. D., Cardenas, L., Chadwick, D. R., and Verhoef, A. (2013) Determination of the gas diffusion coefficient of a peat grassland soil. *European Journal of Soil Science*, 64, 681-687.

Born, M., Dörr, H. and Levin, I. (1990) Methane consumption in aerated soils of the temperate zone. *Tellus*, 42B, 2 - 8.

Bossus, D. A. W. (1984) Emanating Power and Specific Surface Area. *Radiation Protection Dosimetry*, 7, 73-76.

Bozkurt, O., Pennell, K., G., and Suuberg, E., M. (2009) Simulation of the vapor intrusion process for non-homogeneous soils using a three-dimensional numerical model. *Ground Water Monitoring and Remediation*, 29(1), p. 92-104.

Broecker, W. S. and Peng, T. H. (1974) Gas exchange rates between air and sea. *Tellus*, 26, 1-2.

Butterbach-Bahl, K., Rothe, A. & Papen, H. (2002) Effect of tree distance on N_2O and CH_4 -fluxes from soils in temperate forest ecosystems. *Plant and Soil*, 240, 91-103.

Buzinny, M. (1996) A new approach to determining ^{222}Rn in air using liquid scintillation counting. *International Conference on Advances in Liquid Scintillation Spectrometry*, edited by G. T. Coop D. D. Harkness, A. B. MacKenzie, B. F. Miller and E. M. Scott. *RADIOCARBON* 1996, pp. 137 - 140.

Buzinny, M., V. Sakhno and M. Romanchenko (2009) LSC-based approach for radon in soil gas measurements. *Advances in*

Liquid Scintillation Spectrometry, edited by J. Eikenberg, M Jäggi, H. Beer and H. Baehrle, LSC 2008, pp. 7 - 11.

Castelluccio, M., Moroni, M. and Tuccimei, P. (2010) Soil Gas Radon Concentration and Permeability and 'Valle della Caffarella' Test Site (Roma, Italy). Evaluation of Gas Sampling Techniques and Radon Measurements Using Different Approaches. Proceedings of 10th International Workshop on The Geological Aspects Of Radon Risk Mapping, -, -.

Certini, G., Campbell, C. D., and Edwards, A. C. (2004) Rock fragments in soil support a different microbial community from the fine earth. *Soil Biology and Biochemistry*, 36, 1119-1128.

Clarke, R. H. and Southwood, T. R. E. (1989) Risks from ionizing radiation. *Nature*, 338, 197-198.

Chamberlain, A. (1991), *Radioactive Aerosols*. Cambridge University Press.

Chambers, J. E., Wilkinson, P. B., Kuras, O., Ford, J. R., Gunn, D. A., Meldrum, P. I., Pennington, C. V. L., Weller, A. L., Hobbs, P. R. N., and Ogilvy, R. D. (2011) Three-dimensional geophysical anatomy of an active landslide in Lias Group mudrocks, Cleveland Basin, UK. *Geomorphology*, 125, 472-484.

Chanyotha, S., Kranrod, C., Kritsanawanat, R., Lane-Smith, D. and Burnett, W. C. (2016) Optimizing Laboratory-Based Radon Flux Measurements for Sediments. *Journal of Environmental Radioactivity*, 158-159, 47-55.

Chauhan, R. P., Nain, M. and Kant, K. (2008) Radon diffusion studies through some building materials: Effect of grain size. *Radiation Measurements*, 43, S445-S448.

Chesworth, W. (2007), *Encyclopedia of Soil Science*. Springer.

Chhangte, L. Z., Rohmingliana, P. C., Sahoo, B. K., Sapra, B. K., Hmingchungnunga, Vanramlawma, Pachuau, Z., and Zoliana, B. (2019) Determination of radon mass exhalation rate in the region of highest lung cancer incidence in India. *Radiation Environment and Medicine*, 8(2), 113-117.

Chitra, N., Danalakshmi, B., Supriya, D., Vijayalakshmi, I., bala Sundar, S., Sivasubramanian, K., Baskaran, R., and Jose, M. T. (2018) Study of radon and thoron exhalation from soil samples of different grain sizes. *Applied Radiation and Isotopes*, 133, 75-80.

Clever, H. I. (Ed.) 1979. *Krypton, Xenon and Radon, Solubility Data Series 2*, vol. 18. Pergamon Press, Oxford, UK.

Unavailable. Cited in Huxtable et al., 2017.

Crank, J., and Nicolson, P. (1947). A practical method for numerical evaluation of solutions of partial differential equations of the heat conduction type. *Proc. Camb. Phil. Soc.* 43, 50-67. Accessed as: Crank, J., and Nicolson, P. (1996). A practical method for numerical evaluation of solutions of partial differential equations of the heat conduction type. *Advances in Computational Mathematics* 6, 207-226.

Crank, J. (1967). *The Mathematics of Diffusion*. Oxford University Press.

Davidson, E. A. and Trumbore, S. E. (1995) Gas diffusivity and production of CO₂ in deep soils of the eastern Amazon. *Tellus B: Chemical and Physical Meteorology*, 47:5, 550-565.

Delta-T Ltd. www.delta-t.co.uk/product/pr2. Accessed 11/06/2018.

De Jong, E. and Schappert, H. J. V. (1972) Calculation of Soil Respiration and Activity from CO₂ Profiles in the Soil. *Soil Science*, 113(5), 328 - 333.

Dmitriev, E. M. (2018) Influence of Atmospheric Radon Transport on a Radon Flux from the Surface. *Izvestiya, Physics of the Solid Earth*, 54(5), 775-781.

Dörr, H. and Munnich, K. O. (1987) Annual variation in soil respiration in selected areas of the temperate zone. *Tellus*, 39B, 114-121.

Dörr, H. & Munnich, K. O. (1990) Rn-222 flux and soil air concentration profiles in West-Germany. Soil 222Rn as tracer for gas transport in the unsaturated soil zone. *Tellus B*, 42B, 20 - 28.

Durrani, S. A. and Ilic, R. (Ed.s, 1997) Radon measurement by etched track detectors. World Scientific Publishing, Singapore.

Elío, J., Crowley, Q., Scanlon, R., Hodgson, J., and Long, S. (2019) Rapid radon potential classification using soil-gas radon measurements in the Cooley Peninsula, County Louth, Ireland. *Environmental Earth Sciences*, 78, 359.

Etiopé, G. and G. Martinelli (2002) Migration of carrier and trace gases in the geosphere: an overview. *Physics of the Earth and Planetary Interiors*, 129, 185 - 204.

E-Z LOK. <https://www.ezlok.com/316-stainless-steel-properties>. Last accessed: 02/01/2020.

Feng, S., Wang, H., Cui, Y., Ye, Y., Li, X., Xie, D., He, Z., and Yang, R. (2019) Monte Carlo method for determining radon diffusion coefficients in porous media. *Radiation Measurements*, 126, 106130.

Fitzpatrick, R. (2006). University of Texas Lecture Series. Available at: <http://farside.ph.utexas.edu/teaching/329/lectures/node92.html>. Accessed on 12/02/2020.

Fitzpatrick, R. (2006a). University of Texas Lecture Series. Available at: <http://farside.ph.utexas.edu/teaching/329/lectures/node78.html>. Accessed on 12/02/2020.

Folkerts, K. H., Keller, G. and Muth, H. (1984) Experimental investigations on diffusion and exhalation of ^{222}Ra and ^{220}Rn from building materials. *Radiation Protection Dosimetry*, 7, 41–44. Unavailable. Cited in: Hassan et al., 2009.

Freijer, J. I. (1994) Calibration of Jointed Tube Model for the Gas Diffusion Coefficient in Soils. *Soil Science Society of America Journal* 58(4), 1067-1076. Unavailable online. Cited in: Moldrup et al., 2000.

Friedmann, H., Baumgartner, A., Bernreiter, M., Graser, J., Gruber, V., Kabrt, F., Kaineder, H., Maringer, F. J., Ringer, W., Seidel, C. and Wurm, G. (2017) Indoor Radon, Geogenic Radon Surrogates and Geology - Investigations on their Correlation. *Journal of Environmental Radioactivity*, 166, 382-389.

Fu, C. C., Yang, V. F., Walia, V., Liu, T-K., Lin, S-J., Chen, C-H., and Hou, C-S. (2009) Variations of soil-gas composition around the active Chihshang Fault in a plate suture zone, eastern Taiwan. *Radiation Measurements*, 44, 940-944.

Fuhrmann, M., Michaud, A., Salay, M., Benson, C. H., Likos, W. J., Stefani, N., Waugh, W. J. and Williams, M. M. (2019) Lead-2019 profiles in radon barriers, indicators of long-term radon-222 transport. *Applied Geochemistry*, 110, 10443-4.

Fujiyoshi, R., Haraki, Y., Sumiyoshi, T., Amano, H., Kobal, I. and Vaupotic, J. (2010) Tracing the Sources of Gaseous Components (^{222}Rn , CO_2 and its Carbon Isotopes) in Soil Air under a Cool-Deciduous Stand in Sapporo, Japan. *Environ. Geochem. Health*, 32, 73-82.

Fujiyoshi, R., Okabayashi, M., Sakuta, Y., Okamoto, K., Sumiyoshi, T., Kobal, I. and Vaupotic, J. (2013) Soil Radon in Winter Months Under Snowpack in Hokkaido, Japan. *Environmental Earth Sciences*, 70, 1159-1167.

Fukuda (1954) Air and vapor movement in soil due to wind gustiness. *Soil Science*, 79(4), 249 - 256.

Garcia-Torano, E. (2006). Current Status of Alpha-particle Spectrometry. *Appl. Radiat. Isot.* 64, 1273-1280.

Genereux, D. P. and H. F. Hemond (1991) Measurement of the radon-222 content of soil gas by liquid scintillation counting. *Chemical Geology (Isotope Geoscience Section)*, 87, 265-275.

George, A. C. (1984). Passive Integrated Measurement of Indoor Radon Using Activated Carbon. *Health Physics* 46, 867-872. Unavailable. Cited in: Chamberlain 1991.

Georgiev, S., Mitev, K., Pressyanov, D., Dimitrova, I. and Boshkova, T. (2012) Numerical Modelling of the Activity Concentration Measurements of Beta-Radioactive Noble Gases by Absorption in Polycarbonates and External Beta-Counting. *Radiation Measurement*, 47, 303-310.

Gilfedder, B. S., H. Hofmann and I. Cartwright (2013) Novel Instruments for in Situ Continuous Rn-222 Measurement in Groundwater and the Application to River Bank Infiltration. *Environmental Science and Technology*, 43, 993-1000.

Gilmore, G. (2008). Practical Gamma-ray Spectrometry. 2nd. Wiley (2008). Cited in: IAEA (2010)

Girault, F. and F. Perrier (2012) Measuring effective radium concentration with large numbers of samples. Part I - experimental method and uncertainties. *Journal of Environmental Radioactivity*, 113, 177-188.

Girault, F. and Perrier, F. (2012) Measuring effective radium concentration with large numbers of samples. Part II - general properties and representativity. *Journal of Environmental Radioactivity*, 113, 189-202.

Gwosdz, S., West, J. M., Jones, D., Rekoczy, J., Green, K., Barlow, T., Blothe, M., Smith, K., Steven, M., and Kruger, M. (2016) Long-term CO₂ injection and its impact on near-surface soil microbiology. *FEMS Microbiology Ecology*, 92, 1-10.

Häberli, A. (2009) Rn-222 as a tracer for gas transport in soil and fluxes at the soil-atmosphere interface. MSc Report, Swiss Federal Institute of Technology (ETH), 20.

Hansen, J. S. and Damkjaer, A. (1984) Determining ²²²Rn diffusion lengths in soils and sediments, *Health Phys.*, 53, 455-459. Unavailable. Cited in: Hassan et al., 2009.

Hirst and Harrison (1939) The diffusion of radon gas mixtures. *Proceedings of the Royal Society A*, 169:939.

Hoehn, E. and von Gunten, H. R. (1989) Radon in groundwater: a tool to assess infiltration from surface waters to aquifers. *Water Resources Research*, 25(8), 1795-1803.

Holý, K., Múllerová, M., Palušová, V., and Bulko, M. (2017) Comparison of Various Approaches to Determining CO₂ Fluxes from the Soil by ²²²Rn Calibrated Method. *Radiation Protection Dosimetry*, 10, 1-5.

Hooper, D., Coughlan, J. and Mullen, M. R. (2008) Structural Equation Modelling: Guidelines for Determining Model Fit. The Electronic Journal of Business Research Methods 6(1), 2008, 53-60

Hou, X. and Ross, P. (2007) Critical Comparison of Radiometric and Mass Spectrometric Methods for the Determination of Radionuclides in Environmental, Biological and Nuclear Waste Samples. Radiation Research Department, Riso National Laboratory, Roskilde, Denmark. Unavailable. Cited in IAEA (2010)

Hunkeler, D., E. Hoehn, P. Hohener and J. Zeyer (1997) Rn-222 as a partitioning tracer to detect diesel fuel contamination in aquifers: laboratory study and field Observations. Environmental Science and Technology, 31, 3180-3187.

Huxol, S., Brennwald, M., Henneberger, R. and Kipfer, R. (2013) $^{220}\text{Rn}/^{222}\text{Rn}$ isotope pair as a natural proxy for soil gas transport. Environmental Science & Technology, 47 (24), 14044–14050.

Ichedef, M. (2019) Controlled Laboratory Experiments on Radon Diffusion Coefficient. Sakarya University Journal of Science, 23(3), 308-312.

Insitu Test Pty. Ltd., www.insitutest.com.au. Last accessed: 13/12/2019.

IPCC (2001), Assessment Report 3.

IPCC (2013), Assessment Report 5.

Iskandar, D., Yamazawa, H., and Iida, T. (2004) Quantification of the dependency of radon emanation power on soil temperature. Applied Radiation and Isotopes, 60, 971-973.

Israel (1951). Radioactivity of the Atmosphere. Compendium of Meteorology (ed. Malone, T. F.), Boston. P.155-61. Unavailable. Cited in Chamberlain 1991.

Jin, Y. and Jury, W. A. 1996. Characterizing the dependence of gas diffusion coefficient on soil properties. Soil Science Society of America Journal, 60(1), 66-71. Unavailable online. Cited in: Moldrup et al., (2000).

Kikaj, D., Jeran, Z., Bahtijari, M. and Stegnar, P. (2016) Radon in Soil Gas in Kosovo. Journal of Environmental Radioactivity, 164, 245-252.

Knoll, G. F. (2010), Radiation Detection and Measurement. John Wiley and Sons, Inc.

Konert, M., and Vandenberghe, J. (1997) Comparison of laser grain size analysis with pipette and sieve analysis: a solution for the underestimation of the clay fraction. Sedimentology 44, 523-535.

Krishnaswami, S. and Seidemann, D. E. (1988) Comparative Study of ^{222}Rn , ^{40}Ar , ^{39}Ar and ^{37}Ar leakage from rocks and minerals: Implications for the role of nanopores in gas transport through natural silicates. Geochimica et Cosmochimica Acta, 52, 655-658.

Langton, D. D. (1999). The Panda lightweight penetrometer for soil investigation and monitoring material compaction. Ground Engineering.

Lauria, D. C., Ribeiro, F. C. A., Conti, C. C. and Loureiro, F. A. (2009) Radium and uranium levels in vegetables grown using different farming management systems. Journal of Environmental Radioactivity, 100, 176-183.

Lehmann B. E., Lehmann, M., Neftel, A., Gut, A., and Tarakanov, S. V. (1999) Radon-220 calibration of near-surface turbulent gas transport. *Geophysics Research Letters*, 26(5), 607-610.

Lehmann, B. E., Lehmann, M., Neftel, A., and Tarakanov, S. V. (2000) Radon-222 monitoring of soil diffusivity. *Geophysics Research Letters*, 27(23), 3917-3920.

Lockhart et al., (1960) Fission product radioactivity in the air along the 80th meridian (west) during 1959. *Journal of geophysical research* 65(12), 3987-3997. Not available online. Cited in: Chamberlain 1991.

Lucas, H. F. (1957) Improved low-level alpha-scintillation counter for radon. *The Review of Scientific Instruments*, 28(9), 680-683.

Ma, S., Baldocchi, D. D., Hatala, J. A., Detto, M., and Yuste, J. C. (2012) Are rain-induced ecosystem respiration pulses enhanced by legacies of antecedent photodegradation in semi-arid environments? *Agricultural and Forest Meteorology*, 154-155, 203-213.

Markkanen, M, and Arvela, H. (1992) Radon Emanation from Soils. *Radiation Protection Dosimetry*, 45, 269-272.

Marshall, T. J. (1959) The Diffusion of Gases Through Porous Media. *The Journal of Soil Science*, 10(1), 79-82. Not available online. Cited in Moldrup et al., (2000).

McAlary, T., A., Nicholson, P., Groenvelt, H., and Bertrand, D. (2009) *Ground Water Monitoring and Remediation* 29(1), p. 144-152.

McNerney, J. J. and Buseck, P. R. (1973). Geochemical exploration using mercury vapor. *Economic Geology* 68(8), 1313-1320.

Meslin, P-Y., Adler, P. M. and Sabroux, J-C. (2010) Diffusive Transport of gases in Wet Porous Media. Application to Radon. *Soil Physics*, 74 (6), 1871-1885.

Mitev, K., Dustov, Ch., Georgiev, S., Boshkova, D., and Pressyanov, D. (2018) Unperturbed, high spatial resolution measurement of Radon-222 in soil gas depth profile. *Journal of Environmental Radioactivity*.

Mitev, K., Georgiev, S., Dimitrova, I. and Pressyanov, D. (2016) Application of Scintillation Counting Using Polycarbonates to Radon Measurements. *Radiation Measurements*, 92, 32-38.

Moldrup, P., Olesen, T., Gamst, J., Schjonning, P., Yamaguchi, T. and Rolston, D. E. (2000) Predicting the Gas Diffusion Coefficient in Repacked Soil: Water-Induced Linear Reduction Model. *Soil Sci. Soc. Am. J.*, 64, 1588-1594.

Moldrup, P., Olesen, T., Rolston, D. E. and Yamaguchi, T. 1997. Modeling diffusion and reaction in soils: VII. Predicting Gas and ion diffusivity in undisturbed and sieved soils. *Soil Science* 162(9), 632-640.

Moldrup, P., Olesen, T., Schjonning, P., Yamaguchi, T., and Rolston, D. E. (2000) Predicting the Gas Diffusion Coefficient in Undisturbed Soil from Soil Water Characteristics. *Soil Sci. Soc. Am. J.*, 64, 94-100.

Monnin, M. and Seidel, J. L. (1998) An automatic radon probe for earth science studies. *Journal of Applied Geophysics*, 39, 209 - 220.

Myrick, Berven and Haywood (1983) Determination of Concentrations of Selected Radionuclides in Surface Soil in the U.S. *Health Physics* 45(3), 631-642. Not available online. Cited in: Nazaroff 1992

Nazaroff, W. (1992) Radon transport from soil to air. *Reviews of Geophysics*, 30(2), 137 - 160.

Nazaroff, W. W. and R. G. Sextro (1989) Technique for measuring the indoor ²²²Rn source potential of soil. *Environmental Science & Technology*, 23, 451 - 458.

Nielson, K. K. et al., (1984). Diffusion of Radon Through Soils – A Pore Distribution Model. *Soil Science Society of America Journal* 48(3), 482-487. Unavailable online. Cited in: Moldrup et al., 2000

Nemitz, E., Loubet, B., Lehmann, B. E., Cellier, P., Neftel, A., Jones, S. K., Hensen, A., Ihly, B., Tarakanov, S. V. and Sutton, M. A. (2009) Turbulence characteristics in grassland canopies and implications for tracer transport. *Biogeosciences Discussions*, 6, 437-489.

Nero, A. V. and Nazaroff W. W. (1983) Characterizing the source of radon indoors. *Radiation Protection Dosimetry*, 7 (1-4), 23-39.

Nguyen, P. T. H., Nguyen, V. T., Vu, N. A., Nguyen, V. D., and Cong, H. L. (2018) Soil radon gas in some soil types in the rainy season in Ho Chi Minh City, Vietnam. *Journal of Environmental Radioactivity*, 193-194, 27-35.

O’Riordan et al., (1982). Unavailable. Cited in: Chamberlain 1991.

Papastefanou, C. (2007) Measuring radon in soil gas and groundwaters: a review. *Annals of Geophysics*, 50, 569–574.

Papendick, R. I., and Runkles, J. R. (1965) Transient-state oxygen diffusion in soil: I. The case when rate of oxygen consumption is constant. *Soil Science* 100(4), 251-261.

Passo, C. J. and Floekher, J. M. (1991) The LSC approach to radon counting in air and water. In: *Scintillation Counting and Organic Scintillators*, eds. H. Ross, J. E. Noakes and J. D. Spaulding, 32, 375-384.

Petersen, L. W., Rolston, D. E., Moldrup, P and Yamaguchi, T. (1994) Volatile Organic Vapor Diffusion and Adsorption in Soils. *J. Environ. Qual.*, 23, 799-805.

Pingintha, N., Leclerc, M. Y., Beasley Jr., J. P., Zhang, G. and Senthong, C. (2010) Assessment of the Soil CO₂ Gradient Method for Soil CO₂ Efflux Measurements: Comparison of Six Models in the Calculation of the Relative Gas Diffusion Coefficient. *Tellus*, 62B, 47-58.

Pourbakhtiar, A., Poulsen, T. G., Wilkinson, S., and Bridge, J. W. (2017) Effect of wind turbulence on gas transport in porous media: experimental method and preliminary results. *European Journal of Soil Science*, 68, 48-56.

Prichard, H. M. and Gesell, T. F. (1977) Rapid measurements of ²²²Rn concentrations in water with a commercial liquid scintillation counter. *Health Physics*, 33(6), 577-581.

Przylibski, T. A. (2000) Estimating the radon emanation coefficient from crystalline rocks into groundwater. *Applied Radiation and Isotopes*, 53, 473-479.

Quindós Poncela, L. S., Fernandez, P. L. and Arozamena, J. G. (2005) A method for measuring active radon diffusion coefficients in radon barriers by using modified Lucas cells, *Radiation Measurements*, 39, 87-89.

Rama and Moore, W. S. (1990) Micro-crystallinity in radioactive materials. *Int. J. Radiat. Appl. Instrum. Part E, Nucl. Geophys.* 4, 475-478, 1990. Cited in: Nazaroff (1992).

Reimer, G. M. (1980) Use of soil gas helium concentrations for earthquake prediction: limitations imposed by diurnal variation. *Journal of Geophysical Research*, 85(B6), 3107-3114.

Righi, S. and Bruzzi, L. (2006) Natural radioactivity and radon exhalation in building materials used in Italian dwellings. *Journal of Environmental Radioactivity*, 88, 158-170.

Rogers, V. C. and Nielson, K. K. (1991) Correlation for predicting air permeability and ^{222}Rn diffusion coefficient of soils. *Health Phys.*, 61, 225-230. Not available online. Cited in: Hassan et al., 2009.

Rowell, D. L. 1994 "Soil Science: Methods and Applications", Taylor and Francis. Sections 4.1, 4.2, 6.4.

Rubio, V. E. and Detto, M. (2017) Spatiotemporal variability of soil respiration in a seasonal tropical forest. *Ecology and Evolution*, 1-13.

Russell, E. J. and Appleyard, A. (1915) The atmosphere of the soil: its composition and the causes of variation. *Journal of Agricultural Science*, 8, 1-48.

Sakoda, A., Ishimori, Y. and Yamaoka, K. (2011) A Comprehensive Review of Radon Emanation Measurements for Mineral, Rock, Soil, Mill Tailing and Fly Ash. *Applied Radiation and Isotopes*, 69, 1422-1435.

Savovic, S., Djordjevich, A., Tse, P. W., and Nikezic, D. (2011) Explicit Finite Difference Solution of the Diffusion Equation Describing the Flow of Radon Through Soil. *Applied Radiation and Isotopes*, 69, 237-240.

Scatterly (1908). The amount of Ra emanation in the atmosphere. *Philosophical Magazine* 16, 584-615.

Unavailable. Cited in Chamberlain 1991.

Schery, S. D., Gaeddert, D. H. and Wilkening, M. H. (1980) Two-filter monitor for atmospheric ^{222}Rn . *Review of Scientific Instruments*, 51(3), 338-343.

Schroth, M.H., W. Eugster, K.E. Gómez, G. Gonzalez-Gil, P.A. Niklaus, P. Oester (2012) Above- and below-ground methane fluxes and methanotrophic activity in a landfill-cover soil. *Waste Management*, 32, 879 - 889.

Schubert, M. and H. Schulz (2002) Diurnal radon variations in the upper soil layers and at the soil-air interface related to meteorological parameters. *Health Physics*, 83(1), 91 - 96.

Shakhova, N., Semiletov, I., Salyuk, A. and Kosmach, D. (2008) Anomalies of methane in the atmosphere over the East Siberian shelf: Is there any sign of methane leakage from shallow shelf hydrates? *Geophysical Research Abstracts*, 10.

Shakhova, N., Semiletov, I., Salyuk, A., Kosmach, D. and Bel'cheva, N. (2007) Methane Release on the Arctic East Siberian Shelf. *Geophysical Research Abstracts*, 9.

Smith, G. D. *Numerical Solution of Partial Differential Equations: Finite Difference Methods* 3rd Ed. Oxford Applied Mathematics and Computing Science Series. Oxford University Press.

Steele, D. D. and Nieber, J. L. (1994) Network Modeling of Diffusion Coefficients for Porous Media: I. Theory and Model Development. *Soil Sci. Soc. Am. J.*, 58, 1337-1345.

Stranden, E., Kolstad, A. K. and Lind, B. (1984) Radon exhalation: moisture and temperature dependence. *Health*

Phys. 47, 480-485. Not available online. Cited in Hassan et al., 2009.

Sun, K., Guo, Q., and Cheng, J. (2004). The effect of some soil characteristics on soil radon concentration and radon exhalation from soil surface. *Journal of Nuclear Science and Technology*, 41(11), p. 1113-1117.

Szabó, K. Z., G. Jordan, Á. Horváth, C. Szabó (2013) Dynamics of soil gas radon concentration in a highly permeable soil based on a long-term high temporal resolution observation series. *Journal of Environmental Radioactivity*, 124, 74-83.

Tanner, A. B. (1980) Radon Migration in the Ground: A Supplementary Review, 5-56.

Tanner (1964). Unavailable. Cited in: Nazaroff 1992.

Thawatchai Itthipoonthankorn (2017) PhD Thesis. The University of Nottingham.

Troeh, F., Jabro, J. D. and Kirkham, D. (1982) Gaseous Diffusion Equations for Porous Materials. *Geoderma*, 27(3), 239-253.

Tomarken, A. J., and Waller, N. G. (2003). Potential problems with "well fitting" models. *Journal of Abnormal Psychology*, 112(4), 578-598

Tucker, B., Donakowski, J., and Hays, D. (2012) Comparison of Activity Determination of Radium 226 in FUSRAP Soil using Various Energy Lines. WM2012 Conference. February 26-March 1 2012, Phoenix, AZ, USA. Conference.

Turekian, K. K., Nozaki, Y. and Benninger, L. K. (1977). Geochemistry of Atmospheric Radon and Products. *Annual Review of Earth Planetary Science* 5, 227-255. Unavailable. Cited in: Chamberlain 1991.

Uchida, M., Nojiri, Y., Saigusa, N., and Oikawa, T. (1997) Calculation of CO₂ flux from forest soil using ²²²Rn calibrated method. *Agricultural and Forest Meteorology*, 87, 301-311.

Uhlemann, S., Chambers, J., Wilkinson, P., Maurer, H., Merritt, A., Meldrum, P., Kuras, O., Gunn, D., Smith, A., and Dijkstra, T. (2017) Four-dimensional imaging of moisture dynamics during landslide reactivation. *Journal of Geophysical Research*, 122, 398-418.

Uhlemann, S., Smith, A., Chambers, J., Dixon, N., Dijkstra, T., Haslam, E., Meldrum, P., Merritt, A., Gunn, D., and Mackay, J. (2016) Assessment of ground-based monitoring techniques applied to landslide investigations. *Geomorphology*, 253, 438-451.

Ullom, W. L., Soil Gas Sampling. In: *Handbook of Vadose Zone Characterisation & Monitoring*, CRC Press. Wilson, L. G., Everett, L. G., and Cullen, S. J. (Ed.s), 2018).

UNSCEAR, 1988. Sources, Effects and Risks of Ionizing Radiation. United Nations Scientific Committee on the Effects of Atomic Radiation. Report to the General Assembly with Annexes. United Nations Publication, New York, USA. Cited in: Righi and Bruzzi 2006, p.159.

United Nations Scientific Committee on the Effects of Atomic Radiation (1993). Sources and effects of ionizing radiation: UNSCEAR 1993 Report to the General Assembly, with Scientific Annexes. United Nations. ISBN 978-92-1-142200-9.

UNSCEAR, 2000. Effects and Risks of Ionizing Radiations. United Nations Scientific Committee on the Effects of Atomic Radiation. United Nations, New York, USA. Cited in: Singh et al., 2005, p. 437.

Urban, M. and Piesch, E. (1981) Low level environmental radon dosimetry with a passive track etch detector device. *Radiation Protection Dosimetry*, 1(2), 97-109.

van Bavel, C. H. M. (1952) Gaseous Diffusion and Porosity in Porous Media. *Soil Science*, 73(2), 91.

Victor, N. J., Siingh, D., Singh, R. P., Singh, R., and Kamra, A. K. (2019) Diurnal and seasonal variations of radon (^{222}Rn) and their dependence on soil moisture and vertical stability of the lower atmosphere at Pune, India. *Journal of Atmospheric and Solar-Terrestrial Physics*, 195, 105118.

Vonk, J. E. and Gustafsson, O. (2013) Permafrost-carbon complexities. *Nature Geoscience*, 6, 675-676.

Watnick et al., (1986) A ^{222}Rn Monitor Using Alpha Spectroscopy. *Health Physics* 50(5), 645-646. Unavailable. Cited in: Chamberlain 1991.

Whitfield, J. M., Rogers, J. J. W. and Adams, J. A. S. (1959) The relationship between the petrology and the thorium and uranium contents of some granitic rocks. *Geochimica et Cosmochimica Acta*, 17, 248-271.

Wilkening, Clements and Stanley; Adams, J. A. S., Lowder, W. M. and Gesnell, T. F. (ed.) (1972). *Radon Flux Measurements in Widely Separated Regions. Natural Radiation Environments II*, Springfield. P. 717-730.

Willoughby, I., Jinks, R. L., Kerr, G., and Gosling, P. G. (2004) Factors affecting the success of direct seeding for lowland afforestation in the UK. *Forestry*, 77(5), 467-482.

Wrixon et al., (1988). Public Exposure to Radon Daughters, *Radioprotection* 23(4), 347-352. Unavailable. Cited in: Chamberlain 1991.

Ye, Y., Chen, G., Dai., X., Huang, C., Yang, R., and Kearfott, K. J. (2019) Experimental study of the effect on water level and wind speed on radon exhalation of uranium tailings from heap leaching uranium mines. *Environmental Science and Pollution Research*, 26, 27502-27511.

Zhang, L., Lei, X., Guo, Q., Wang, Q., Wang, S., Ma, X., and Shi, Z. (2012) Accurate measurements of the radon exhalation rate of building materials using the closed chamber method. *Journal of Radiological Protection* 32, 315.

Zhang, W., Zhang, Y., and Sun, Q. (2019) Analyses of influencing factors for radon emanation and exhalation in soil. *Water Air Soil Pollution*, 230, 16.

10 Appendix: Scripts

10.1 Authorship

The model employed as part of the presented research was written and developed by Lewis S. Rose whilst a PhD student at the University of Nottingham.

10.2 Conversion of particle size analyser results

Script written in Microsoft Visual Basic.

```
Sub ConvertXls()  
    Dim strPath As String  
    Dim strFile As String  
    Dim wbk As Workbook  
  
    ' Path must end with backslash  
    strPathRead = "existingInputFolder"  
  
    ' Write path must direct to pre-existing folders  
    strPathWrite = "existingOutputFolder"  
    strFile = Dir(strPathRead & "*.xls")  
    Do While strFile <> ""  
        If Right(strFile, 3) = "xls" Then  
            Set wbk =  
                Workbooks.Open(FileName:=strPathRead &  
                    strFile)  
            wbk.SaveAs FileName:=strPathWrite &  
                strFile & ".x", _  
                FileFormat:=xlOpenXMLWorkbook
```

```
        wbk.Close SaveChanges:=False
    End If
    strFile = Dir
Loop
End Sub
```

10.3 Soil gas diffusion model

10.3.1 Primary algorithm: *Main()*

```
from datetime import datetime
startTime = datetime.now()
beginTime = datetime.now()
print('Started at', beginTime)
import numpy as np, csv, pandas as pd
from Diff_1D_251119_static import DiffusionModel
from Ressumofsquares_251119 import checkRes
infile = np.loadtxt('inputfile.txt')
sourcefile = np.loadtxt('sourcefile.txt')
dt = infile[0]
dx = infile[1]
dstart = infile[2]
dend = infile[3]
runcycle = int(infile[4])
measurements = int(infile[5])
equilibrium = infile[6]
subdivisions = int(infile[7])
profileDepth = infile[8]
resultsToOutput = list()
# for the final output file
mesh = int((profileDepth / dx)+40)
# 40*dx of buffer
profilemesh = int(profileDepth/dx)
rd1 = (dt / (dx*dx))*dstart
# value of diffusion coefficient implicitly included
rd2 = (dt/ (dx*dx))*dend
print(rd1, rd2)
```

```

if rd1 > 40 or rd2 > 40:
    print('WARNING: System may be unstable. \n rd = (dt /
        (dx)^2)*D \n if this occurs try rd < 40.')

# output progress to screen
print("Profile depth is", profileDepth)
print("Number of measurements is", measurements)
print("Mesh is", mesh)
chunk_size = measurements

# maximum number of measurements in a profile
def split(df, chunk_size):
    indices = index_marks(df.shape[0], chunk_size)

# df.shape[0] gives the number of rows
    print(indices)
    return np.split(df, indices)

def index_marks(nrows, chunk_size):
    return range(1 * chunk_size, (nrows // chunk_size) *
        chunk_size, chunk_size)

df = pd.read_csv('radonMeasurements.csv')

# reads all measured values into dataframes
waterdf = pd.read_csv('VWCMeasurements.csv')
soildf = pd.read_csv('soilFile.csv')

# soil physical characteristics for emanation calculation
chunks = split(df, chunk_size)

# splits the dataframes into individual profiles
waterchunks = split(waterdf,10)

# default 10 cm VWC measurements
if df.shape[0] % measurements != 0 or waterdf.shape[0] %
10 != 0 or len(chunks) != len(waterchunks):
    print('Some measurement profiles cannot be evenly
        split. Please correct!')
    raise SystemExit

# prepares soil data

```

```

rawRn = np.delete(soildf.values,[1,2,3],axis=1).ravel()
sand = np.delete(soildf.values,[0,2,3],axis=1).ravel()
silt = np.delete(soildf.values,[0,1,3],axis=1).ravel()
clay = np.delete(soildf.values,[0,1,2],axis=1).ravel()
# main loop
chunkNum = 0
for currentChunk in chunks:
    divide = 0
    drange = np.geomspace(dstart,dend,runcycle,
        endpoint=True)
# generates diffusion coefficient values
    initialconditions = np.full(mesh, 100000.0)
# large initial conditions
    print('Chunk is', chunkNum, '\n')
    currentChunk = currentChunk.dropna(how='any')
# "any" drops the row if any values are missing
    currentVWC = waterchunks[chunkNum]
    concChunk =
    np.delete(currentChunk.values,[1,2],axis=1)
# extracts concentration values (cols 1 and 2)
    errChunk = np.delete(currentChunk.values,[0,1],axis=1)
# should remove to error col only
    vwcChunk = np.delete(currentVWC.values,[0],axis=1)
    chunkNum += 1
    meas = concChunk.ravel()
# converts to an array, ready to pass to diffusion model
    err = errChunk.ravel()
    vwc = vwcChunk.ravel()
    best = float("inf")
    bestcoeff = np.array([])
    for firstRange in range(runcycle):
# passes data to model and then residual checker

```

```

coeff = drange[firstRange]
if chunkNum-1 != 0 and firstRange == 0:
    initialconditions = firstInitialConditions
if 1 == 1:
    mod, trued, newInitialConditions =
    DiffusionModel(coeff, dt, dx, equilibrium,
    measurements, sourcefile, initialconditions,
    mesh, profilemesh, meas, firstRange)
    rss, simpleMod = checkRes(mod, coeff,
    meas, measurements, mesh, profileDepth,
    err)
    print(coeff, 'took', datetime.now()-startTime)
    startTime = datetime.now()
    if firstRange == 0:
        firstInitialConditions =
        np.copy(newInitialConditions)
    else:
        initialconditions = newInitialConditions
    if firstRange == 0 or rss <= best:
        best = rss
# all-time best diffusion coefficient (min residuals)
        bestcoeff = np.append(bestcoeff,
        drange[firstRange])
# the best diffusion coefficients
        finald = trued
        finalres = simpleMod
        finalnorm = np.sqrt(rss)
        print('best')
    else:
        print('subdividing')
        try:
# only one value means only one diffusion coefficient

```

```

drange =
np.geomspace(drange[firstRange
], bestcoeff[-2], runcycle)
except:
drange =
np.geomspace(drange[firstRange
], bestcoeff[-1], runcycle)
break

```

straight to subdivisions

```

for dividingDs in range(subdivisions):
for division in range(1,runcycle-1):

```

as above, no values rerun

```

coeff = drange[division]
mod, trued, newInitialConditions =
DiffusionModel(coeff, dt, dx, equilibrium,
measurements, sourcefile, initialconditions,
mesh, profilemesh, meas, dividing)
rss, simpleMod = checkRes(mod, coeff,
meas, measurements, mesh, profileDepth,
err)
print(coeff, 'took', datetime.now()-startTime)
startTime = datetime.now()
initialconditions = newInitialConditions
if rss <= best:
best = rss
bestcycle = drange[division]
bestcoeff = np.append(bestcoeff,
drange[division])
finald = trued
finalres = simpleMod
finalnorm = np.sqrt(rss)
print('best')

```

```

else:
    print('subdividing')
    try:
# only one value means only one diffusion coefficient
        drange =
            np.geomspace(drange[division],
                bestcoeff[-2], runcycle)
    except:
        drange =
            np.geomspace(drange[division],
                bestcoeff[-1], runcycle)
    break

# finished
    resultsToOutput.append(concChunk)
# appends the measured values to aid identification
    resultsToOutput.append(finald)
# collates results to write to file
    resultsToOutput.append(finalnorm)
# normalised residuals of the data to the model for the
given value
    for writing in range(len(simpleMod)):
# a single iterable, rather than an interable of iterables
        resultsToOutput.append(simpleMod[writing])
with open("NewOutput %s .csv" % datetime.now().date(),
"a") as f:
# 'a' appends to the output file.
    writer = csv.writer(f)
    writer.writerow(resultsToOutput)
# single iterable means writerow() rather than
writerows() is appropriate
print('Finished. The fitted value for d is', bestcoeff[-1], 'with
rss value', best.round(3))

```

```
print('Finished at:', datetime.now(), '\n Total run:',  
datetime.now()-beginTime)  
# tracks total run time
```

10.3.2 Secondary algorithm: *Diff_1D()*

```
def DiffusionModel(coeff, dt, dx, equilibrium, measurements,
sourcefile, initialconditions, mesh, profilemesh, meas,
coeffRange):
# include diffusion coefficient within calculations
    rd = (dt / (dx * dx)) * coeff
# calculate the source terms from sourcefile and vwc
    source = np.zeros(measurements)
    for calculateSource in range(measurements):
        sandSource = rawRn[calculateSource] * (0.1 * (1
        + 1.53 * (1 - np.exp(-21.8 *
        vwc[calculateSource])))) * sand[calculateSource]
        siltSource = rawRn[calculateSource] * (0.1 * (1 +
        1.73 * (1 - np.exp(-20.5 *
        vwc[calculateSource])))) * silt[calculateSource]
        claySource = rawRn[calculateSource] * (0.1 * (1
        + 1.85 * (1 - np.exp(-18.8 *
        vwc[calculateSource])))) * clay[calculateSource]
        source[calculateSource] = sandSource +
        siltSource + claySource
    print('source is', source)
    res = np.zeros(profilemesh)
# concentration vector
    origmat = np.zeros((mesh,mesh))
# Crank-Nicolson matrix (original and for manipulation)
    ansmat = np.copy(initialconditions)
    ansmat2 = np.copy(ansmat)
    compare = np.ones(profilemesh)
# for comparison with previous timestep
    steps = 0
```

```

# tracks current timestep
    point = np.ones(profilemesh)
    temppoint = np.ones(profilemesh)
    realtime = np.array([])

# populate the C-N matrix
    for n in range(1, mesh-1):
        origmat[n,n-1] = -rd
        origmat[n,n] = 2 + 2*rd
        origmat[n,n+1] = -rd

# implement boundary conditions
    origmat[0,0] = 2 + 2*rd
    origmat[0,1] = -rd
    origmat[mesh-1,mesh-1] = 2 + rd
    origmat[mesh-1,mesh-2] = -rd

# Crank-Nicolson solver
    while all(item > equilibrium*dt for item in compare):

# checks all nodes for equilibrium criteria
        mat = np.copy(origmat)

# copies of the matrix LHS for calculation
        mat2 = np.copy(origmat)
        steps += 1

# the number of timesteps
        if coeffRange == 0:
            minRun = 10800/dt

# minimum run time of 3 h in the model
        else:
            minRun = 2

        if steps > minRun:
            temppoint = np.copy(res)
            if steps%dt == 0:

# check every second of model time
                for points in range(profilemesh):

```

```

compare[points] =
abs(point[points]-
temppoint[points])
point = np.copy(temppoint)
sourceNum = 0
for sourceterm in range(len(source)):
    for soilLayer in
range(len(source)*sourceNum,
len(source)*(sourceNum+1)):
        ansmat[soilLayer] = ansmat[soilLayer]
        * (0.9999979**dt) +
        source[sourceNum] * dt
# accounts for varying dt and mesh size
sourceNum += 1
for extraLayers in range(len(source)*sourceNum,
len(ansmat)):
    ansmat[extraLayers] = ansmat[extraLayers]
    * (0.9999979**dt) + source[-1] * dt
ansmat2 = np.copy(ansmat)
# manipulate solution vector for boundary conditions
for n in range(1, mesh-1):
    ansmat2[n] = rd*ansmat[n-1] + (2-
2*rd)*ansmat[n] + rd*ansmat[n+1]
ansmat2[0] = (2-2*rd)*ansmat[0] +
rd*ansmat[1]
ansmat2[mesh-1] = rd*ansmat[mesh-2] + (2-
rd)*ansmat[mesh-1]
ansmat = np.copy(ansmat2)
# manipulation LHS (pivoting):
for pivcol in range(mesh-1):
    pivot = mat[pivcol,pivcol]
    for pivrow in range (pivcol, len(mat)):

```

```

        if abs(mat[pivrow,pivcol]) >=
        abs(pivot):
            pivot = mat[pivrow,pivcol]
            checkrow = pivrow
            checkcol = pivcol
        if checkrow != checkcol:
# ...row switching...
            for switchrow in range(mesh):
                mat2[pivrow,switchrow] =
                mat[pivcol,switchrow]
                mat2[pivcol,switchrow] =
                mat[pivrow,switchrow]
            ansmat2[pivrow] = ansmat[pivcol]
            ansmat2[pivcol] = ansmat[pivrow]
            mat = np.copy(mat2)
            ansmat = np.copy(ansmat2)
# ...row reduction...
            for n in range(pivcol+1, mesh):
                f = mat[n,pivcol] / mat[pivcol,pivcol]
                for x in range(mesh-pivcol):
                    mat2[n,pivcol+x] =
                    mat[n,pivcol+x] -
                    mat[pivcol,pivcol+x] * f
                    ansmat2[n] = ansmat[n] -
                    ansmat[pivcol] * f
            mat = np.copy(mat2)
            ansmat = np.copy(ansmat2)
# ...backward substitution...
            for y in range(mesh-2, -1, -1):
                for l in range(y, -1, -1):
                    f = mat[l,y+1] / mat[y+1,y+1]

```

```

        mat2[l,y+1] = mat[l,y+1] -
        mat[y+1,y+1] * f
        ansmat2[l]=ansmat[l]-ansmat[y+1]*f
    mat = np.copy(mat2)
    ansmat = np.copy(ansmat2)
# ...division through each row...
    for z in range(mesh):
        ansmat2[z] = ansmat[z]/mat[z,z]
    for extractingres in range(profilemesh):
        res[extractingres] = ansmat2[extractingres]
    newInitialConditions = np.copy(ansmat2)
    ansmat = np.copy(ansmat2)
    return res, d, newInitialConditions

```

10.3.3 Tertiary algorithm: RSS()

```
def checkRes(mod, runcycles, meas, measurements, mesh,
profileDepth, err):
    simpleMod = np.array([])
# simplified array for output
    sumsquare = np.zeros(measurements)
    sums = np.copy(sumsquare)
    if measurements != 6 or measurements != 10:
        print("Measurement number not currently
supported")
        raise SystemExit
    if measurements == 6:
        tempMod = np.split(mod, 4)
        simpleMod = np.array([])
        simpleMod = np.append(simpleMod, mod[4])
        simpleMod = np.append(simpleMod, mod[9])
        for finalFour in range(len(tempMod)):
            pickLayer = tempMod[finalFour]
            simpleMod = np.append(simpleMod, pickLayer[-1])
    if measurements == 10:
        tempMod = np.split(mod,10)
        for values in range(10):
            pickLayer = tempMod[values]
            simpleMod = np.append(simpleMod, pickLayer[-1])
    for calcrss in range(len(meas)):
# calculates residual sums of squares
        sums[calcrss] = (simpleMod[calcrss] - meas[calcrss])
        sumsquare[calcrss] = (simpleMod[calcrss] -
meas[calcrss])**2
    rss = sum(sumsquare)
```

```
for printing in range(len(simpleMod)):
    print(simpleMod[printing])
return rss, sums, simpleMod
```